



INTERNATIONAL ATOMIC ENERGY AGENCY
UNITED NATIONS EDUCATIONAL, SCIENTIFIC AND CULTURAL ORGANIZATION



INTERNATIONAL CENTRE FOR THEORETICAL PHYSICS
34100 TRIESTE (ITALY) - P.O.B. 586 - MIRAMARE - STRADA COSTIERA 11 - TELEPHONES: 224281/23456
CABLE: CENTRATOM - TELEX 460392-1

SMR/98 - 41

AUTUMN COURSE ON GEOMAGNETISM, THE IONOSPHERE
AND MAGNETOSPHERE

(21 September - 12 November 1982)

WAVES AND WAVE-PARTICLE INTERACTIONS IN THE MAGNETOSPHERE.

R. GENDRIN

CNET/CRPE
92131 Issy-les-Moulineaux
FRANCE

These are preliminary lecture notes, intended only for distribution to participants.
Missing or extra copies are available from Room 230.

WAVES AND WAVE-PARTICLE INTERACTIONS IN THE MAGNETOSPHERE

Lectures given at the International Center for Theoretical Physics

Trieste, Italy, October 1982

by

Roger GENDRIN

Centre de Recherches en Physique de l'Environnement
Centre National d'Etudes des Télécommunications
3, avenue de la République, 92131 Issy-les-Moulineaux, France

CHAPTER II

HYDROMAGNETIC WAVES WITH HIGHER FREQUENCIES

CHAPTER II

HYDROMAGNETIC WAVES WITH HIGHER FREQUENCIES

APPENDIX B

THEORY OF GYRORESONANT INTERACTIONS

CHAPTER II - HYDROMAGNETIC WAVES WITH HIGHER FREQUENCIES

In the 1950's and later sensitive magnetic detectors (0.1 nT or less) were made available in the frequency range around 1 Hz ($\sim 0.1 - 5$ Hz). It soon appeared that this part of the frequency spectrum was also occupied by natural emissions originating in the Earth's environment. The amplitude and/or frequency characteristics versus time of these emissions can be 'regular' or 'irregular', similarly to what exists for the long period pulsations (LPP).^{*} These emissions can last for hours or for only tens of minutes or even less. They occur during magnetically quiet or disturbed conditions, the 'regular' ones occurring preferentially during quiet conditions, the 'irregular' ones being mostly observed during magnetically active periods. A more precise description of these waves, as observed on the ground, is given in Section 2.1.

For both experimental and theoretical reasons, it soon became evident that these waves were generated in the outer region of the magnetosphere ($3 \leq L \leq 8$) and that they were propagating along magnetic field lines in a manner similar to VLF 'whistler' waves whose propagation characteristics were just interpreted at that time. These waves share two properties with LPP's : *first*, their phase velocity is of the order of the Alfvén velocity V_A , because their frequency is smaller than the proton gyrofrequency at the apex of the field line and therefore much smaller than f_{ci} everywhere else ; *second*, the ionosphere also modifies the characteristics of the waves before they reach the ground. But contrarily to LPP's and because their frequency is larger, there are many wavelengths along the field line^{**}. Consequently one can speak of propagating waves and the inhomogeneity of the medium does not play a fundamental role as far as their generation mechanism is concerned, and which can be considered as localized in space. Besides, f being not much smaller than f_{ci} ,

* The appellations Pc ('Pulsations continues', i.e. continuous pulsations) and Pi ('Pulsations irrégulières', i.e. irregular pulsations) are also valid in this frequency range.

** Assuming $L = 4$, $V_A = 1000 \text{ km.s}^{-1}$ and $f = 1 \text{ Hz}$ gives $\lambda = 50 \lambda$

dispersion effects are important and the phase and group velocities of these waves are generally frequency-dependent. Moreover the inhomogeneity of the medium and the anisotropic properties of the dispersion relation impose the use of ray tracing techniques. All these problems will be discussed in Section 2.2.

As far as the generation mechanisms of these waves are concerned, the cyclotron resonance instability induced by energetic protons ($\sim 10 - 100 \text{ keV}$) having an anisotropic distribution function ($T_{\perp}/T_{\parallel} > 1$) soon became popular for both experimental and theoretical reasons. The theory of this instability will be presented in Section 2.3. The linear theory gives the frequency of the emission as a function of the hot and cold plasma parameters. The quasi-linear theory explains the reaction of the wave on the particle distribution function, which leads to pitch angle and energy diffusion.

Recently spacecraft bearing detectors almost as sensitive as the ground ones have been launched into the equatorial magnetosphere. Hydromagnetic waves ($0.1 < f < 10 \text{ Hz}$) could thus be observed in the region of space where they are generated. These observations lead scientists to modify the too simple picture which had arisen from ground measurements alone. First it was shown that the presence of even a small concentration of cold Helium ions completely changes the propagation and generation characteristics of waves with $f < f_{ci}$, with important consequences on the heavy ion energetics in the magnetosphere (section 2.4). Second a new category of waves was discovered in the frequency range $f > f_{ci}$, with a wave normal vector almost perpendicular to the DC magnetic field ; such waves cannot be detected on the ground (Section 2.5). The two last Sections of this Chapter will be devoted to irregular pulsations : IPDP's (Irregular Pulsations of Diminishing Periods) and SIP's (Short Irregular Pulsations). The previous ideas on the nature and origin of these pulsations have been also modified by the results obtained in situ with spacecraft.

2.1. Overall properties and classification

As said in the introduction these natural emissions can be divided into two main categories : Pc and Pi. Both Pc's and Pi's can be subdivided into different subcategories of which the principal ones are illustrated on Figures 2.1 and 2.2, by both their amplitude-versus-time variation and their representation in the frequency-time domain. Their characteristics are described below ; they are summarized in Table 2.1 (Gendrin, 1970).*

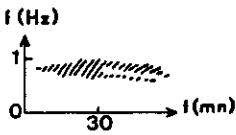
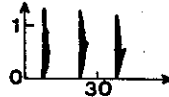
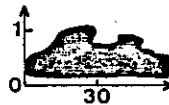
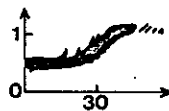
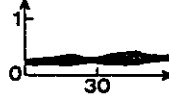
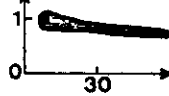
The 'pearl oscillations', originally discovered by Troitskaya (1961), owe their name to the shape of their amplitude versus time diagram (Figure 2.1.a). They are also called 'structured Pc 1 events'. Because of their very regular characteristics they are precious tools for studying the propagation and generation properties of h.m waves in this frequency range (see Section 2.2 and 2.3). Within each pearl element, the frequency increases almost linearly, the slope $s = df/dt$ of successive elements being in general a decreasing function of time (Figure 2.1.c). Such a property is due to the cumulative effect of dispersion along the many bounces that these waves make along the field line between two conjugate points. By analogy with what occurs in the VLF range these emissions have been called 'hydromagnetic whistlers' (Obayashi, 1965). Sometimes s is not a decreasing function of time, a phenomenon which is interpreted as being due to the competing action of generation and propagation processes (Section 2.3). The mean frequency of the wave, f_0 is a decreasing function of latitude whereas the repetition period T of the elements increases. The product $f_0 T$ is approximately constant (Gendrin, 1963 ; Tepley, 1965)

$$f_0 T \sim 100 - 150 \quad (1)$$

A qualitative interpretation of this empirical relation (Figure 2.3) is that the frequency of the wave is approximately a constant fraction of the gyrofrequency at the apex of the field line ($f_0/f_{ceq} \sim 0.2$). As the L value of the field line increases, its length increases and so does T

* A more detailed classification has been made recently by Fukunishi et al. (1981) on the basis of ~ 3000 events recorded at the Japanese antarctic base of Syowa ($L \sim 6.5$).

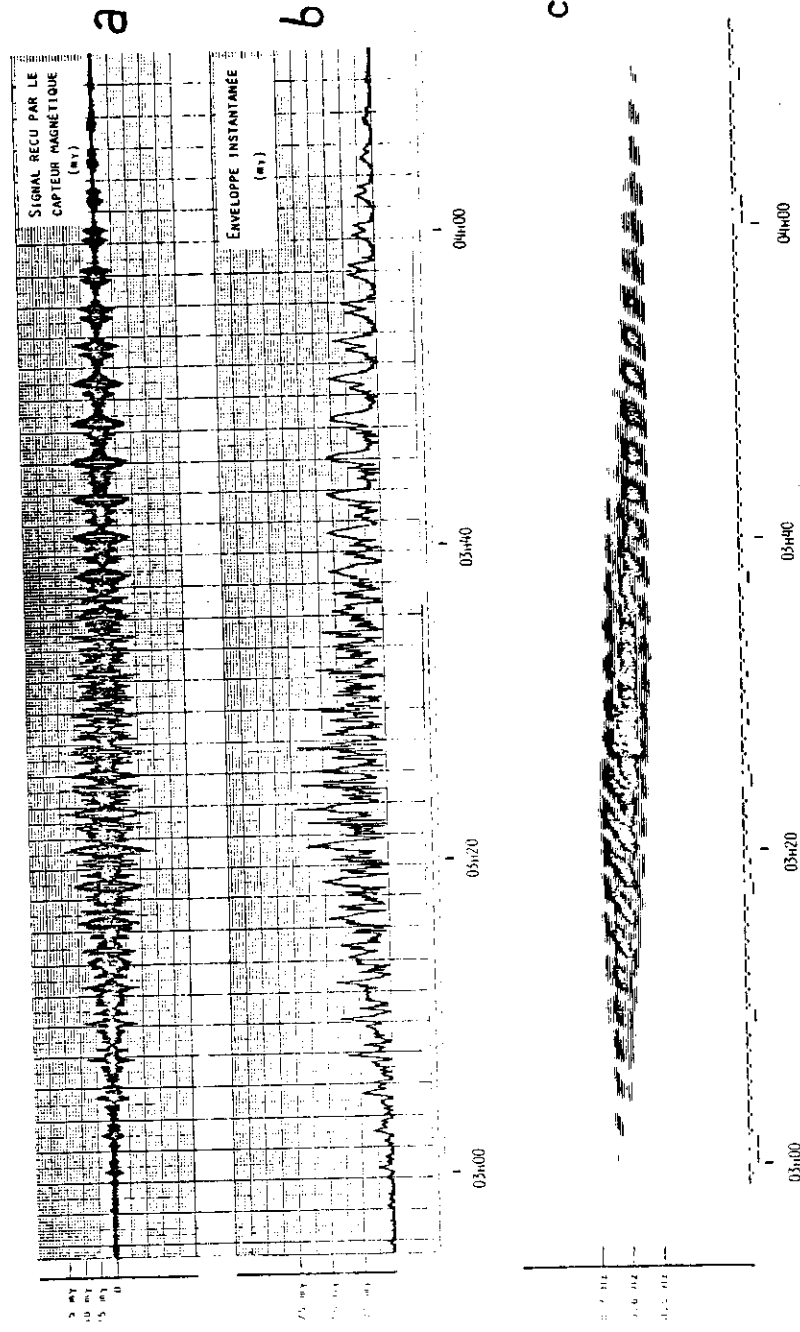
TABLE 2.1.
Characteristics of short period micropulsations
(amplitude and time occurrence are given for Kerguelen, except for the 4-sec band noise which is principally observed in the auroral zone)

Name	Spectral shape	Mean spectral intensity (mV·Hz ^{-1/2})	Mean amplitude* (V)	Time of occurrence ^b (L.T.)	Observations
Pearls		80	0.1	0212	
S.I.P. (short irregular pulsations)		70	0.2	2205	Often accompanied with A.I.P.
A.I.P. (auroral irregular pulsations)		130	0.3	0208	Often accompanied with S.I.P.
I.P.D.P. (irregular pulsations with diminishing periods)		50	0.1	1601	Notice the structured elements and the Pc 1 event which often follows the I.P.D.P.
4-sec band noise		35	0.035	1220 2302	Chiefly observed during summer
I.P.I.P. (irregular pulsations with increasing periods)		200	0.5	1416	Maybe a badly resolved Pc 1 event (see Figure 4)

* observed with a receiver of frequency band from 0.1 to 5 Hz
* at 6 dB occurrence

Gendrin, Space Sci. Rev., 11, 54, 1970

Fig. 2.1.



KERGUELEN 25-FEB-1980

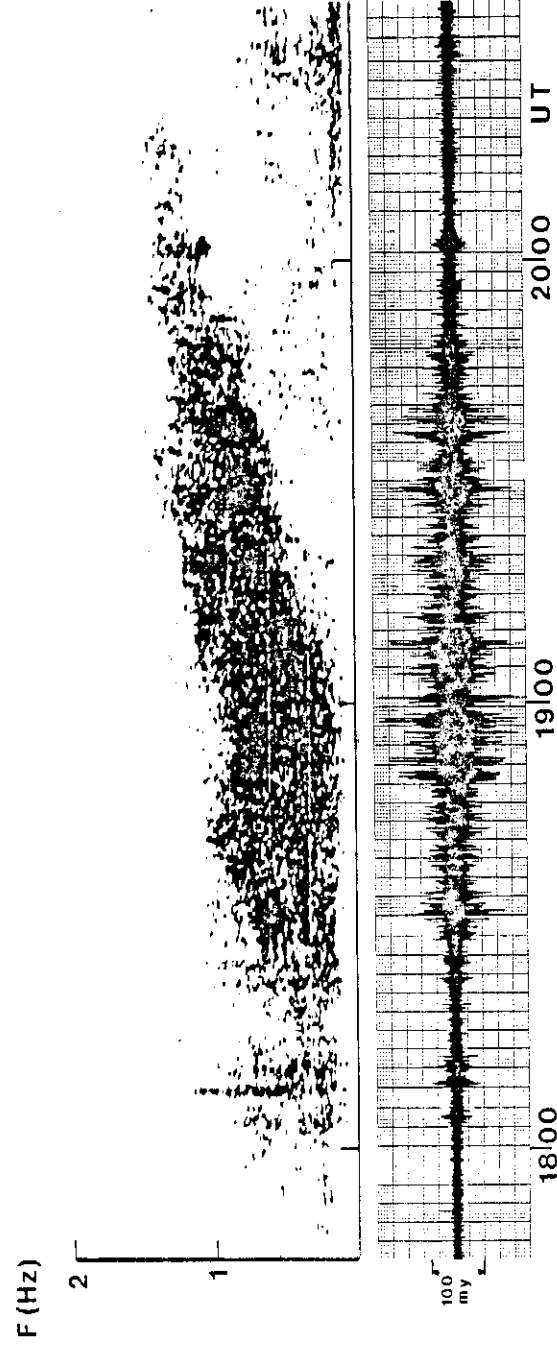


Fig : 2.2.a. Irregular Pulsations of Diminishing Periods (IPDP)

KERGUELEN 28. FEB. 1980

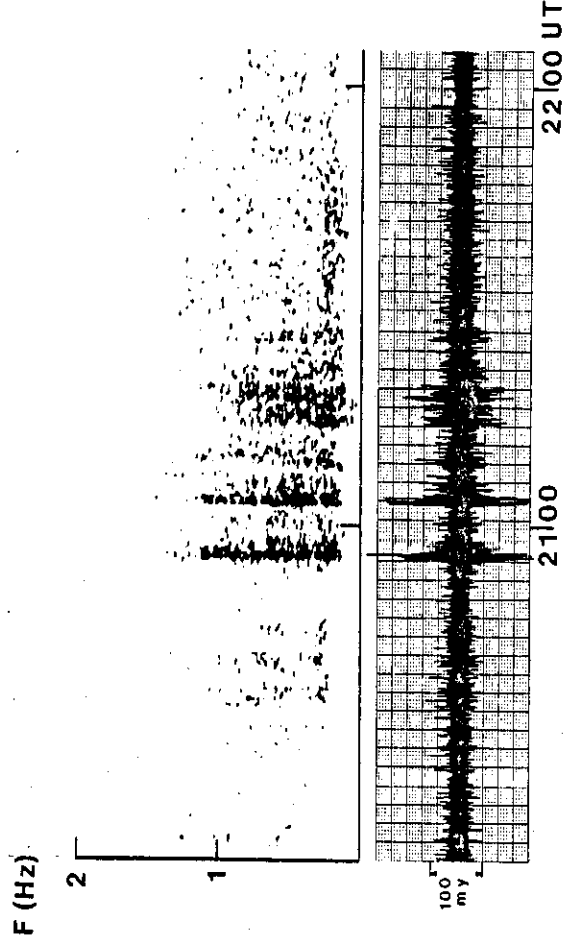


Fig: 2.2.b. Short Irregular Pulsations(SIP)

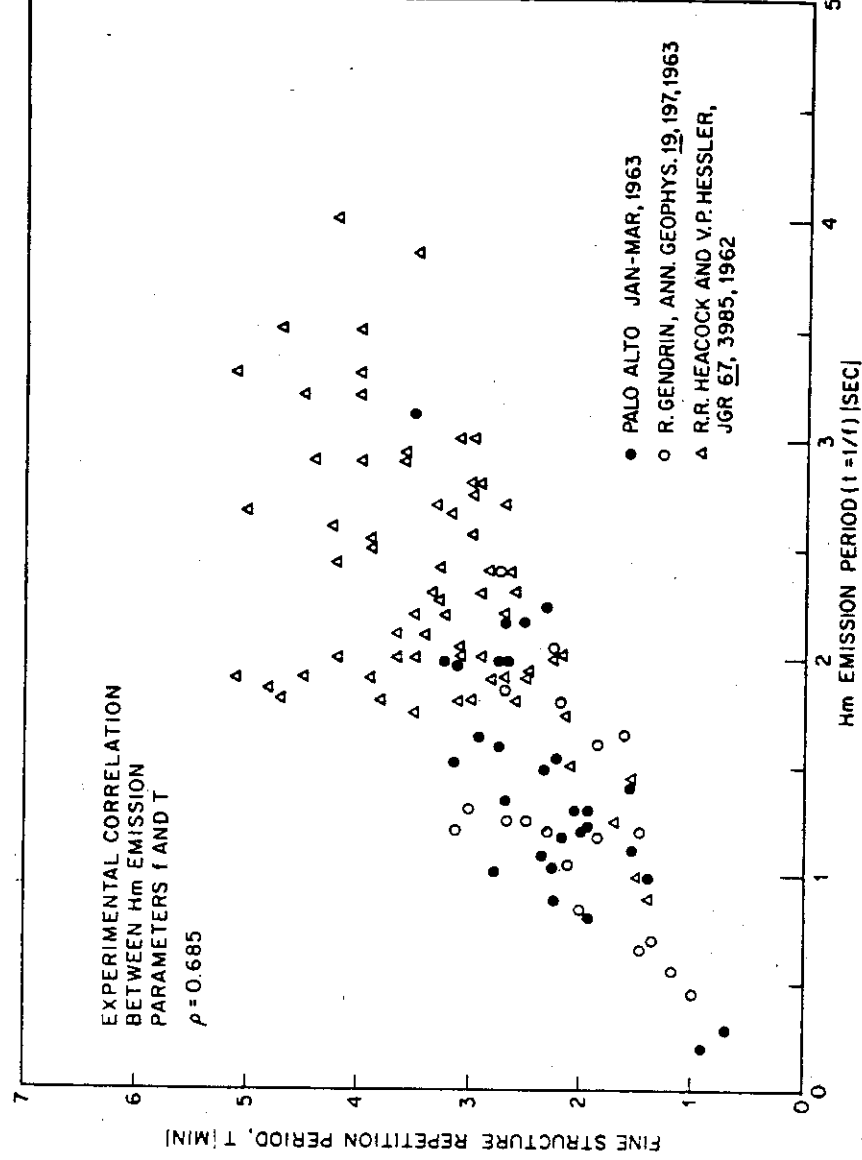


Fig. 2.3. Corrélation entre la période de répétition et la fréquence moyenne des oscillations hydro-magnétiques structurées. (D'après TEPLEY, 1965.)

whereas f_o decreases. At $L = 4$ for instance, $f_{ci} = 6.5$ Hz and one observes pearls with $f_o \sim 1 - 1.5$ Hz. For $V_A \sim 1000 \text{ km.s}^{-1}$, $T \sim 100$ s (see Chapter 1), which leads to (1). However, both experimental observations (Gendrin et al., 1978) and theoretical modelling (Antonova et al., 1981) show that at latitudes higher than 65° , the product $f_o T$ has higher values ($\sim 200 - 300$). This may be due to the increase of the equatorial value of f_{ci} because of the dayside compression of the magnetosphere. Such an effect is not only statistical ; it may be observed for example on individual events (Hirasawa, 1981) when an emission is in progress during an SSC (Sudden Storm Commencement) (Figure 2.4). On the contrary, for high L-values, the equatorial plasma density is much lower, an effect which should lead to an increase of V_A and therefore to a decrease of T .

The 'irregular pulsations of diminishing periods' (IPDP) are not structured in time except at the end of some events. They have a wider frequency spectrum the central frequency of which suddenly increases with time. These events are observed in the dusk sector during proton injection events following substorm onsets. An example of one such emission is given on Figure 2.2.a.

The 'short irregular pulsations' (SIP) are bursts of wide band noise with a short duration (~ 1 mn) and a repetitive structure (Lacourly, 1969). They are often associated with 'auroral irregular pulsations' (AIP) which consist of an intense wide band noise extending to very low frequencies*. These phenomena are observed at high latitudes, in conjunction with visible aurorae. All these events have definite occurrence relationships with local time and magnetic activity. On Figure 2.5 the mid-latitude ($L \sim 3.7$) local time dependence for the three main pulsation categories is represented. Note that different curves can be observed at different latitudes not only because of the L-dependence of the generation efficiency but also because of the different transmission properties of the ionosphere (Section 2.2).

* figure 2.2.b.

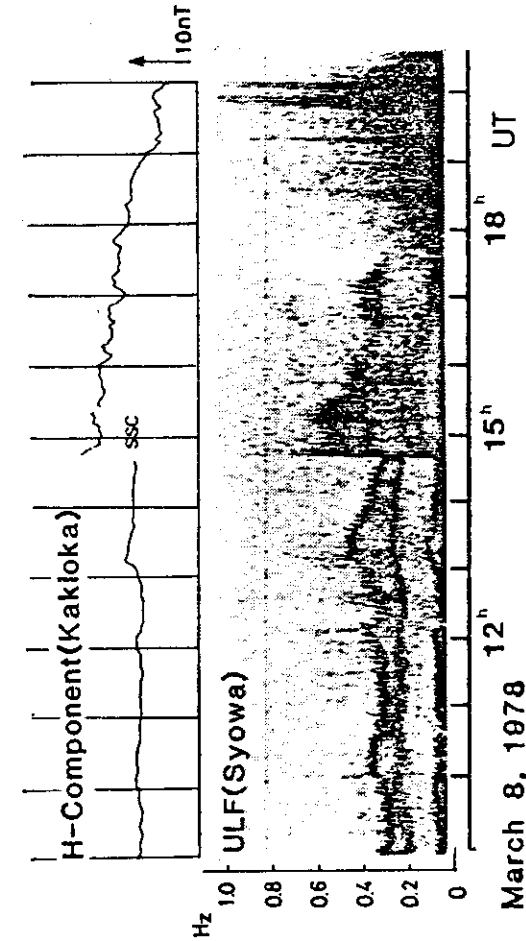


Fig. 2.4. Magnetic H-component variation recorded at low-latitude station, Kakioka (top) and f-1 diagram of ULF emission (HM chorus) at Syowa Station (bottom).
T. Hirasawa, *Memoirs of the NIPR, Tokyo, 18, 127-151, 1981*

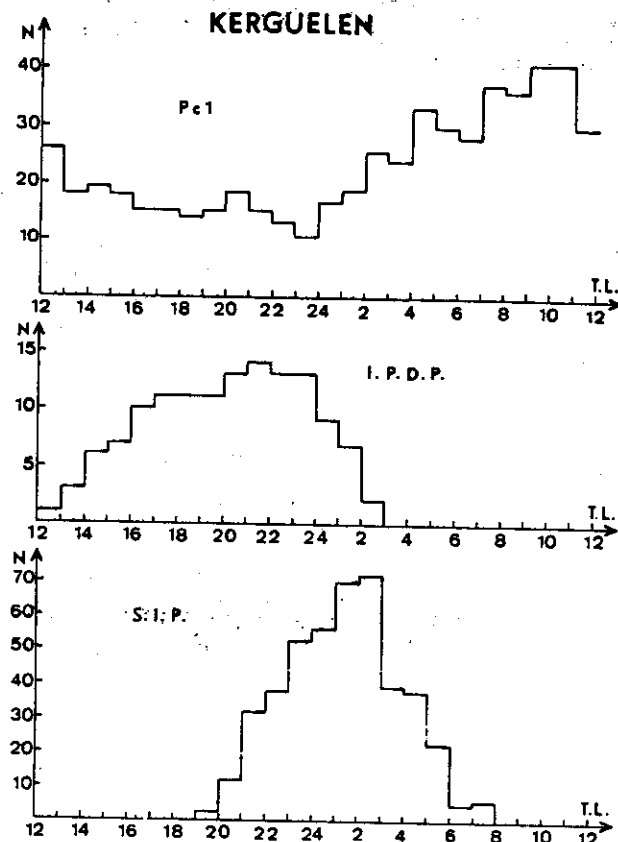


Fig. 2.5. Statistical occurrence of Pc 1's, IPDP's and SIP's at Kerguelen for the years of 1965 or 1966. (The upper part of the figure is taken from the work of Gendrin and Vigneron (1966); the other statistics have been kindly communicated by Miss Lacourly.

Gendrin, 1970.

2.2. Propagation effects

In this Section we will study the propagation characteristics of ULF waves with frequencies slightly smaller than the equatorial value of the proton gyrofrequency ($\sim f_{ci}/10 < f < f_{ci}$). The anisotropic and dispersive properties of these waves will be analysed. The experimental facts which support the theory and which concern mainly hydromagnetic whistlers (or 'pearl oscillations') will be presented. Finally the way in which the ionosphere modifies some of the wave characteristics will be discussed.

2.2.1. Anisotropy, dispersion and time delay

In the frequency range $f < f_{ci}$ two modes can propagate that have different polarization and dispersive characteristics. One of them is completely isotropic in the limit $f \rightarrow 0$ and is right-hand polarized. The other is strongly anisotropic and is left-hand polarized. For a given wave normal angle $\theta = (\underline{k}, \underline{B})$ the variation of the phase velocity with frequency is also different for the two modes (see Appendix A).

The curves representing the shape of the index surfaces for the two modes are given on Figure 2.6 (Jacobs and Watanabe, 1964 ; Dowden, 1965 ; Jacobs, 1970). Because the wave energy propagates in the direction which is perpendicular to the index surface (the ray direction \underline{R}), the energy is focused within a small cone around the direction of the DC magnetic field for the L mode whereas it is dispersed in the whole space for the R mode. This is demonstrated in a quantitative manner on Figure 2.7. For the L mode, the angle $\theta_R = (\underline{R}, \underline{B})$ remains smaller than $\sim 9^\circ$ for all value of θ when $X = f/f_{ci} < 0.5$ (Figure 2.7.a). Consequently the energy of the wave can be guided along the magnetic field lines. On the contrary the ray direction makes a large angle with \underline{B} for the R mode (Figure 2.7.b). It is only when f becomes larger than f_{ci} that θ_R becomes smaller than $\sim 20^\circ$. Such an effect is related with the guidance of whistler waves (which also propagate in the R mode also) at higher frequencies (see Chapter 3).

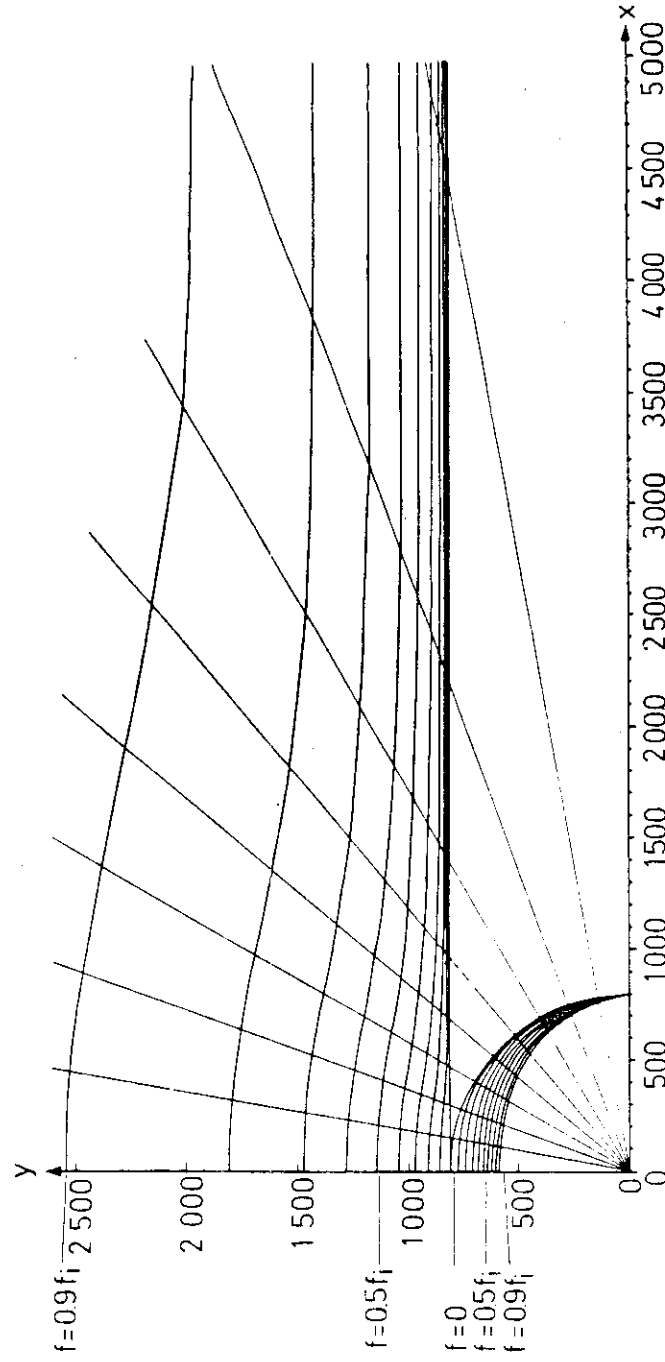


Fig. 2.6. Surfaces of refractive index for waves in a homogeneous plasma permeated by an external magnetic field. (After J. A. Jacobs and T. Watanabe)

b

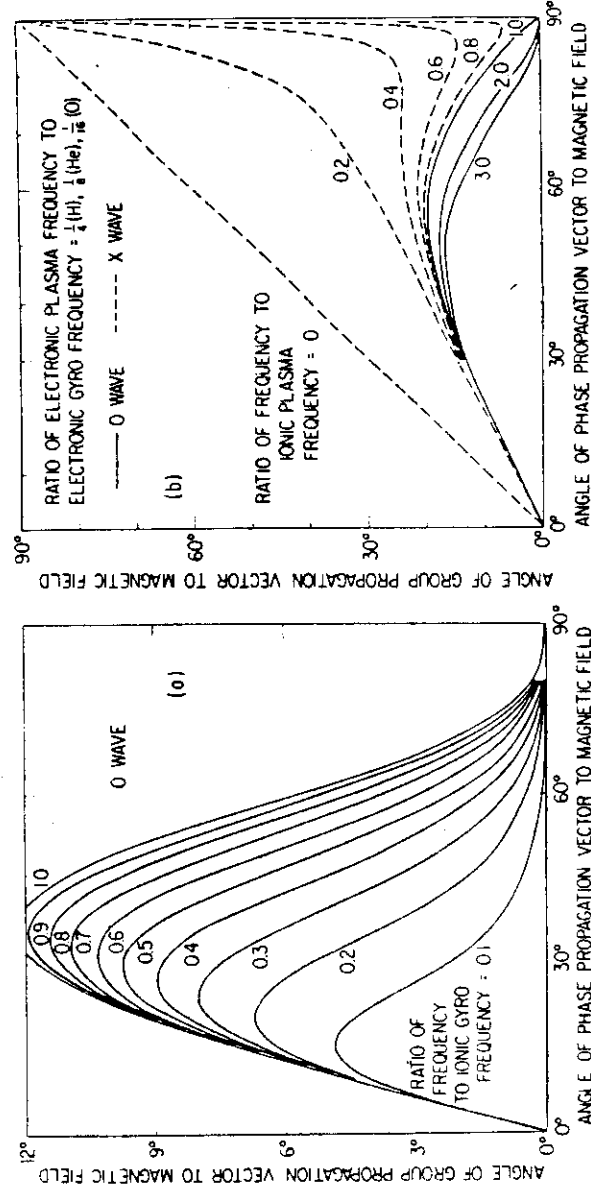


Fig. 2.7. — Angle de propagation de l'énergie par rapport au champ magnétique en fonction de la normale à l'onde, pour différentes valeurs du rapport f/f_B .
a) Pour le mode L. Le rapport $\alpha = f/\omega_B$ est pris égal à $1/4$ si les ions sont des protons, $1/8$ s'il s'agit d'ions He^+ , $1/16$ s'il s'agit d'ions O^+ . On remarque qu'on a guidage pour le mode R dès que $f > f_B$ (d'après Booker et Dyer, 1965).

Since θ_R is large, waves propagating in the R mode are not guided by the magnetic field; they cannot make many bounces between conjugate points. Therefore 'pearl oscillations' are likely to correspond to L waves*.

Moreover the frequency dependence of the L mode group velocity is such that one can interpret the slope of the signal dispersion in a frequency-time diagram. The group velocity is related to the phase velocity by the relation

$$v_g = d\omega/dk = c/n_g \quad (2.2)$$

where

$$n_g = n_\phi + \omega dn_\phi/d\omega \quad (2.3)$$

For the L mode and for strictly longitudinal propagation ($\theta = 0$) the phase velocity $v_\phi = c/n_\phi$ is given by**

$$v_\phi = V_A (1 - X)^{1/2} \quad (2.4)$$

so that

$$v_g = V_A (1 - X)^{3/2} / (1 - X/2) \quad (2.5)$$

which shows that v_g is a decreasing function of frequency. Therefore the propagation time is longer for higher frequencies. An opposite variation would be found for the R mode.

Assuming that the same wave packet is bouncing back and forth between the two hemispheres, the repetition period between two successive elements of a pearl event recorded at a given station would be approximately given by

$$T = 2 \int \frac{ds}{v_g} \quad (2.6)$$

* The mechanism by which waves are generated in this frequency range also plead in favour of the L-mode.

** Equation (A.24).

where the integral is taken along the field line between the two conjugate points. Clearly T is an increasing function of the frequency and, for each new bounce, the slope $s = df/dt$ must decrease, which is what is observed (see Figure 2.2).

For the computation of T, the model which is used for representing the variation of the cold plasma density along the field line is not so important. Indeed, as it is usual in this sort of integral, the equatorial region (where V_A is minimum) plays the dominant role. An example of results obtained for a model in which the equatorial plasma density is equal to 10^4 cm^{-3} (a rather high value for $L = 4-5$) is given on Figure 2.8. The shape of the recorded signals, as well as the orders of magnitude of T are correctly interpreted if one assumes that the true signal occupies just a restricted frequency range (Obayashi, 1965). The period of repetition is an increasing function of latitude, whereas the high frequency cut-off (the frequency for which $T \rightarrow \infty$) decreases with latitude. It is equal to the equatorial value of the proton gyrofrequency ($v_g \rightarrow 0$ when $X \rightarrow 1$).

In fact the integral is not to be taken along the field line but along the ray trajectory. Although the angle θ_g between \underline{B} and the ray direction remains small it is not equal to zero. The ray deviates from the magnetic field line. The medium being inhomogeneous, Descartes-Snell's law implies that the wave normal angle itself has to vary. Consequently θ_g is different; the ray propagates in another region of the magnetosphere where the plasma parameters are still different, θ varies again and so on. Ray tracing techniques must be used, which take into account all these related variations. In general these techniques involve the numerical integration of the Haselgrove's (1957) equations*.

* The general formalism which leads to these equations can be found for instance in Quemada (1968) pp. 218-223. The practical equations valid in the ULF range for a multi-component plasma, have been worked out by Rauch (1981.)

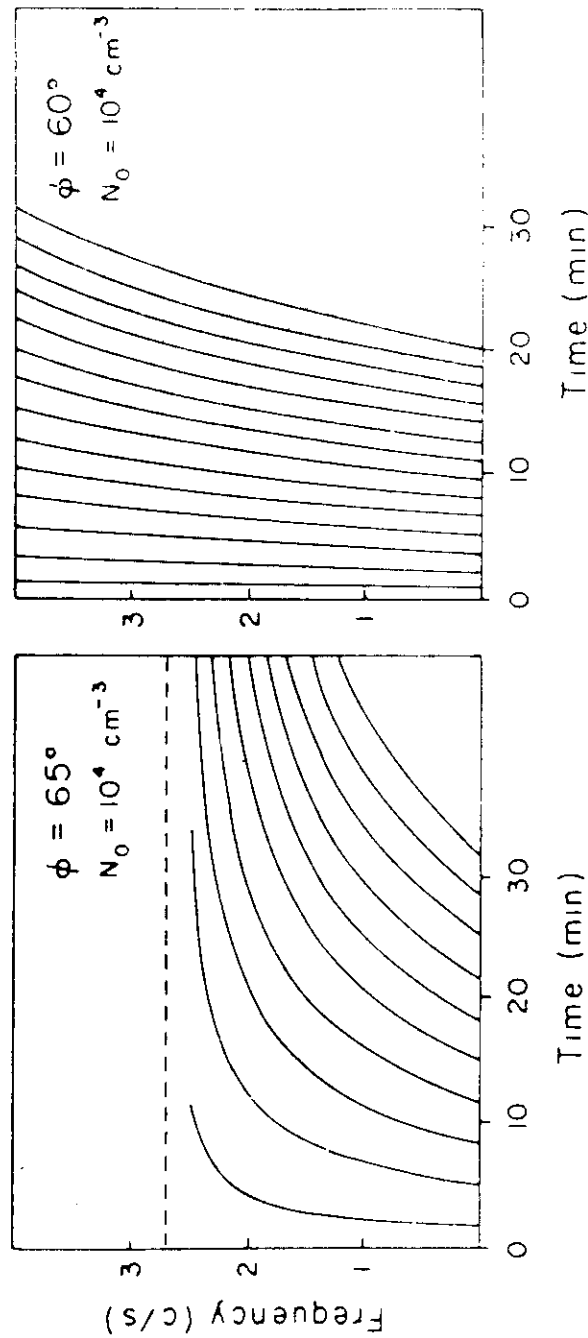


Fig. 2.8. Sonagramme théorique d'un sifflement hydromagnétique pour deux latitudes. La variation de la densité électronique avec la distance géométrique L est donnée par la loi $N = N_0(r_c/r)^3$. (D'après OBAYASHI, 1965.)

An example of the results thus obtained is presented on Figure 2.9 which shows that the travel time for a wave with a given frequency may vary by a factor of 2 depending on the initial value of the wave normal angle at the injection point. At the opposite end of the field line, the wave normal angle θ always reach the value of 90° which prevents any further propagation (Kitamura and Jacobs, 1965). However, Glangeaud and Lacoume (1971) have shown that for waves propagating in the vicinity of a density gradient, the wave normal never departs from the magnetic field direction by more than 30° . More recent computations (Rauch, 1981 ; Rauch and Roux, 1982) have been done for a plasma containing more than one ion species. Their results will be presented in Section 2.4.

2.2. Observations

Initial ground measurements, especially those made at conjugate observatories, have supported the theoretical ideas presented above. Figure 2.10 gives two examples of signals recorded at the two stations of Kerguelen Island (Indian Ocean) and Borok (Soviet Union) which are almost conjugated ($L \sim 3.7$). The similarity of the frequency-time structure at the two stations (lower part of the figure) is evident, although there are differences in the relative intensities in some frequency ranges. The amplitude-versus-time diagrams (upper part of the figure) do present identical characteristics which are delayed in time by almost half the repetition period, as expected for waves bouncing back and forth between the two hemispheres.

Two techniques have been used in the past to qualitatively and quantitatively evaluate the similarities and differences of signals received in conjugate areas. The first one is illustrated in Figure 2.11 (Tepley, 1964). Transparencies of the f-t diagrams obtained for the two signals are superposed and shifted in time until one gets the appearance of a unique signal. In that figure the h.m emission was recorded on two islands situated in the Pacific Ocean at approximately 23° in latitude and 260° in longitude (both geomagnetic). In the

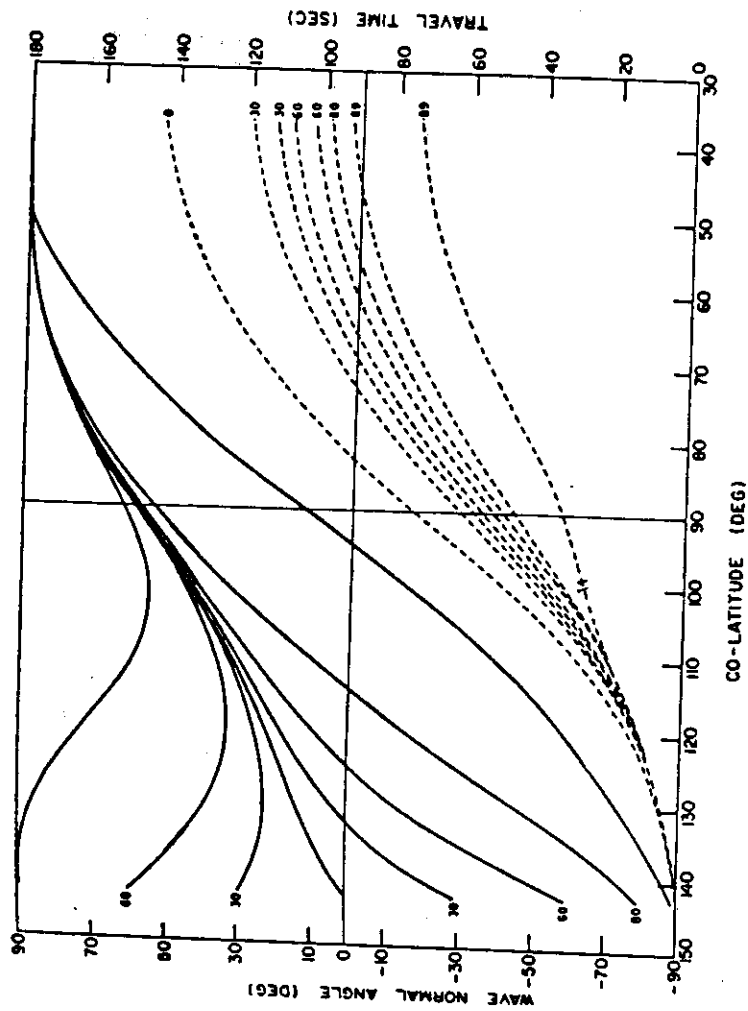
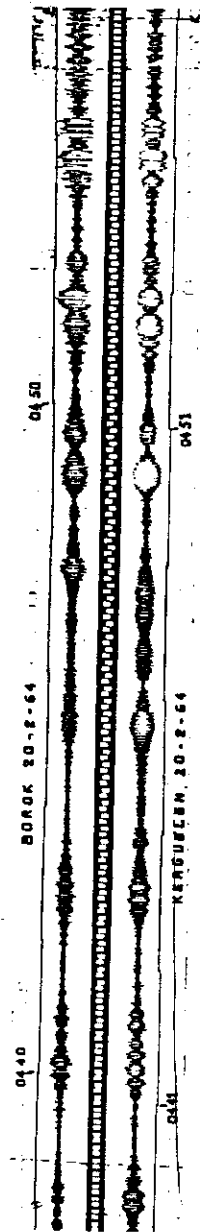
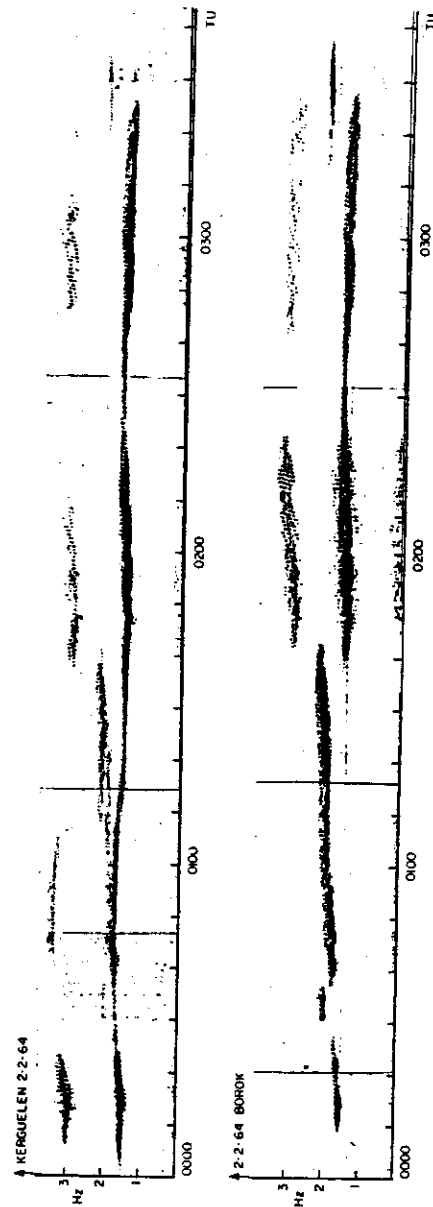


Fig. 2.9. Wave normal angle (solid lines) and travel time (dotted lines) along the ray path, as a function of colatitude, for different initial wave normal angles. The ray is assumed to start in the southern hemisphere, on an $L = 5$ magnetic field at an altitude of 5000 km. The frequency is 1 Hz. A magnetic model for the electron density profile has been assumed with $N_0(L=5) = 100 \text{ cm}^{-3}$ (after Kitamura and Jacobs, 1968)



Amplitude time displays obtained from the magnetic tape.

This is an example of the method described in section 5.1. One can see that the two patterns are not exactly shifted by half the repetition period. In this case, the signal at Kerguelen is delayed by 80 sec and 56 sec later there appears at Borok another signal of different shape.



Sonagrams from Borok and Kerguelen.

The similarity of the two signals received at the two stations is a very striking one. Nevertheless the relative intensity of each frequency component is sometimes different (for instance between 0100 and 0140).

Fig. 2.10. Gendrin and Troitskaya, Radio Sci., 69D, 1107, 1965

17 FEB 1963, 1347-1423 GMT

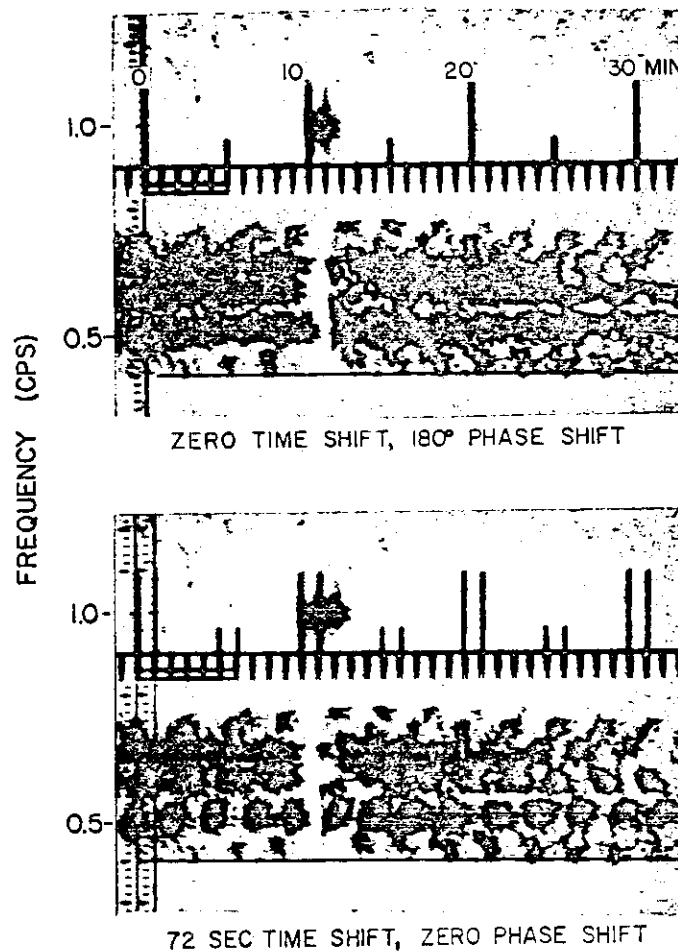


Fig. 2.11 Illustration of conjugate-point 180° fine-structure phase shift. The transparency overlay technique for measurement of phase shift is shown. The data sample is taken from the event shown in Figure 2. In the top photograph is a superposition of transparencies from Kauai and Tongatapu for the 35-min time interval indicated. The photograph includes an accurate frequency-time scale which actually consists of two superimposed identical frequency-time scales. Note the over-all darkness of the hm-emission bands, and in particular note that the band at 0.5 cps appears as a dark line. Compare this photograph with the lower one, which was obtained by shifting the Kauai transparency to the left a distance equivalent to a time interval of 72 sec. On the lower picture the emission bands are lighter, and the band at 0.5 cps appears as a series of equally separated dark spots. Note also the change in appearance of the time-scale which now appears as two scales separated by 72 sec. The isolated structural element above the scale at about 11 minutes is an hourly calibration signal which occurs at the same time at both stations. Thus it appears as a single signal in the top photograph, but becomes 'doubled' in the lower picture.

Tepley, J. G. R., 69, 2273, 1964.

second method the envelopes of the signals recorded at the two stations are correlated (Gendrin and Troitskaya, 1964). For an ideal case the correlation function should be equal to -1 for zero time-lag and it should reach the value of +1 for a time equal to $\pm T/2$. Figure 2.12 shows that this is not the case. Differences of spectral densities in different frequency ranges is the cause of this poor correlation, because a non filtered signal was used. However it is clear that there is a time shift τ of the order of $T/2$ between the two signals, although the difference between τ and $T/2$ exceeds the experimental errors, a discrepancy which has not yet received a satisfactory explanation.

A more recent technique consists of measuring the coherency function between the two signals themselves and not between their envelopes. If the two signals are shifted by the right amount of time, the phase of this coherency function is constant over the whole signal bandwidth. Otherwise this phase is an increasing or decreasing function of frequency. One adjusts the time shift until one obtains a constant phase*. Figure 2.13 shows for instance that the time delay between two signals recorded at stations situated in the same hemisphere and separated by ~ 500 km is of the order of 1.7 s. Between two conjugate stations this time delay is of the order of 95 s (Glangaud et al, 1980). The same technique has been applied (Figure 2.14) in order to compute the time delay of ULF signals detected in the equatorial region of the magnetosphere on board the GEOS spacecraft and at its conjugate point in Iceland (Gendrin et al, 1978). The time delays which are measured at this high L-value ($L \sim 6.7$) correspond to very long repetition periods ($T \sim 5-6$ mn).

As far as the polarization of Pc 1's is concerned observations made on the ground in conjugate areas have not given results in complete agreement with the simple picture of a lefthand wave propagating more or less along a given field line in the same mode (Gendrin et al., 1966).

* The advantage of this technique is that it works for signals having a wide frequency band and no apparent structure.

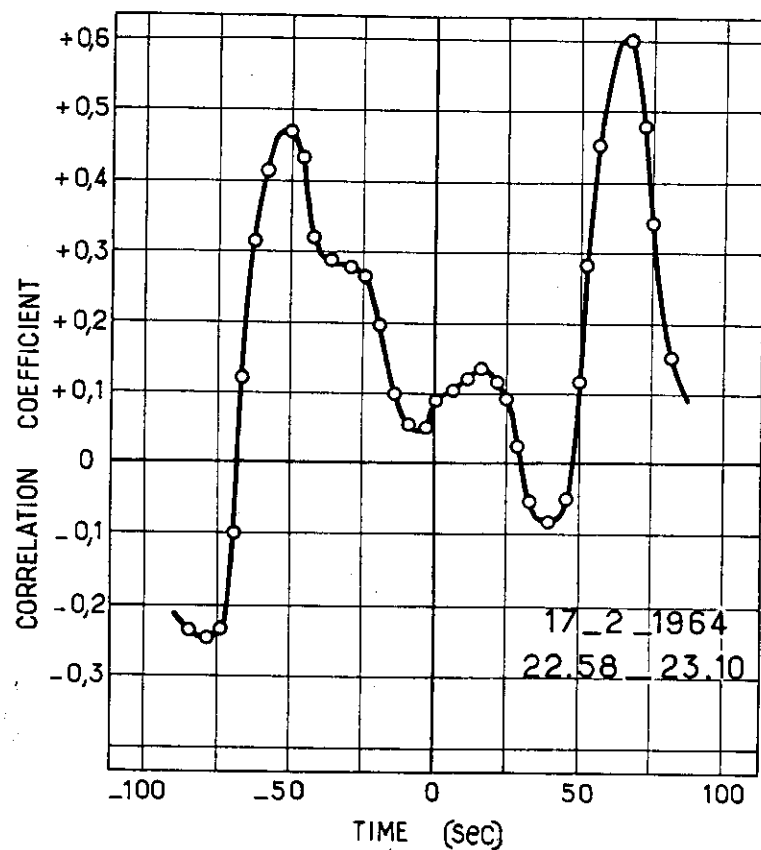


FIGURE 2.12. Correlation function of the envelopes of signals received at Borok and Kerguelen.

The two maxima do not have the same amplitude and are not symmetric around the value $\Delta t = 0$. The correlation function being taken between $K(t)$ and $B(t + t)$, and the greatest maximum occurring for $\Delta t = +70$ sec, it is better to say that the signal appears at Kerguelen 70 sec after its appearance at Borok than to say that it appears at Borok 50 sec after its appearance at Kerguelen. This is often the case (see fig. 12).

GLANGEAUD ET AL.: CROSS-SPECTRAL ANALYSIS OF PC I
J.G.R., 85, 4115, 1980

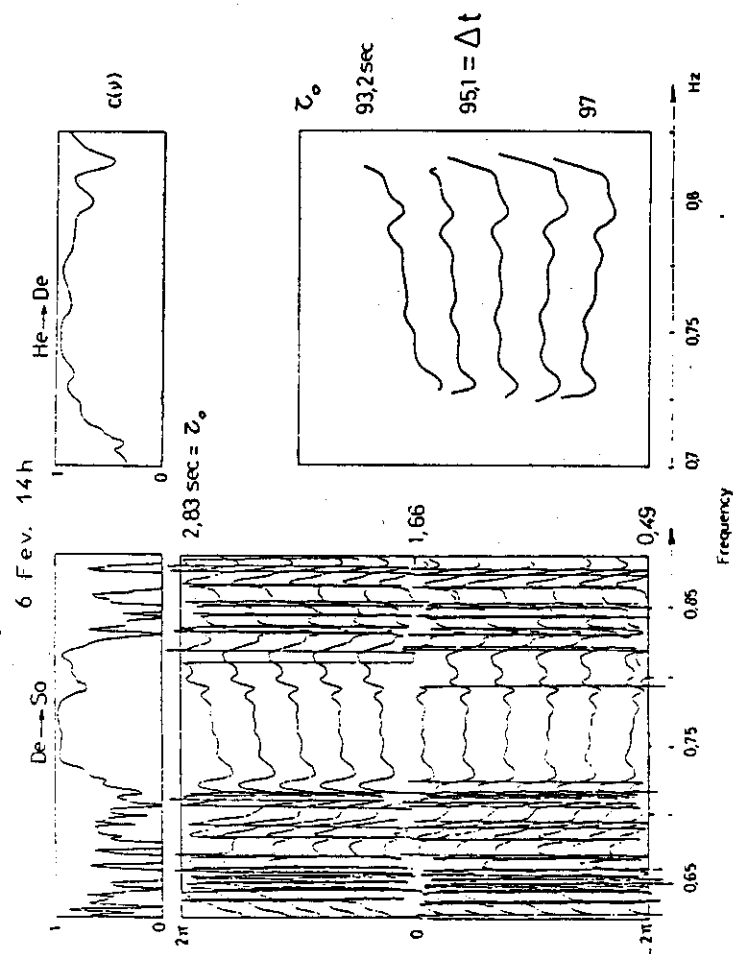


Fig 2 13. Determination of time delay in the same hemisphere (De-So) and between conjugate points (He-De). The different curves correspond to various artificial delays Δt . In the upper part of the figure the modulus of the coherency coefficient is also represented. $N = 4.5$.

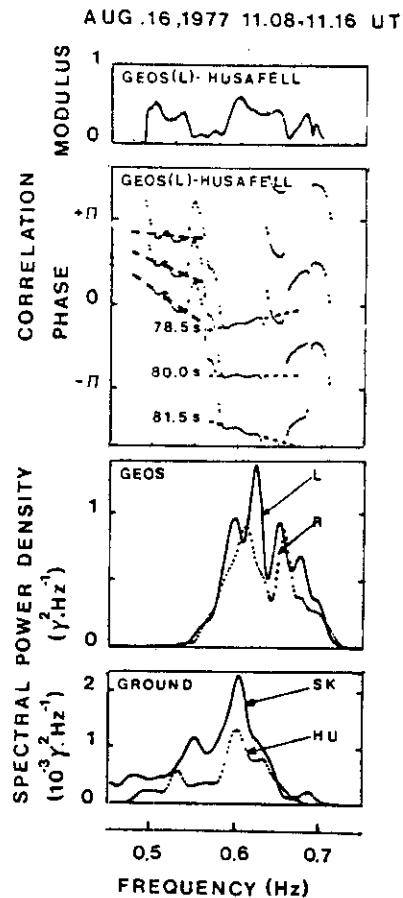


Fig. 2.14. Coherency analysis of ULF signals. From top to bottom: modulus of the coherency function between the GEOS left hand mode and the Husafell X component; phase of this coherency function; autospectra of GEOS left hand right hand modes; autospectra of the X components recorded at Skibotn and Husafell.

Gendrin et al., *Space Sci. Rev.*, 22, 433, 1978

If this situation were always occurring one should always observe a wave vector rotating in the counterclockwise direction (CCW, as seen from above) in the northern hemisphere and a clockwise rotation (CW) in the southern one (Figure 2.15). Such a configuration is often observed (Figure 2.16, left) but the reverse configuration, which corresponds to a right-hand wave, is also observed (Figure 2.16, right).

The RH characteristic of the wave may be an intrinsic property (the wave being RH polarized along its whole trajectory) or it may be the consequence of a more localized effect. The first hypothesis is not very likely since RH waves are not guided along the magnetic field lines (see Section 2.2.1); moreover there is no mechanism which one could think of, presently, to explain their generation in the equatorial region*. Consequently the wave must be generated in the LH mode; it must propagate in this mode for a reasonable fraction of the distance along the field line in order to be guided; then it could be coupled with an RH wave. Two possible coupling mechanisms are: a) the one which occurs in the ionosphere (see below) and b) the one which is due to the presence of an heavier ion, such as He^+ (see Section 2.4).

2.2.3. The role of the ionosphere

As for long-period pulsations (LPP) the ionosphere modifies the characteristics of the ULF waves before they reach the ground. There are two aspects in the role of the ionosphere on propagation in this frequency range.

A first aspect concerns the vertical propagation of the wave. At their arrival onto the ionosphere, the waves are partially reflected, partially absorbed and partially transmitted to the ground. The ionospheric ...

* The most favoured generation mechanism (cyclotron resonance with energetic protons) leads to the generation of an LH (respectively RH) wave if the perpendicular temperature T_{\perp} of the proton distribution is larger (respectively lower) than its parallel temperature T_{\parallel} . Both the theory of proton injection into the equatorial magnetosphere and experimental measurements on board spacecraft show that $T_{\perp}/T_{\parallel} > 1$, so that only LH waves can be generated. However if the protons do have a small bulk velocity, it is possible to generate RH waves (section 2.3.7).

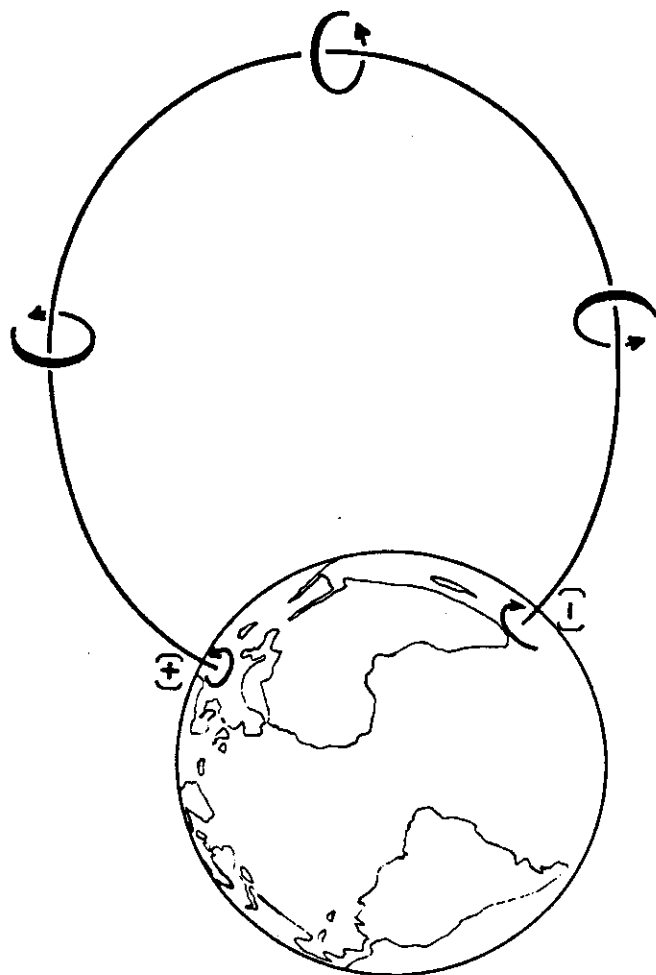
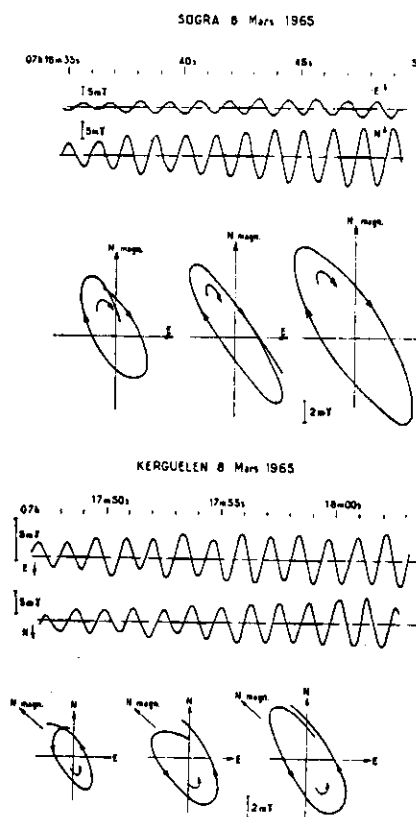


Fig. 2.15. Sens de rotation observé en deux points conjugués, pour une onde se propageant d'un hémisphère à l'autre dans le mode polarisé circulairement à gauche (mode anisotrope).

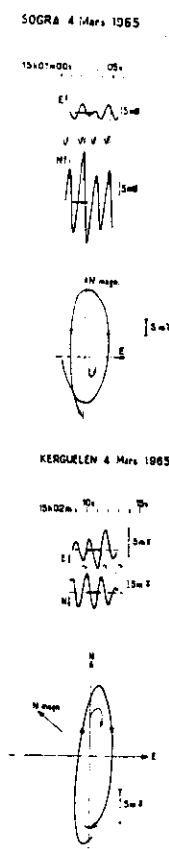
Gendrin et al., Ann. Geophys., 22, 329, 1966.



a. — Enregistrements analogiques et ellipses de polarisation pour un cas simple.

Pour cet événement, le sens de rotation (qui se conserve au cours du temps) est positif à Kerguelen, et négatif à Sogra. On a tenu compte du décalage en temps correspondant à la propagation d'un hémisphère à l'autre.

Gendrin et al., Ann. Geophys., 22, 329, 1966.



b. — Enregistrements analogiques et ellipses de polarisation pour un cas simple.

Pour cet événement le sens de rotation (qui se conserve au cours du temps) est négatif à Kerguelen et positif à Sogra.

Voir le sonagramme correspondant sur la figure 4.

Fig. 2.16.

The ionospheric transfer functions (which take into account all these effects*) are much different for the L mode and the R mode. They also much depend on the ionospheric characteristics (electron content, inclination of the DC magnetic field). Consequently the intensity of the field which is detected on the ground will depend on the observing conditions (day or night, sunspot minimum or sunspot maximum, high latitudes or low latitudes). The observed polarization will also depend on these conditions, even if the original polarization remains identical. These effects have the same origin as the ones which occur for LPP's. However, because the frequency is much larger in that case, theories which have been described in Chapter 1 cannot be applied. The ionosphere cannot be considered as a thin layer, the scale heights being not negligible with respect to the wavelength. Another difference is that waves can be considered as plane waves ($\partial/\partial x = \partial/\partial y = 0$). Besides the wavelengths being much shorter than the length of the field line one may apply Descartes-Snell's laws at the entrance into the ionosphere. The index of refraction being very large (see Figure 2.6) and the ionosphere being horizontally stratified, the wave normal becomes immediately vertical so that only vertical incidence has to be considered..

A second aspect is related to the horizontal propagation of these waves, which is made possible because of the existence of a sort of wave-guide around the ionospheric F_2 peak for these frequencies. At the F_2 peak altitude, the Alfvén velocity passes through a maximum ($V_A \sim 250 \text{ km.s}^{-1}$ for $f_{pe} \sim 6 \text{ MHz}$, $f_{ci} \sim 30 \text{ Hz}$ **). Above and below the height of this maximum, the Alfvén velocity presents important vertical gradients which play the role of partial reflectors. The width of this cavity is of the order of the wavelength (at 1 Hz, $\lambda \sim 250 \text{ km}$ for the same parameters). Waves can therefore be guided horizontally as in a classical wave guide. The names which such a 'guide' or 'cavity' have received are 'Sub-Magnetospheric-Ionospheric Guide' (SMIG) or 'Sub-Magnetospheric-Ionospheric Cavity' (SMIC)***. Because ...

* Plus the ground reflection which doubles the intensity of the magnetic field.

** At these altitudes, the dominant ion is O^+ .

*** This cavity must not be confused with the Earth-Ionosphere-Cavity which is at the origin of the Schumann resonances at higher frequencies ($f_n \sim 8, 14, 21, \dots \text{ Hz}$).

Because the waves can propagate horizontally, they can be detected at far distances ($\sim 2000 \text{ km}$) from their entry points.

Starting first by the vertical propagation it is worth recalling the main relevant properties of the ionosphere. Besides of the variation of the Alfvén velocity with height, the ionosphere is characterized by varying collision frequencies which are the dominant factors in its transmission properties. Three distinct regions can be defined in the ionosphere (Figure 2.17). They are characterized by the relative magnitude of ω (the wave frequency), ν_i the ion-neutral collision frequency) and ω_{ci} (the ion gyrofrequency) Quoting Jacobs (1970), these regions are :

- " a) The Hall region. This is the region in which the inequality $\omega \ll \omega_{ci} < \nu_i$ is satisfied, i.e. where the collision frequency is the dominant frequency.
- " It lies between about 80 and 130 km. The boundaries of this region are independent of ω provided that $\omega \ll \omega_{ci}$.
- " b) The transition region. This region is defined by the inequality $\omega < \nu_i < \omega_{ci}$ and lies between about 130 and 350 km, the location of the upper boundary depending on the wave angular frequency .
- " c) The Alfvén region. This is the region in which the inequality $\nu_i < \omega \ll \omega_{ci}$ is satisfied. It lies therefore above about 350 km and is assumed to be semi-infinite in extent. In it the disturbance propagates as a pure Alfvén wave.

" The actual functional form of the frequency enters only in the transition region. For both L and R modes of propagation the Alfvén region is a lossless and non dispersive medium. On the other hand the Hall region appears quite different for the two modes. For the R mode*, the index of refraction is real and the mode thus propagates without attenuation

* For a certain time there has been some confusion about the definition of the R and L modes, as far as the ionospheric effects are concerned. In the following works (and probably others), what is called R-mode is in fact the L-mode and vice-versa : Karplus et al., 1962 ; Jacobs and Watanabe, 1962 ; Akasofu, 1965 ; Field and Greifinger, 1965 ; Gendrin, 1967 a, b ; Jacobs, 1970. The situation has been clarified by Campbell (1967) and the review by Gendrin (1970) contains the correct definitions. The present quotation from Jacobs (1970, p. 77) has been corrected accordingly.

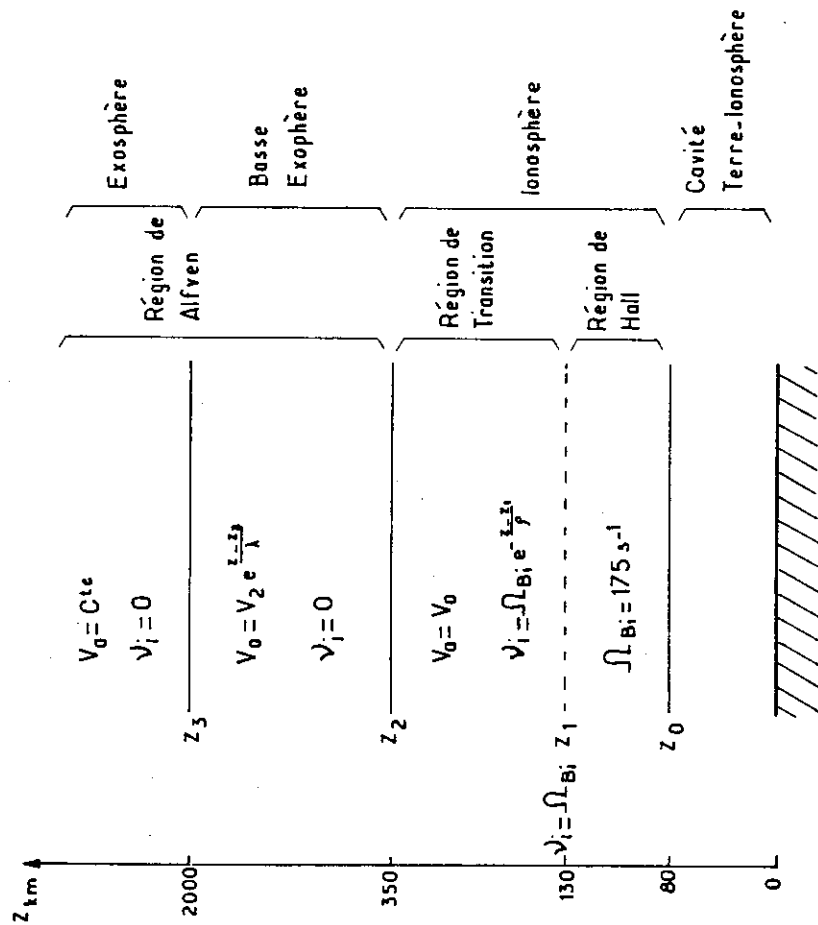


Fig. 2.17. Les différentes régions de l'ionosphère intervenant dans le calcul de la transmission des ondes E.B.F. (D'après FIELD et GREIFINGER, 1965.)

- " (although with dispersion). For the L-mode, the index of refraction is
- " purely imaginary and the mode is thus evanescent. Because of this, the
- " transmission coefficient for the L-mode drops off very rapidly with
- " frequency and it is mainly the R mode that gets through the ionosphere.
- " In the transition region the index of refraction of both modes is complex
- " so that in this region each mode undergoes both attenuation and dispersion."

These properties are easily demonstrated* by considering the phase velocity expressions given in the Appendix which are modified in order to include the effects of collisions. An important consequence of these expressions is that, except at the geomagnetic pole, the propagation is quasi-transverse (QT) at high altitudes and QL at low altitudes. Once this is understood it is easy to follow the apparent complexity of the changes which occur in the wave propagation and polarization characteristics. Let us examine this point.

The QT condition, which one can deduce from (A.26) in which one introduces the modifications defined in Section A.5 of the Appendix A, becomes :

$$\left(\frac{\sin^2 \theta}{2 \cos \theta} \right)^2 \gg \left(\frac{\omega - i\nu_i}{\omega_{ci}} \right)^2 \quad (2.7)$$

At high altitude, $\nu_i \ll \omega \ll \omega_{ci}$ so that this condition is satisfied even for very small values of θ . If $\nu_i = 0$, $f \sim 1$ Hz, $f_{ci} \sim 350$ Hz (which is valid at an altitude of ~ 2000 km at a latitude of 60°) the condition is satisfied as soon as $\theta \gtrsim 2^\circ$. The wave normal being vertical θ is equal to the zenith angle of the magnetic field direction. Therefore, except in the near vicinity of the geomagnetic pole, ULF waves propagate in the upper ionosphere in the QT approximation. Equations (A.27), (A.28) and (A.45), modified by the introduction of the collision frequency become

* analytically and not as the result of numerical computations.

$$\begin{aligned}
 W_+^2 &= \frac{V_A^2}{1 - i\nu_i/\omega} \\
 W_-^2 &= \frac{V_A^2 \cos\theta}{1 - i\nu_i/\omega} \\
 p_+ &= \frac{i \sin^2\theta}{2\cos\theta} \cdot \frac{\omega_{ci}}{\omega - i\nu_i} \\
 p_- &= \frac{2i \cos\theta}{\sin^2\theta} \cdot \frac{\omega - i\nu_i}{\omega_{ci}}
 \end{aligned} \quad (2.8)$$

In the limit $\nu_i \ll \omega$, the waves are non dispersive and the polarization is almost linear. On the contrary in the Hall region, the QL approximation becomes valid because of the large values of ν_i/ω and ν_i/ω_{ci} . Equation (A.30), also modified by the introduction of collision terms becomes :

$$W_{\pm}^2 = V_A^2 \frac{[1 \pm (\omega - i\nu_i)/\omega_{ci}]}{1 - i\nu_i/\omega} \quad (2.9)$$

which leads to

$$W_{\pm}^2 = \pm V_A^2 \frac{\omega}{\omega_{ci}} \quad (2.10)$$

whereas the polarization factor keeps the same value

$$p_{\pm} = \mp i \quad (2.11).$$

In the Hall region, the L mode (W_-) is evanescent and only the R mode can propagate with an RH circular polarization. However, it is in this same region that there is a strong coupling between the two modes, when the zenith angle of the geomagnetic field is different from zero.

The ionospheric transfer function is therefore defined by a matrix (Altman and Cory, 1969 a, b, ; Altman and Fijalkow, 1969).

$$\begin{pmatrix} B_L^{(2)} \\ B_R^{(2)} \end{pmatrix} = \begin{pmatrix} T_{LL} & T_{RL} \\ T_{LR} & T_{RR} \end{pmatrix} \begin{pmatrix} B_L^{(1)} \\ B_R^{(1)} \end{pmatrix}$$

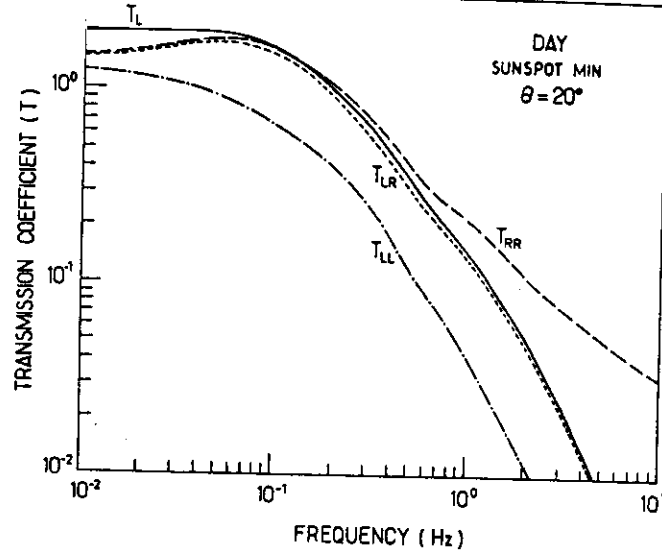
where $B_L^{(2)}$ and $B_R^{(2)}$ are the two circularly components of the wave magnetic field detected at the ground and $B_L^{(1)}$ and $B_R^{(1)}$ are the equivalent quantities above the ionosphere. Computations show that T_{RL} is very small so that an incident R-wave is detected at the ground almost as a pure R-wave. The values of the three other coefficients, as well as the value of $T_L = T_{LL} + T_{LR}$ which corresponds to the total transmission of an L-wave regardless of its final polarization, are given as a function of frequency, for a magnetic dip angle of 20° on Figure 2.18. From this figure, one may conclude that

a. The ionosphere is more transparent during the night than during the day.

b. It is more transparent for R-waves than for L-waves.

c. At high frequencies ($f > 1$ Hz) and during the day a wave polarized in the R-mode at the top of the ionosphere may be observed at the ground with an almost pure RH polarization ($T_{LL}/T_{LR} < 4$), this polarization change being negligible during the night.

The consequences of such effects on the polarization of Pc 1 events have been studied in detail by Perraut (1974). They partially explain the possibility of detecting R waves on the ground even if they are generated in the L-mode inside the magnetosphere. The diurnal variation of the occurrence of the events and the relationships between the observed polarization and their central frequency are also interpreted. However



Day-time transmission coefficients versus frequency for $\theta = 20^\circ$
(after Altman and Fijalkow, 1969).

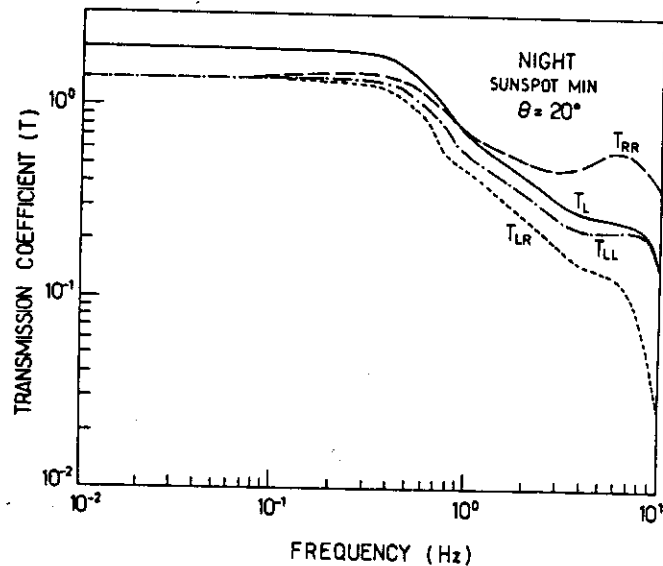


Fig. 2.18. Night-time transmission coefficients vs. frequency for $\theta = 20^\circ$
(after Altman and Fijalkow, 1969).

a) The observation of events consisting of two simultaneous emissions of waves with slightly different frequencies but with opposite polarizations cannot be explained by such effects, the frequency difference between the two emissions being rather small : $2(f_2 - f_1) / (f_2 + f_1) \lesssim 0.4$. One has to consider the possibility of the simultaneous generation of waves in the two modes (Perraut, 1974 ; Gendrin, 1981 a).

b) The coupling between the R- and L-modes may occur in the magnetosphere, well before the wave reaches the ionosphere (Section 2.4).

As far as the horizontal propagation of ULF waves in the SMIC is concerned the reader is referred to the (rather old) review by Gendrin (1970) and to the lectures which will be given by Pr. D.M. Walker.

2.3. Generation mechanisms

As discussed in the previous Section, the study of the frequency-time structure of Pc 1 emissions led to the conclusion that such phenomena were associated with waves propagating along field lines crossing the equatorial plane at large geocentric distances. In this region of the magnetosphere, energetic particles are continuously injected and their distribution in pitch angle is highly anisotropic. The simultaneous existence of cold plasma (which supports the wave propagation) and of hot anisotropic particles (which are far from thermodynamic equilibrium) is a favourable condition for gyroresonant interactions to take place. The general theory of such interactions is presented in Appendix B. In this section, we will restrict ourselves to the application of these principles to the interaction of protons with left-handed ULF waves with frequencies smaller than the proton gyrofrequency*. As far as these interactions are concerned the main results of the theory may be summarized as follows :

* A few words will also be said on other interactions taking place in this frequency range (Section 2.3.7).

1. For bi-maxwellian distributions the growth rate, γ' of the instability is given by :

$$\frac{\gamma'}{\omega_{ci}} = \sqrt{\pi} \frac{n_h}{n_c} \frac{(1-x)}{x(2-x)} \cdot [A - (A+1)x] \sqrt{\gamma_2} \exp(-\gamma_2) \quad (2.12)$$

where the different quantities are defined in the Appendix (section B.3) and where $\gamma' = -\gamma$. Equation (2.12) is valid only when $n_h \ll n_c$.

2. The frequency of the waves which may be amplified ($\gamma' > 0$) verifies :

$$f = x f_{ci} < f_c \quad (2.13)$$

with

$$f_c = f_{ci} \cdot A / (A+1) \quad (2.14)$$

3. The growth rate at a given frequency is a function of the anisotropy A , and of the ratio of the thermal parallel energy, $U_{//}$ to the Alfvén velocity, v_a . Both quantities characterize the proton distribution function.

4. The growth rate increases when the hot particle density, n_h increases. But the variation of γ' with the cold plasma density, n_c is not so simple. There exists an optimum cold plasma density, n_c^* for which the growth rate is maximized.

5. The quasi-linear reaction of the waves upon the energetic particles lead to the diffusion of these particles in pitch angle (and energy) and to their subsequent precipitation into the ionosphere.

The detailed application of these general properties to ULF wave generation is made in the following sub-sections.

2.3.1. Variation of the growth rate with the characteristic parameters of the distribution function

The growth rate defined by equation (2.12) can be plotted as a function of x for different values of the anisotropy A , $U_{//} / v_a$ being kept constant, or for different values of $U_{//} / v_a$, the anisotropy being kept constant (Gendrin et al., 1971). This is done on Figures 2.19 and 2.20.

Figure 2.19 shows that γ' is positive (i.e. waves are amplified) for frequencies smaller than the critical frequency defined by equation (2.14). When A increases the frequency range of the instability increases. At a given frequency, the absolute value of the growth rate also increases. The frequency f_m for which γ' is maximum is not much dependent on the anisotropy.

Figure 2.20 shows that the growth rate increases when $U_{//} / v_a$ increases. Simultaneously f_m decreases. Let us call V_M the parallel velocity of the particles which resonate at the frequency f_m and $E_M = m V_M^2 / 2$ the corresponding energy. Gendrin et al. (1971) have shown (see their Figure 2.8) that, for values of A larger than ~ 1 , V_M does not depend much on the anisotropy and that, for values of $U_{//} / v_a$ larger than ~ 2 , V_M is approximately equal to the velocity $U_{//}$ which characterizes the distribution function with respect to $v_{//}$. Since $\langle v_{//}^2 \rangle = U_{//}^2 / 2$ (equation (B.29)), $V_M \sim \sqrt{2} \langle v_{//}^2 \rangle^{1/2}$, i.e.

$$E_M \sim 2 E_{//} \quad (2.15)$$

where $E_{//} = m \langle v_{//}^2 \rangle / 2$ is the mean parallel energy of the distribution function. This relation is interesting since, from the measurement of f_m , one can deduce the characteristic parallel energy of the interacting protons provided one knows n_c and B , the two parameters which allow to compute V_M once f_m is known*. It is not necessary to know the value of A for making this computation.

* These two parameters are evaluated from the measurement of the dispersive properties of the waves (see below).

Gendrin et al., J.A.T.P., 19, 165, 1971.

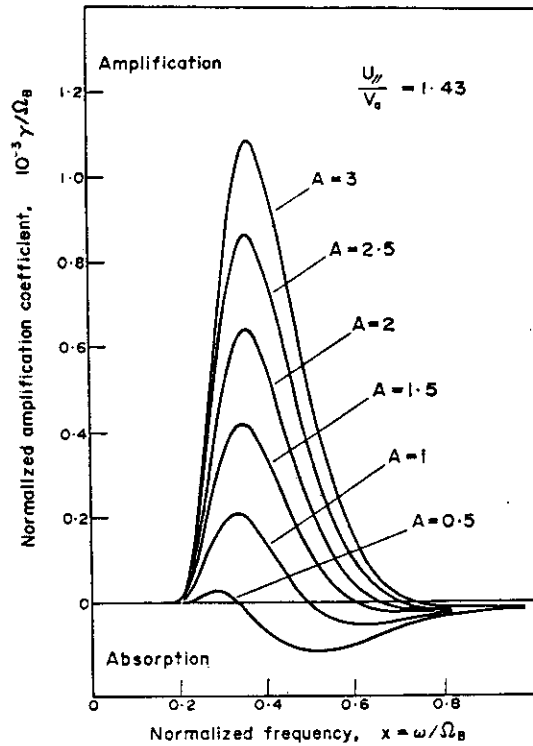


FIG. 2.19. AMPLIFICATION COEFFICIENT AS A FUNCTION OF FREQUENCY (BOTH QUANTITIES BEING NORMALIZED TO THE PROTON GYROFREQUENCY), FOR DIFFERENT VALUES OF THE ANISOTROPY COEFFICIENT.

The mean parallel velocity (U_{\parallel}) of the hot particles is the same. For increasing anisotropies, the bandwidth of the emission and the amplitude of the growth rate increase, but the frequency for which maximum amplification occurs remains more or less the same.

Gendrin et al., J.A.T.P., 19, 165, 1975.
WAVE PACKET PROPAGATION IN AMPLIFYING MEDIUM AND Pc 1 EVENTS

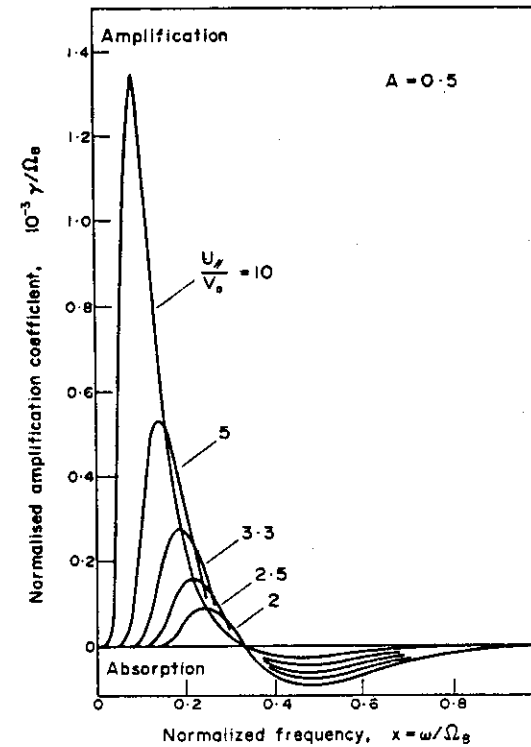


FIG. 2.20. AMPLIFICATION COEFFICIENT AS A FUNCTION OF FREQUENCY (BOTH QUANTITIES BEING NORMALIZED TO THE PROTON GYROFREQUENCY), FOR DIFFERENT VALUES OF THE MEAN PARALLEL VELOCITY OF THE HOT PARTICLES.

The anisotropy has been chosen equal to 0.5, so that amplification can occur for frequencies smaller than $F_B/3$, whatever U_{\parallel} is. The frequency for which maximum amplification occurs decreases with increasing parallel velocity.

TABLE 2.2

MODELLING OF ION-CYCLOTRON INTERACTIONS IN THE MAGNETOSPHERE

2.3.2. Spatial variation of the amplification

Different attempts have been made to model the ULF-proton interaction in the whole magnetosphere in order to predict the frequency which corresponds to the maximum amplification and to evaluate this amplification. The variation of the growth rate, γ' as a function of latitude along a given field line (Liemohn, 1967) or as a function of longitude at a given radial distance in the equatorial plane (Solomon, 1975 ; Lin and Parks, 1976) has been studied. Three attempts have been made (Criswell, 1960 ; Perraut et al., 1976 ; Kaye et al., 1979) to compute the field-line integrated growth rate

$$\Gamma = \int \frac{\gamma' ds}{v_g} \quad (2.16)$$

as a function of both longitude (i.e. local time) and radial distance of the apex of the field line (i.e. L).

Such modellings are based upon assumptions concerning the cold plasma density variation along the field lines and in the equatorial plane. Specific velocity distributions for the energetic protons must also be assumed and care must be taken of their variation with latitude, longitude or radial distance. The parameters which were used in these modelling exercises are listed in Table 2.2. Some of the obtained results are described below.

Liemohn (1967) has considered the latitudinal variation of the spatial growth rate $k_i = -\gamma/v_g$ as a function of latitude, λ (Figure 2.21). Since the anisotropy factor m of the proton distribution function is equal to 2, the critical frequency $f_c = 0.5 f_{ci}$ (equations (B.26) and (B.32)). Therefore only waves with frequencies smaller than half the equatorial value of f_{ci} can be amplified along the whole field line. Waves of higher frequencies are absorbed at the equator but they are amplified above a certain latitude

AUTHOR	OBJECTIVES	COLD PLASMA DENSITY MODEL	ENERGETIC PROTON DISTRIBUTION FUNCTION
<u>Liemohn</u> (1967)	Variation of k_i as a function of latitude on a given field line ($L = 4$)	$n_c \propto \exp [C/r]$	$\propto E^{-n} \sin^m \alpha$
<u>Criswell</u> (1969)	Variation of $\Gamma = \int \gamma' ds/v_g$ for different frequencies on different field lines	along the field line : $n_c \propto \exp [C_1/r]$ inside the plasmasphere, $n_c \propto (C_2/r)^n$ in the plasmatrough equatorial profile : deduced from Carpenter's measurements ⁽¹⁾	$\propto E^{-n} \sin^m \alpha$
<u>Solomon</u> (1975)	Variation of γ' and $f_{\gamma' \max}$ as a function of time after an injection for different longitudes ($L = 6.6$)	$n_c = \text{constant}$	$\propto E^m \exp \left[-\frac{E}{E_0} \right] \sin^{2m} \alpha$
<u>Lin and Parks</u> (1976)	ditto	$n_c = \text{constant}$ or $n_c = \text{constant in longitude but varying with time}$	$\propto V^{-1/2} \exp \left[-\frac{V}{V_0} \right] \sin^m \alpha$
<u>Perraut et al.</u> (1976)	variation of $\Gamma = \int \gamma' ds/v_g$ and of $f_{\gamma' \max}$ as a function of L for night, noon and dusk sectors, taking into account the variation of T_\perp and T_\parallel due to inward displacement	along the field line : $n_c \propto B$ equatorial profile : adapted from Chappell's measurements ⁽²⁾	$\propto \exp \left[-\frac{V_\perp^2}{U_\perp^2} - \frac{V_\parallel^2}{U_\parallel^2} \right]$ (initial anisotropy at $L = 7 : A = 0.5$)
<u>Kaye et al.</u> (1979)	Variation of γ' and Γ as a function of L and local time taking into account the full trajectories of protons in a magnetospheric electric field model.	along the field line : $n = \text{constant}$ equatorial profile : $0.5(10/L)^4$ outside the plasmasphere $100 (6/L)^4$ inside the plasmasphere	$\propto \exp -\frac{E}{E_0}$ and $\propto \left(1 + \frac{E}{E_0} \right)^{-m}$ (isotropic at the injection boundary : $L = 10$)

(1) CARPENTER, D.L. J. Geophys. Res., 71, 693, 1966

(2) CHAPPELL, C.R., Rev. Geophys. Space Phys., 10, 951, 1972.

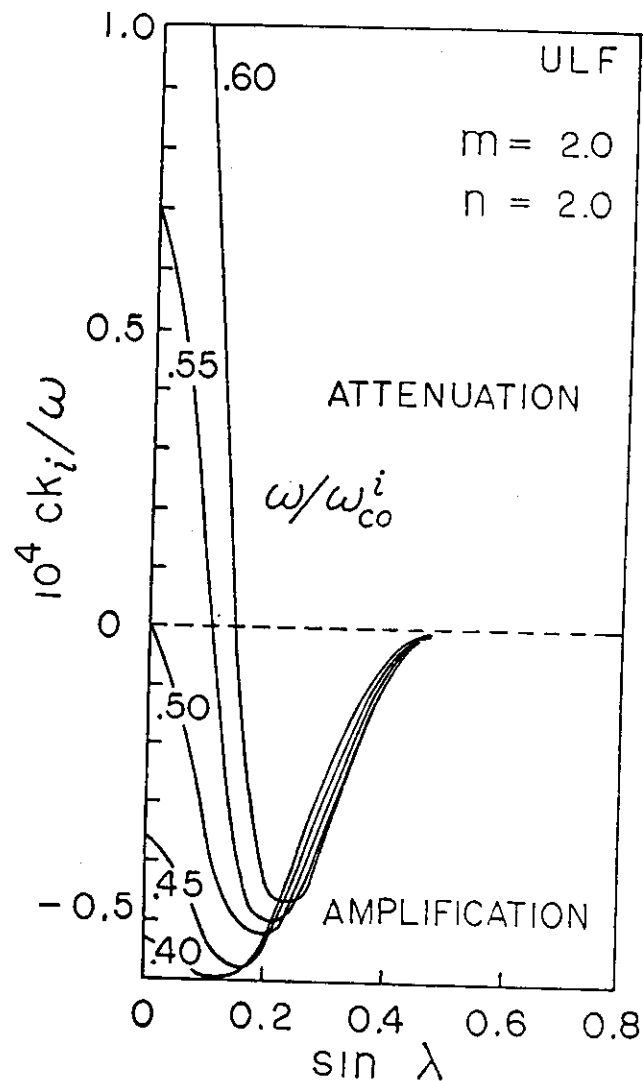


Fig. 2.21. ULF amplitude exponent k_i as a function of geomagnetic latitude λ .

Liemohn, J.G.R., 72, 39, 1967.

since the factor $[A - (A+1)x]$ increases with λ . Because of the mirroring effect the number of energetic particles that are present at higher latitudes diminishes (n_h decreases) so that there is a latitude at which k_i is maximum. This figure gives an idea of the latitudinal extent of the amplification region* : $\pm 15^\circ$.

Criswell (1969) computed the total amplification Γ for different frequencies as a function of L (Figure 2.22). The right order of magnitude of the amplified frequencies is obtained ($0.2 < f < 1.5$ Hz for $3.5 < L < 6$). The L -value for which Γ is maximum at a given frequency f_0 is a decreasing function of this frequency : higher frequencies have to be observed at lower L -values, for which the repetition period T is shorter. The product $f_0 T$ can be computed and Criswell (1969) has shown that for $\Gamma > 10$, one has

$$130 < f_0 T < 200 \quad (2.17)$$

in reasonable agreement with the observed values of this product (see equation (2.1) and Figure 2.3). Figure 2.22 also shows that the curve $\Gamma_{\max}(L)$ presents a maximum near $L = 3.5$, which corresponds to the latitude where most of the well-structured Pc 1 events are observed, and a minimum near $L = 5$. The further ascent of the $\Gamma_{\max}(L)$ curve near the border of the assumed plasmopause is due to the sharp decrease of n_c which leads to an increase of γ' . We will come back to this point in the next subsection.

A third interesting attempt was made by Solomon (1975) who studied the effect of the differential drift to which protons are submitted on a given L -shell. An injection was assumed to take place at time $t = 0$ in the

* Other arguments, which are based upon the distance along the field line over which particles and waves remain in resonance, help evaluating the length of interaction (see section 2.3.6).

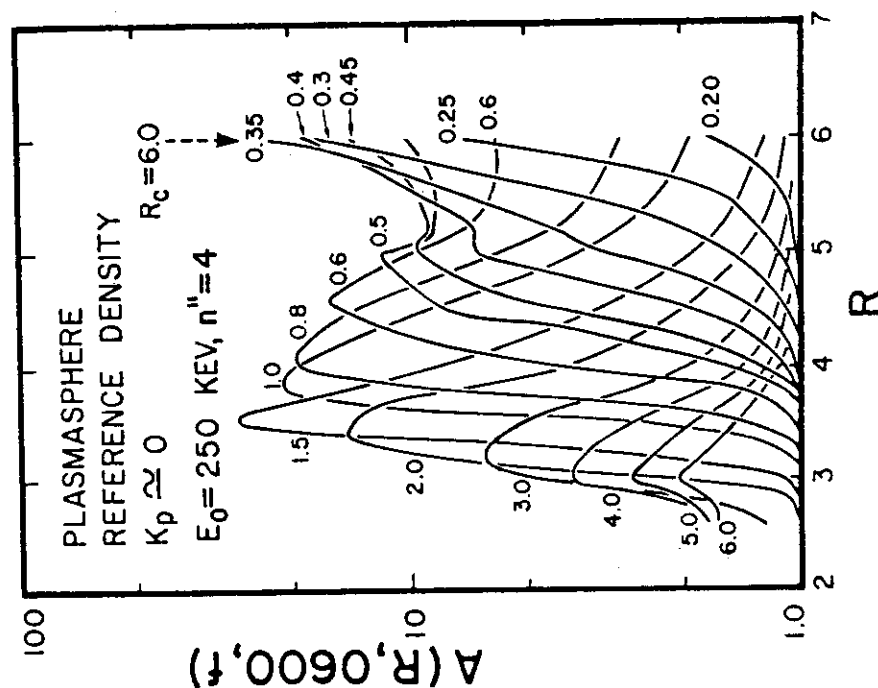


Fig. 2.22. An amplification profile for the quiet time plasmasphere. (After D. R. Criswell)

midnight sector within a range of longitude $\Delta\phi = 30^\circ$. After a certain time the protons arrive in the dusk sector ($\phi = 90^\circ$) but the particles with large pitch angles arrive before the particles with small pitch angles so that the local anisotropy, at the beginning of the event, is larger than the initial anisotropy of the injected particles. Then the anisotropy decreases since only the low pitch angle particles continue to arrive. Similarly, the proton drift velocity being proportional to their energy, high energy particles arrive first and the characteristic energy of the local distribution function at $\phi = 90^\circ$ starts to increase and then decreases. The same is true for the energetic particle density n_h , but the characteristic time of this last variation is longer than the characteristic times of the two first ones (upper part of Figure 2.23). The time variation of these parameters being known it is possible to compute $f_m(t)$ and the associated function $\gamma'_{\max}(t)$. The results are presented on the lower part of Figure 2.23. On this example the maximum growth rate which is observed in the dusk sector is reached some 20 mn after the injection. Its value is $\sim 0.07 \omega_{ci}$ and the corresponding frequency is $\sim \omega_{ci}/4$. The time duration over which γ' changes by one order of magnitude is of the order of one hour. The frequency which corresponds to γ'_{\max} does not change much during the course of an event ($0.22 f_{ci} < f < 0.28 f_{ci}$). These conclusions are in agreement with the first *in situ* observations of Pc 1 waves made on board ATS-1 (Mc Pherron et al., 1972).

Lin and Parks (1976) have followed a similar approach. They computed iso- γ contours in the f - t plane for different longitudes, ϕ and in the ϕ - t plane for different times, t . Results obtained in the first case are reproduced on Figure 2.24. They confirm Solomon's (1975) computations. They also show that the frequency $f_{\gamma_{\max}}$, which is at every longitude a slightly increasing function of time, is almost the same for all longitudes. The growth rate reaches its maximum maximum value some 20 mn after the injection at the longitude $\phi \sim 30^\circ$.

Though interesting they are these theories do not take into account the radial drift of the particles. However this inward displacement, which occurs especially during injection events and which is due to the magnetospheric convection electric field, is as much important as the azimuthal

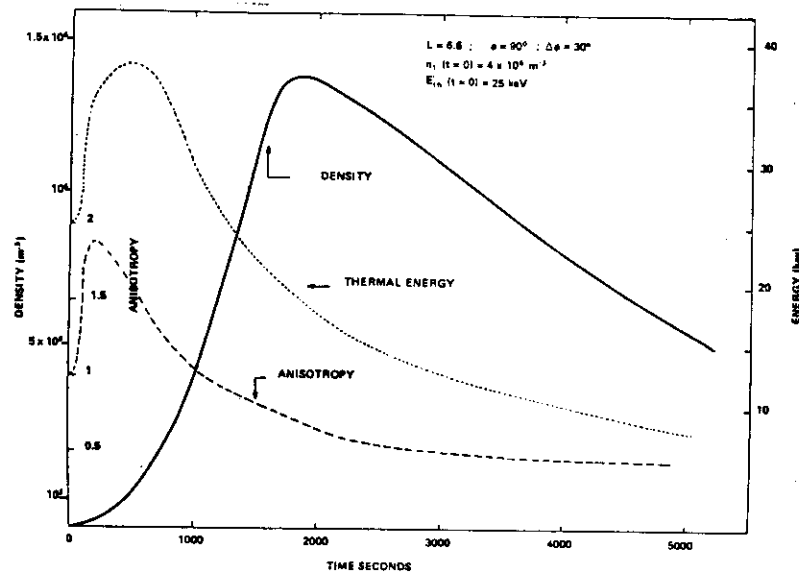


Fig. Plot of the density, the anisotropy and the thermal velocity of the hot protons vs time, for a given ϕ . For the anisotropy, we have fixed $V_R^2 = 2v_{th}^2$.

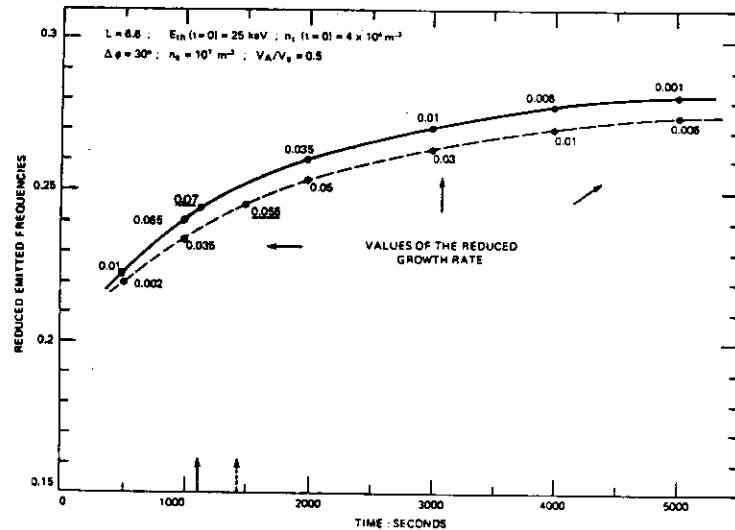


Fig.2.23 Plot of the emitted frequencies for which the growth rate is maximum vs time, for $\phi = 90^\circ$ (solid line) and $\phi = 120^\circ$ (dashed line), and given initial parameters (on top of the curves). The corresponding values of the reduced growth rate ω_i/ω_{ci} are also indicated on the curves.

Solomon, in 'The Magnetospheres of the Earth and Jupiter', D. Reidel, 1975, 153

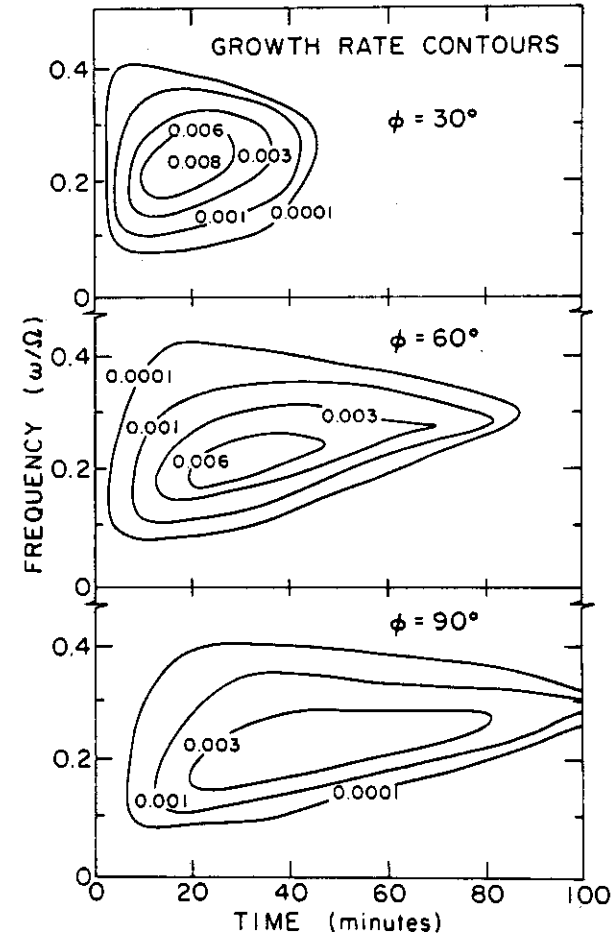


Fig. 2.24. The γ contours in the ω - t plane for three positions in space away from the particle source.

Lin@ Parks, J. C. R., 81, 3919, 1976.

drift, especially for low energy particles. The last modelling attempts which we would like to describe take into account such an effect (Perraut et al., 1976 ; Kaye et al., 1979). However before describing it, the controversial question of the role which is played by the cold plasma density on ULF-proton interactions should be discussed.

2.3.3. Role of the cold plasma density

The in situ observations of protons on board OGO-3 and Explorer 45 have shown that drastic changes occur both in the flux intensity and in the shape of the distribution function when the plasmopause is encountered. The inner edge of the ring current protons ($E \sim 40$ keV) coincides with the plasmopause boundary (Russel and Thorne, 1970 ; Cornwall et al., 1970). At low L-values their pitch angle distributions are rounded with a peak at 90° , indicative of a weak diffusion process, whereas at higher L-values the distributions are flat with an empty loss-cone, indicative of the absence of diffusion, the boundary between the two regimes being situated at higher L-values for higher energies (Williams and Lyons, 1974). These experimental observations have been interpreted as a consequence of gyroresonant interactions between protons and ion cyclotron waves and to the strengthening of these interactions in the presence of an increased cold plasma density. This interpretation is based upon the following arguments.

Because of the existence of a critical frequency above which no interaction can take place, protons which intervene in the interaction must have a parallel velocity which exceeds a certain value, to which corresponds the critical resonant energy, E_c . Replacing x by x_c , as given in equation (2.14), in the equation defining the resonant velocity for protons interacting with LH waves :

$$\frac{v_r}{v_a^+} = \frac{(1-x)^{3/2}}{x} \quad (2.18)$$

one gets

$$E_c = \frac{E_m}{A^2(A+1)} \quad (2.19)$$

where $E_m = (m v_a^{+2}) / 2 = B^2 / 2\mu_0 n_c$ is the Alfvén energy i.e. the magnetic energy per cold particle (see also Table B.2). For a dipolar magnetic field one has

$$E_m = 2.4 \left(\frac{10}{L} \right)^6 \cdot \frac{1}{n_c} \quad (2.20)$$

where E_m is in keV and n_c in cm^{-3} . The associated variation of E_c and A for different values of n_c is represented on Figure 2.25 (Cornwall et al., 1970).

Energetic protons whose (total) energy is smaller than E_c cannot interact with ion/cyclotron waves. Therefore they cannot be diffused in pitch angle : their distribution function is isotropic and the loss-cone is empty. On the contrary protons whose total energy exceeds the critical energy* may interact with ion cyclotron waves. In that case because of quasi-linear effects (see Section 2.2.5), they diffuse in pitch angle towards the loss-cone. Their distribution function is rounded and because of the subsequent precipitation into the atmosphere, their flux is lowered. Due to the variation of n_c and B with L, the Alfvén energy does present a minimum at the inner border of the plasmopause. So does the critical energy.

On Figure (2.26) the variation of E_c with L for two different values of the anisotropy is represented. For the cold plasma density profile which is assumed and for $A = 0.5$, protons with an energy equal to 3 or 30 keV cannot interact with ion cyclotron waves in the outer magnetosphere since $E < E_c$. But as soon as they enter the plasmasphere their energy is larger than E_c and they are able to interact. The boundary between the region where there is no possible interaction and the region where such interactions are possible is at a higher L-value when the energy is higher, in agreement with some experimental measurements (Williams and Lyons, 1974)**. From the measurement of the position of this boundary as a function of E, and assuming a 'typical' value for the anisotropy ($A \sim 0.2$), Williams et al. (1973) have claimed to be able to 'deduce' a cold plasma density profile.

* This is not a sufficient condition. One must have $E_{\parallel} > E_c$.

** However measurements made onboard low-altitude spacecraft give evidence of an opposite variation of the position of the boundary for higher energy particles (Cornwall et al., 1971 b ; Imhof et al., 1977).

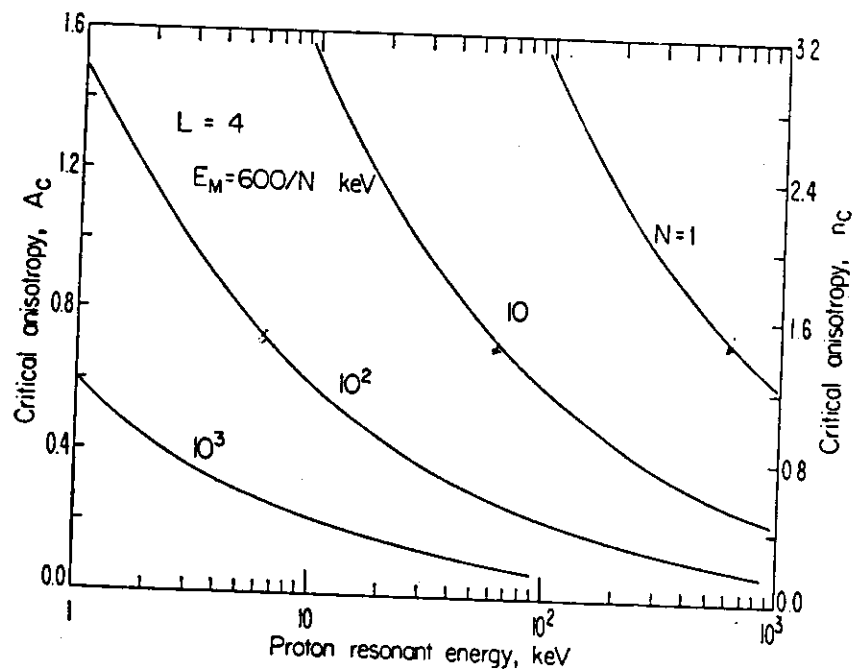


Fig. 2.25. The critical proton pitch angle anisotropy required for ion-cyclotron instability is shown as a function of the proton energy for representative total electron densities in the magnetosphere.

Cornwall et al., JGR, 75, 4699, 1970

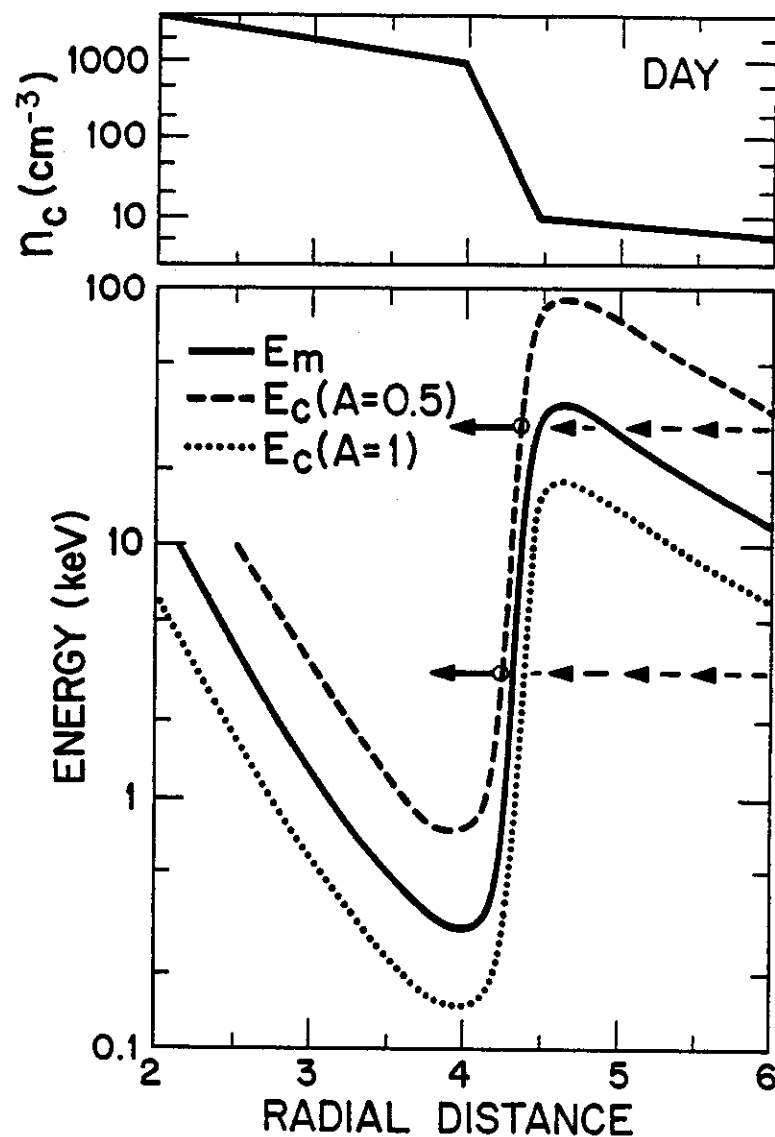


Fig. 2.26 Variation of the Alfvén energy E_m and of the critical resonant energy E_c for the cold plasma density profile which is represented in the upper part of the figure. A dipolar magnetic field is assumed. 30 keV protons can interact with ULF waves ($E > E_c$) at a slightly higher L-value than 3 keV protons.

This simple interpretation has been questioned by Gendrin (1975 a,b) on the basis of both experimental observations and theoretical arguments. The first theoretical difficulty lies in the fact that the anisotropy must be independent of energy for the interpretation to be valid. The second difficulty is that the frequency of the waves which resonate with particles having the critical energy is the critical frequency, i.e. the frequency which corresponds to the marginal stability condition ($\gamma = 0$). Such waves have no chance to be amplified and therefore the 'resonating' protons cannot be precipitated. Waves which can be efficient for proton precipitation are the most intense waves, i.e. waves for which the amplification is maximum. Their frequency f_m is much lower than f_c and therefore the parallel resonant energy of the most efficiently precipitated protons is much higher than E_c . Moreover, outside the plasmasphere, n_c may be of the order of n_h ; consequently the complete expression for the growth rate must be used, and not its approximation (2.12) which is valid only when $n_h \ll n_c$. In fact equation (2.12) is also valid when $n_h \sim n_c$ provided one replaces n_c in the denominator by $n_c + n_h$ and provided that $V_r \gg U_{//}$ (Gendrin et al., 1971). But in the outer magnetosphere $V_r \sim U_{//}$. The argument $\xi = V_r / U_{//}$ of the Fried and Conte function $Z(\xi)$ approaches unity and the usual approximation $Z(\xi) = -1/\xi$ cannot be used, so that (2.12) is not valid.

Following the already reported work of Perraut and Roux (1975) where the correct expression for γ was used, Perraut et al. (1976) have computed the frequency f_m for which $\gamma = \gamma_{\max}$ and the associated value of the resonant parallel energy E_M . In their computation due account was taken of the variation of the anisotropy when the protons move inward under the influence of the magnetospheric convection electric field. Assuming that the two first adiabatic invariants are conserved during this displacement, the proton parallel and perpendicular energies vary respectively like $L^{-5/2}$ and L^{-3} (Cowley and Ashour-Abdalla, 1975), so that

$$A = (A_0 + 1) (L_0/L)^{1/2} - 1 \quad (2.21)$$

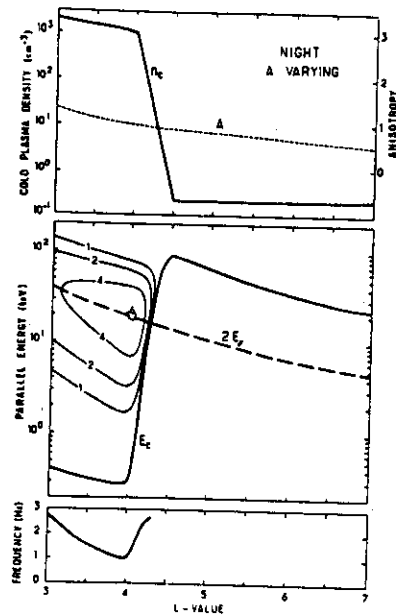
where A_0 is the initial anisotropy at the injection boundary defined by L_0 .

The total amplification $\Gamma = \int \gamma' ds/vg$ was computed and iso- Γ contours in the $E_r - L$ plane were drawn (Figure 2.27), assuming that $L_0 = 7$ and $A_0 = 0.5$. This figure shows that during the night, amplification takes place only within the plasmasphere, at the very near border of the plasmapause. However the resonant energy of particles associated with the large Γ waves, E_M , are much higher (almost 2 orders of magnitude) than the critical energy. During the day and outside the plasmasphere E_c is smaller since n_c is larger so that there is some amplification at large L-values. In this case E_M is not much larger than E_c .

It is worth noting that the model predicts that amplification still exists at higher frequencies well inside the plasmasphere ($\Gamma \sim 4$ for $f \sim 2.5$ Hz at $L = 3$). Such emissions are due to medium energy protons ($E_{//} \sim 30-40$ keV). Recent ground observations confirm this prediction. Using the Soviet-Finnish chain of stations ($57^\circ < \Lambda_{\text{geomagn.}} < 66^\circ$), Baranski et al. (1981) have shown that high frequency emissions ($f \sim 2$ Hz) are generated around $L = 3.2$. This demonstrates that medium energy protons can penetrate well inside the plasmasphere. In other words the interactions which they should in principle be subject to as soon as they enter the plasmasphere are not sufficiently intense to precipitate all of them.

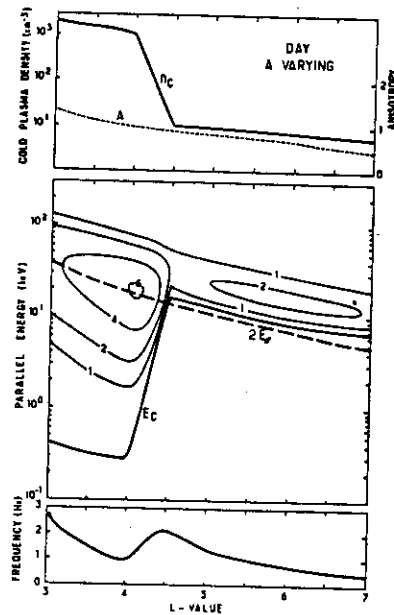
On Figure 2.28 the variations of $E_{//}$, E_c and E_M and Γ_M are represented for three different plasma conditions. On the left and central parts of the Figure, the anisotropy is varying according to equation (2.21); on the right part of the figure, the anisotropy is kept constant. In both cases the mean parallel energy $E_{//}$ is much larger than $E_c/2$ within the plasmasphere so that equation (2.15) is valid and E_M is much larger than E_c . Outside the plasmasphere, E_M is slightly larger than $\max(2E_{//}, E_c)$. As shown on the bottom panels of the figure, Γ_M is large in this region only when A is large. In both Figures 2.27 and 2.28 a constant values for E_1 at $L = 7$ has been chosen ($E_1 = 7$ keV). If $E_1 = E_{//} + E$ is the total mean energy of the distribution function equations (B.29) and (B.30) show that

$$\begin{aligned} E_{//} / E &= (2A + 3)^{-1} \\ E_1 / E &= 2(A + 1) / (2A + 3) \end{aligned} \quad (2.22)$$



a. Iso- Γ contours in the E_R - L plane (night conditions, varying anisotropy). The integrated growth rates are plotted as a function of the proton parallel energy and L -value (solid thin lines). A curve labelled n corresponds to an integrated amplification equal to $20 \log e^+ \text{ dB}$. The variations of twice the parallel thermal energy, $2E_j$ and of the critical energy E_c are also drawn (dashed lines). In the upper part of the figure the cold plasma density profile and the anisotropy variations are represented. The lower panel gives the emitted frequency which corresponds to the maximum value of Γ_M (at a given L). In these conditions, ULF waves are amplified only inside the plasmasphere. The parallel energy of protons which interact with the most amplified waves is approximately equal to twice the thermal parallel energy for every L -value. Both energies are much larger than the critical energy.

Fig. 2.27.



b. Iso- Γ contours in the E_R - L plane (day conditions, varying anisotropy). Same as Fig. 1, except for day conditions. Large amplification occurs inside the plasmasphere. A significant amplification occurs also outside the plasmasphere, involving protons having energies slightly larger than twice the thermal energy.
Perraut *et al.*, J.A.T.P., 38, 1191, 1976.

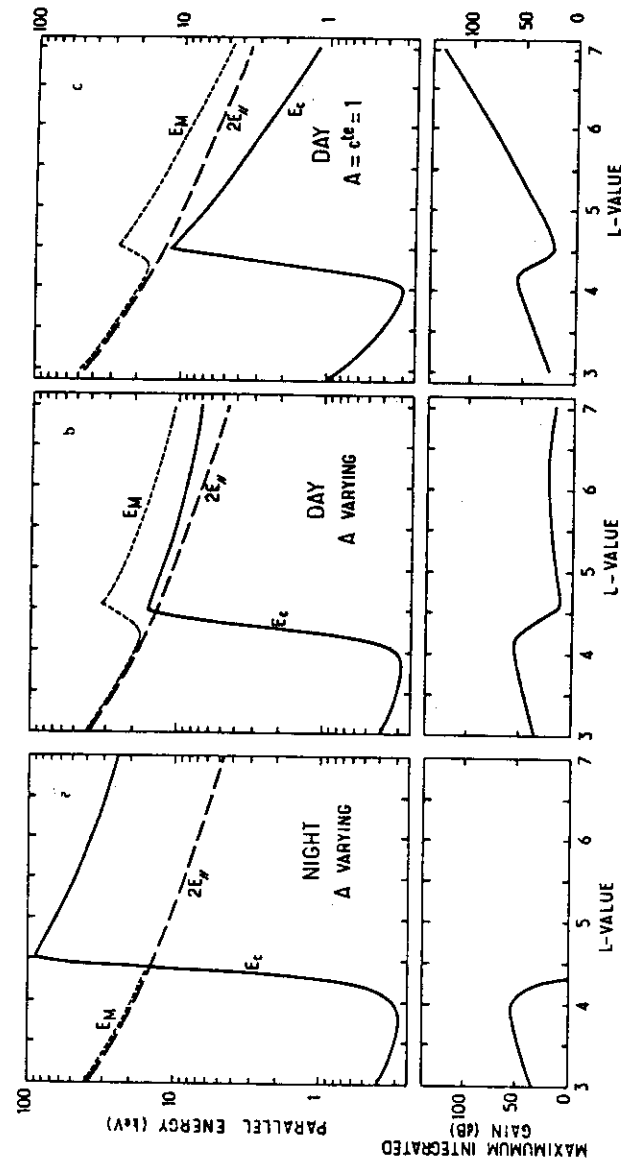


Fig. 2.28 Variation of E_M , E_j , E_c and Γ_M as a function of L . (a) Night conditions, A varying; (b) Day conditions, A varying; (c) Day conditions, A constant. This figure illustrates the relative role of E_j and E_c . Inside the plasmasphere, $2E_j$ is always much larger than E_c and strong amplification takes place. Outside the plasmasphere, when $2E_j$ is only slightly smaller than E_c , some amplification may occur (Fig. 8b). When $2E_j$ is larger than E_c , strong amplification occurs (Fig. 8c). In all cases, when amplification occurs outside the plasmasphere, it involves the high energy part of the distribution function. The value of Γ which is plotted, Γ_M , is the maximum Γ at any given L .

Perraut *et al.*, J.A.T.P., 38, 1191, 1976.

Kaye et al. (1979) made a more refined analysis by considering the full proton trajectories under the influence of convection and corotation electric fields. An interesting result of their study is the appearance of a low-frequency cut-off which is related to the existence of a high-energy cut-off in the distribution of protons within the plasmasphere (Figure 2.29). The low-energy cut-off in this distribution does not play a symmetric role, since it corresponds to high-frequency waves which are not generated because of the low value of the anisotropy. Such an effect restricts the frequency range of the instability mainly in the midnight sector. But it does not change much the overall picture of the total amplification in the dusk sector. The iso- Γ contours which are obtained do not differ significantly from the ones which are presented on Figure 2.27, at least within the plasmasphere. The large discontinuity which is assumed in this work at the plasma-pause boundary ($n_c \sim 100 \text{ cm}^{-3}$ for $LR \leq 6$ and $n_c \sim 4 \text{ cm}^{-3}$ for $L > 6$) does not allow to study the specific role of the cold plasma density in the transition region.

In conclusion one can say that the inner border of the plasmopause is a preferential region for precipitation of medium energy protons. However important precipitation may also occur outside the plasmasphere, depending on the initial anisotropy and mean energy of the injected protons. Besides protons which are most efficiently precipitated within the plasmasphere are not those for which $E_M = E_c$ but those for which $E_r = E_M \sim 2E_{//}$. Finally, at least during quiet conditions, the interactions which take place at the inner border of the plasmopause are not sufficiently intense to put all the interacting protons in strong diffusion; some protons may still penetrate further in and generate ULF waves of higher frequencies.

2.3.4. Competing processes : dispersion versus growth rate

Since waves are amplified over a restricted frequency range, there is a strong variation of the wave amplitude with frequency. Because of dispersive effects the frequency itself is a function of time, $f = f(t)$. We are therefore in the presence of a signal whose both amplitude and frequency vary with time. In such conditions the apparent law $f_m = f_m(t)$

where f_m is the frequency for which the amplitude is maximum differs from the original law $f = f(t)$ (see Chapter 6). Consequently the variation of the slope of the different Pc 1 elements in a frequency-time diagram differs from the one which would be obtained as a consequence of the sole dispersion.

For instance, instead of having a continuously decreasing slope df/dt like it is theoretically predicted for h.m. whistlers (see Figure 2.8), Pc 1 events often present parallel or even reerecting structures (Figure 2.30). This phenomenon has been interpreted by Gendrin et al. (1971) who showed the opportunity which it presents for diagnosing all the plasma parameters. In this study $\gamma(k)$ instead of $\gamma(\omega)$ was considered since the limited spatial extent of the wave packet is easily transposed into the k -space by a Fourier transform. Developing ω and k in the vicinity of the central angular frequency ω_0 and wave number k_0 , for which γ reaches its maximum value γ_0 , one has

$$\begin{aligned} \omega &= \omega_0 + v_{go} (k - k_0) + \frac{v_0}{2} (k - k_0)^2 \\ \gamma &= \gamma_0 - \frac{\mu_0}{2} (k - k_0)^2 \end{aligned} \quad (2.23)$$

where

$$\begin{aligned} v_{go} &= \left. \frac{d\omega}{dk} \right|_{k=k_0} \\ v_0 &= \left. \frac{dv_g}{dk} \right|_{k=k_0} = \left. \frac{d^2\omega}{dk^2} \right|_{k=k_0} \\ \mu_0 &= - \left. \frac{d^2\gamma}{dk^2} \right|_{k=k_0} \end{aligned} \quad (2.24)$$

After the time $t_n = nT$ which corresponds to n back and forth travels through the amplifying region (T being the repetition period), the wave packet has expanded in time. Simultaneously its apparent slope $d\omega/dt$ is an $f - t$ diagram has decreased. Let θ_n be the duration of the wave packet at time t_n , i.e. the time during which the amplitude is larger than half the maximum amplitude. Gendrin et al. (1971) have shown that :

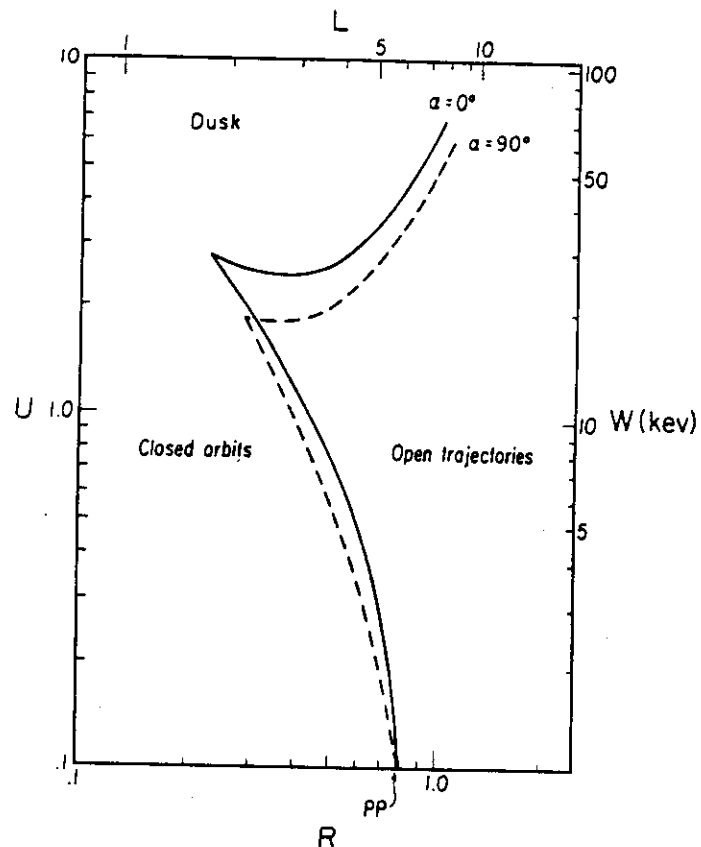


Fig. 229 Boundary between open and closed orbits for $\alpha = 0^\circ$ and $\alpha = 90^\circ$ protons. The normalized scale parameters are defined by $U = 0.42 W(\text{keV})/\phi_T^{1/3}$ and $R = 0.0295 L\phi_T^{1/3}$. The L and W scales are calculated specifically for a cross-magnetospheric potential drop of 90 kV; 'pp' denotes the position of the plasmopause.

Kaye et al., J.G.R., 84, 6397, 1979.

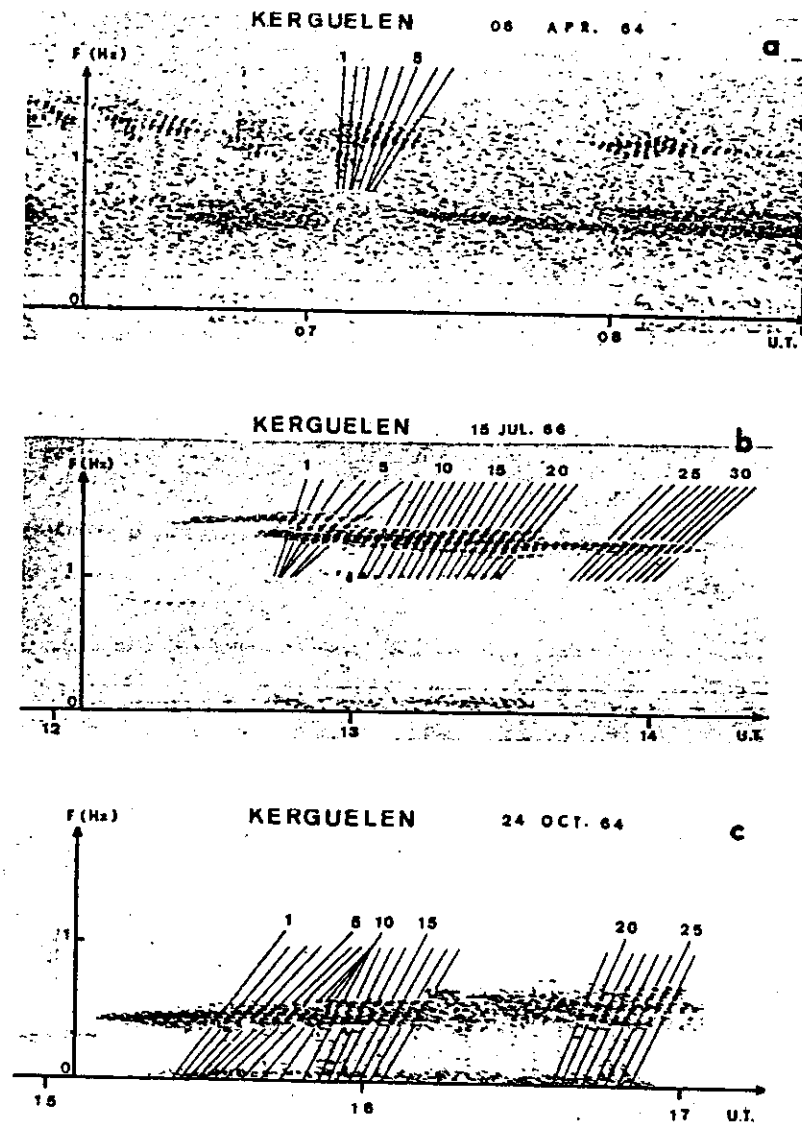


FIG. 230 THIS PICTURE REPRESENTS 3 EXAMPLES OF EVENTS WHICH WERE ANALYSED. Case (a) represents a particularly clear event from which one can think that only the dispersive property of the medium intervenes. Case (b) is more complicated. There are 3 parts for which the dispersion effect is clear (1-6, 14-22 and 23-26). The rest of the time, the pearls seem to remain parallel. In the case (c), 2 successive periods of dispersion separated by a period during which the elements reerect, appear. It is difficult to say if the third dispersive part is the end of the same event or if it is another emission because it is not exactly the same mean frequency.

Gendrin et al., Planet. Space Sci., 19, 165, 1971.

$$\theta_n^2 \sim 8 \ln 2 \frac{\mu_0^2 + \nu_0^2}{\mu_0 \nu_{go}^2} t_n \quad (2.25)$$

$$\left. \frac{d\omega}{d\tau} \right|_{t=t_n} \sim - \frac{\nu_0 \nu_{go}^2}{(\mu_0^2 + \nu_0^2) t_n}$$

Let us introduce the two reduced parameters

$$p = \frac{1}{t_n} \cdot \frac{d\tau}{d\omega} = - \frac{\mu_0^2 + \nu_0^2}{\nu_0 \nu_{go}^2} \quad (2.26)$$

$$q = \frac{\theta_n^2}{t_n} = 5.55 \frac{\mu_0^2 + \nu_0^2}{\mu_0 \nu_{go}^2} \quad (2.27)$$

which will be used later.

If the amplification curve $\gamma(k)$ is not strongly peaked around $k = k_0$, μ_0 is small and one has

$$\frac{d\omega}{d\tau} = - \frac{\nu_{go}^2}{\nu_0 t_n} \quad (2.28)$$

This formula is the one which is valid for propagation in an amplifying medium. In order to demonstrate this statement let us compute $d\tau/d\omega$ at time t_n . Obviously one has :

$$\left. \frac{d\tau}{d\omega} \right|_{t=t_n} = \left. \frac{d\tau}{d\omega} \right|_{t=t_{n-1}} + \frac{d\tau}{d\omega} \quad (2.29)$$

so that

$$\left. \frac{d\tau}{d\omega} \right|_{t=t_n} = n \frac{d\tau}{d\omega} \quad (2.30)$$

But

$$\frac{dT}{d\omega} = - \int \frac{ds}{\nu_g^2} \frac{d\nu_g}{dk} \frac{dk}{d\omega} = - \int \frac{\nu ds}{\nu_g^3} \quad (2.31)$$

Since $\nu = \nu_g d\nu_g/d\omega$, ν is equal to ν_a^{+2} times a certain function of frequency. The same is true for ν_g^2 so that one can write

$$\frac{dT}{d\omega} = F(\omega) \int \frac{ds}{\nu_g} = F(\omega) T \quad (2.32)$$

where $F(\omega) = \nu/\nu_g^2$, so that

$$\frac{dT}{d\omega} = - \frac{\nu}{\nu_g^2} T \quad (2.33)$$

which, with the help of (2.30), demonstrates (2.28).

In the left handed mode one has (see Table B.2) :

$$\nu_g = \nu_a^+ \cdot \frac{(1-x)^{3/2}}{1-x/2} \quad (2.34)$$

from which one deduces

$$\nu = - \frac{\nu_a^{+2}}{\omega_{ci}} \cdot \frac{(1-x)^2 (1-x/4)}{(1-x/2)^3} \quad (2.35)$$

When the event is in its linear phase, i.e. when no more amplification occurs so that the signal is dying out, $d\tau/d\omega$ varies linearly with time and p is a constant. This final value of p is called p_f and it verifies

$$p_f = - \frac{\nu_0}{\nu_{go}^2} \quad (2.36)$$

which, with the help of (2.34) and (2.35) becomes

$$p_f = \frac{1}{\omega_{ci}} \cdot \frac{(1-x_0/4)}{(1-x_0)(1-x_0/2)} \quad (2.37)$$

Consequently from the measurement of p_f and x_0 one can deduce ω_{ci} , the equatorial value of the proton gyrofrequency and hence the L-value of the field line where the wave has been generated. Note that in this method, there is no need to use the repetition period itself nor to assume a specific model for the cold plasma density distribution along the field line. Other methods for computing ω_{ci} and L make use of such assumptions*. Obviously, if one wants to evaluate the value of n_c at the apex of the field line one must measure T itself and one must make some assumption about the cold plasma distribution.

Plots of $dt/d\omega$ as a function of time (Figure 2.31) show that there are in general two periods during which p is constant. The last one is the one which is used for computing ω_{ci} . The results agree well with what is known about the generation region of Pc 1's. The second one allows to define an initial value of p , p_i which is larger than p_f since it verifies (2.26) with $\mu_0 \neq 0$.

As time elapses, ν remains constant but γ and μ decrease because of the diffusion of particles under the influence of the wave (section 2.3.5). The value of p which was constant at the beginning of the event is still constant at the end but is smaller. This is the interpretation which was given by Gendrin et al. (1971) for the variation of the slope $d\omega/dt$ during the course of Pc 1 events.

The amplification coefficient γ and therefore its second derivative μ_0 are proportionnal to n_h/n_c . The proportionality factor is a function of x_0 and of U_{\parallel}/V_a^+ which itself can be obtained from the measurement of x_0 (see Section 2.3.1). The direct measurement of γ is impossible because of wave dissipation effects (see Appendix B, Section B.5). To measure μ_0 is difficult but the ratio μ_0/ν_0 , which is also the product of n_h/n_c by some function of ω_0 and U_{\parallel}/V_a^+ is easy to evaluate. Therefore one has the

* References to these other methods can be found in Gendrin et al. (1971) p. 173.

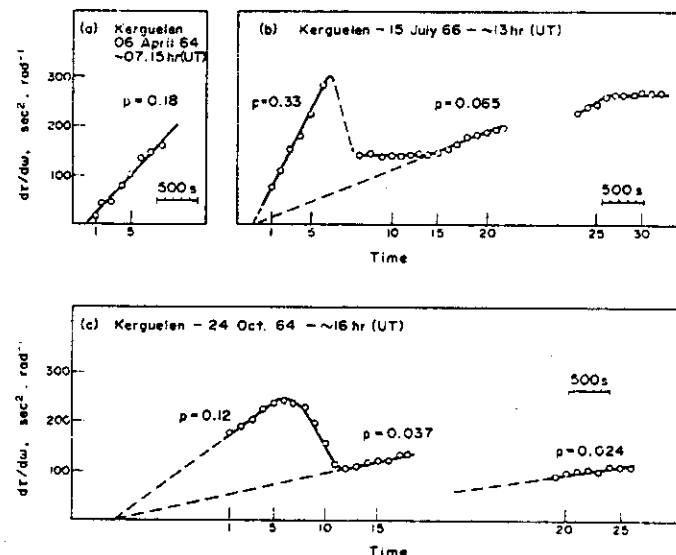


FIG.2.31 SLOPE OF THE ELEMENTS $dt/d\omega$ AS A FUNCTION OF TIME FOR THE THREE EXAMPLES WHICH HAVE BEEN REPRODUCED IN FIG. 2.

One can see clearly the linear increasing of slope at the beginning of the event, followed by a decrease of the slope. Afterwards there is again an increase. Sometimes $dt/d\omega$ remains constant: the pearls remain parallel.

Gendrin et al., *Planet. Space Sci.*, 19, 165, 1971

possibility of measuring n_h/n_c . The ratio μ_0/v_0 can be expressed either by using (2.26) and (2.27) from which one gets

$$\frac{\mu_0}{v_0} = -5.55 \frac{p}{q} \quad (2.38)$$

or by using (2.26) and (2.36) which gives

$$\frac{\mu_0}{v_0} = \sqrt{\frac{p_i}{p_f}} - 1 \quad (2.39)$$

Both methods have been used by Gendrin et al. (1971). They give results which agree together and which are of the right order of magnitude ($n_h/n_c \sim 10^{-3} - 10^{-1}$). The largest ratios are obtained for high L-values ($L \sim 6$), or at lower L-values ($L \sim 4$) but during period of intense magnetic activity. These results are expected from the dynamics of both cold and hot plasmas during injection events.

In summary the slope of successive Pc 1 elements in a frequency-time diagram is the result of a competing action between dispersion and amplification. Due to quasi-linear processes the importance of the second phenomenon with respect to the first one diminishes during the course of the event. The measurement of all the characteristics of the frequency-time structure of Pc 1's at the beginning and at the end of the emission allows to evaluate L, n_c , n_h and U_{\parallel} . The only parameter which is not determined is the anisotropy.

2.3.5. Geophysical consequences of Ion Cyclotron Waves

Once they are generated, ion cyclotron waves (ICW) act upon the magnetospheric particles in different ways. Their reaction upon the energetic protons which are at the origin of their generation has already been studied (Section 2.3.3) where the role of the plasmopause with respect to proton precipitation has been discussed. In Appendix B, the proton lifetime under the influence of quasi-linear diffusion has been also evaluated (Section B.4.4)

as well as the wave intensity which is necessary to bring these protons into strong diffusion (Section B.4.5). In this Section we would like to study the effects that ICW's may produce on particles that are not responsible for their generation. These particles may be protons (in a different energy range), electrons (both thermal and relativistic) or heavy ions. These principal interactions are listed in Table 2.3 and below they are briefly reviewed in the order in which they are listed.

Thermal protons

The fact that isotropic, low energy particles may absorb cyclotron waves near the gyrofrequencies is a consequence of the relationships which exist between wave amplification and particle diffusion (see Appendix B, Section B.4.2). The interaction is gyroresonant in the backward mode and the pitch angle of the interacting particles increases. Since the particles we are concerned with have thermal energies, the resonance occurs at frequencies which are very near to the gyrofrequency ($x \lesssim 1$). Therefore the ratio $v_{\phi}/v_{\parallel} = x / (1-x)$ is very large. The diffusion curves in the v_{\parallel}, v_{\perp} plane are almost straight lines parallel to the v_{\perp} axis and even distributions with a positive anisotropy could produce wave absorption. This is the phenomenon known as cyclotron absorption.

In the case of ICW's the particles which could absorb the waves are thermal or suprathermal protons. Such a mechanism has been invoked to explain the change in the pitch angle distribution of low-energy protons ($3 \leq E \leq 600$ eV) detected onboard the geostationary spacecraft ATS-6 as a function of local time. These distributions are more or less field-aligned in the afternoon and night sector and they change to pancake distributions in the morning sector (Imhof et al., 1982). By using Gendrin's (1968) expression for the pitch angle coefficient $D_{\alpha\alpha}$, these authors were able to show that a low magnetic field power density ($\sim 10^{-3} \gamma \cdot \text{Hz}^{-1/2}$) was sufficient to diffuse 100 -eV protons by $\Delta\alpha = 90^\circ$ in $\Delta t \sim 10^4$ s. Such a spectral density is small as compared to the ones which are commonly observed at geostationary altitudes ($\sim 1 \gamma \cdot \text{Hz}^{-1/2}$) but the problem is that these observed emissions occur at frequencies much smaller than the proton gyrofrequency ($0.2 < x < 0.6$) as expected for waves which are locally generated by energetic particles with

TABLE 2.3.

Consequences of ICW's on particles other than the ones that are involved in their generation.

Particles	Mechanism	Consequence	References
Thermal protons	gyroresonance (backward)	Generation of pancake distributions ($\alpha \searrow$)	<u>Singh et al.</u> , 1982
Relativistic electrons	gyroresonance (forward anomalous)	precipitation ($\alpha \searrow$)	<u>Thorne and Kennel</u> , 1971 <u>Thorne</u> , 1974 a,b.
He^+ ions	gyroresonance (forward normal if $f > H_{\text{He}^+}$)	heating ($E \searrow$, $\alpha \searrow$ or $\alpha \swarrow$)	<u>Gendrin and Roux</u> , 1980
	gyroresonance (backward if $f < F_{\text{He}^+}$)	heating and trapping ($E \searrow$, $\alpha \searrow$)	<u>Mank et al.</u> , 1981 <u>Young et al.</u> , 1981 <u>Roux et al.</u> , 1982
Thermal electrons	Landau absorption ($k_{\perp} \neq 0$)	heating production of SAR arcs	<u>Cornwall et al.</u> , 1971 a <u>Williams et al.</u> , 1976 <u>Lundblad and Söraas</u> , 1978

an anisotropic distribution function. Therefore one must assume that the waves are generated off the equator (with a local value of $x < 1$) by these energetic protons and that they propagate back to the equator where x approaches unity. A similar mechanism was already invoked by Joselyn and Lyons (1976) in order to explain the rounded pitch angle distributions of medium energy protons which were initially unable to generate ICW's.

One may also note that there are other processes by which waves can be generated near the proton gyrofrequency, in the magnetosonic mode and not in the Alfvén mode (see Section 2.4).

Relativistic electrons

The same difficulty does not arise when the absorption of (left-handed) ICW's by energetic electrons is considered. But, because of the large value of the ratio $|\omega_{ce}| / \omega_{ci}$, these electrons must have relativistic energies if an interaction has to occur at frequencies of the order of $\omega_{ci}/2$ (Figure 2.32). The interaction takes place in the backward mode. Absorption is possible because the electrons have a positive anisotropy (see Table B.5). During the interaction the electron pitch angle decreases and the electrons are precipitated.

Taking into account the relativistic variation of the gyrofrequency, Thorne and Kennel (1971) have evaluated the resonant energy of electrons interacting with an ICW such that $\omega/\omega_{ci} = 0.5$ (Figure 2.33). Two assumptions were made concerning the cold plasma density outside the plasmasphere: $n_c = 10 \text{ cm}^{-3}$ corresponding to afternoon values near the bulge and $n_c = 1 \text{ cm}^{-3}$ corresponding to plasmatrough values. The resonant energy expressed in terms of the relativistic factor $\gamma = (1 - v^2/c^2)^{-1/2}$ is given by

$$(\gamma^2 - 1) \cos^2 \alpha = \left(2m^* \frac{E_m}{E_0} \right) \cdot \frac{1-x}{x^2} \quad (2.40)$$

where α is the particle pitch angle, $m^* = 1840$ is the mass ratio between protons and electrons, $E_0 = m_e c^2$ is the electron rest mass and $E_m = B^2 / (\mu_0 n_c)$ is the magnetic energy per cold particle. The figure shows that the region

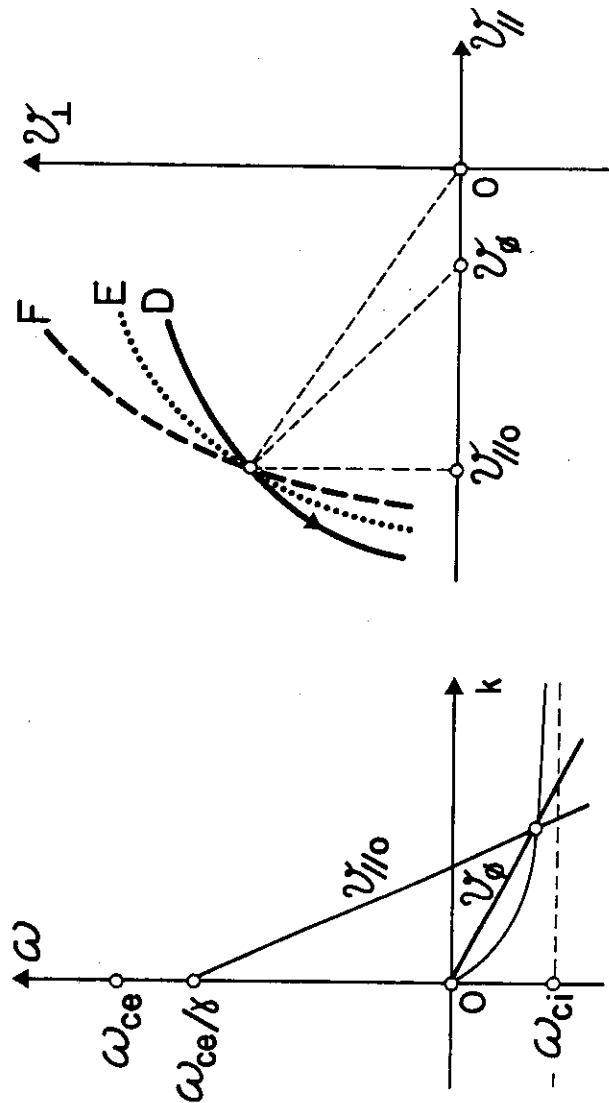


Figure 2.32.

Interaction between relativistic electrons and electromagnetic ion-cyclotron waves.

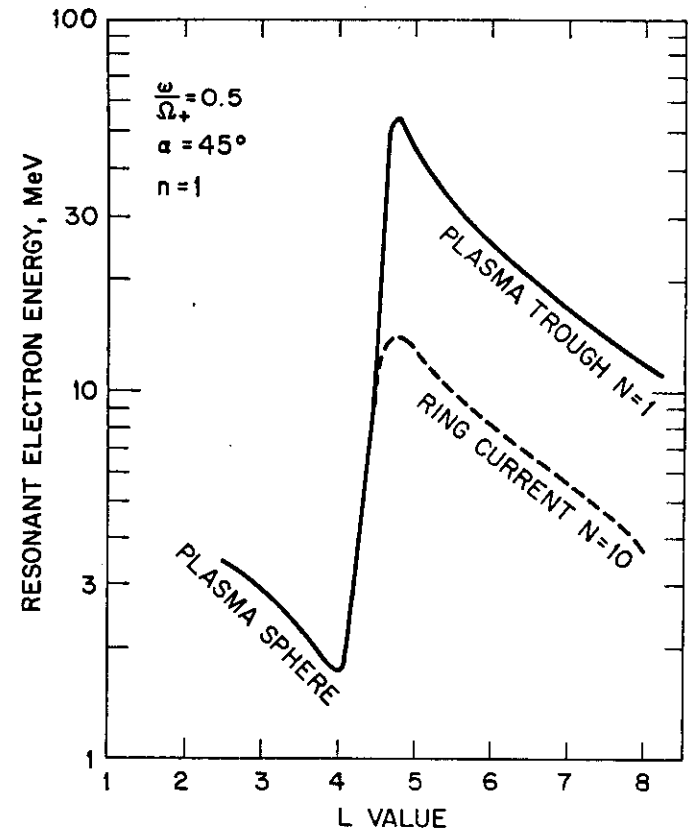


Fig. 2.33. The energy of electrons with 45° pitch angle resonant at the magnetic equator with $\omega/\Omega_e = 0.5$ ion-cyclotron waves is plotted against L value. The sharp increase at $L \approx 4.5$ is caused by the pronounced drop in density at the plasmapause. Beyond the plasmapause two curves have been plotted, one assuming typical thermal plasma densities ($N \approx 1 \text{ cm}^{-3}$) and the other assuming ring current proton densities ($N \approx 10 \text{ cm}^{-3}$).

Thorne & Kennel, J.G.R., 76, 4446, 1971.

of precipitation of electrons ($1 \leq E \leq 3$ MeV) is the inner border of the plasmapause. For the same physical reason (the minimum value of E_m) this is also the region of maximum generation of ICW's.

Thorne and Kennel (1971) have computed the electron pitch angle diffusion time $\tau_\alpha \sim D_{\alpha\alpha}^{-1}$ by using a formula similar to the one given by equation (B.100). For $E = 2$ MeV, $b = 1\gamma$ and $L = 4$ they found $\tau_\alpha \sim 50$ s. In the same conditions, the minimum lifetime $\tau_m = 2T_e/\alpha_0^2$ is 20 s. Then Equation (B.93) allows to compute the precipitated flux, J_p in the equatorial region if one knows the trapped flux, J_T whose measured value is $\sim 5 \times 10^3 \text{ cm}^{-2} \text{ s}^{-1}$, so that $J_p \sim 2 \times 10^3 \text{ cm}^{-2} \text{ s}^{-1}$. The energy diffusion time τ_E being related to the pitch angle diffusion time by the relation*

$$\frac{\tau_E}{\tau_\alpha} \sim \left(\frac{v_r}{v_\phi} \right)^2 \sim \left(\frac{m^*}{\gamma x} \right) \quad (2.41)$$

one can evaluate $\tau_E/\tau_\alpha \sim 10^6$ which means that $\Delta E/(\pi/2)^2 \sim \tau_\alpha/\tau_E \sim 10^{-6}$. In other words a typical relativistic electron of 1 MeV gains approximately 1 eV, an energy which is removed from the ICW's. The total energy flux which is removed is $\sim 2 \times 10^3 \text{ eV.cm}^{-2} \text{ s}^{-1}$ whereas the wave energy flux, for $b = 1\gamma$ and $V_a = 2000 \text{ km.s}^{-1}$ is $\sim 2 \times 10^9 \text{ eV.cm}^{-2} \text{ s}^{-1}$, e.g. 10^5 times larger. This mechanism is therefore efficient in precipitating relativistic electrons without modifying the ICW generation conditions.

Such a process operates principally in the night and dusk sectors at L-values of the order of 4, when the freshly injected protons encounter the plasmapause. At higher L-values ($L \sim 5-6$) the injected protons may drift without suffering much diffusion. But if they encounter detached plasma regions on the morning side, they could generate intense ICW's which could be at the origin of intense relativistic electron precipitation (REP) events (Figure 2.34). These events modify the day side ionospheric conductivity at auroral latitudes (Thorne, 1974 a,b).

* See equation (B.111).

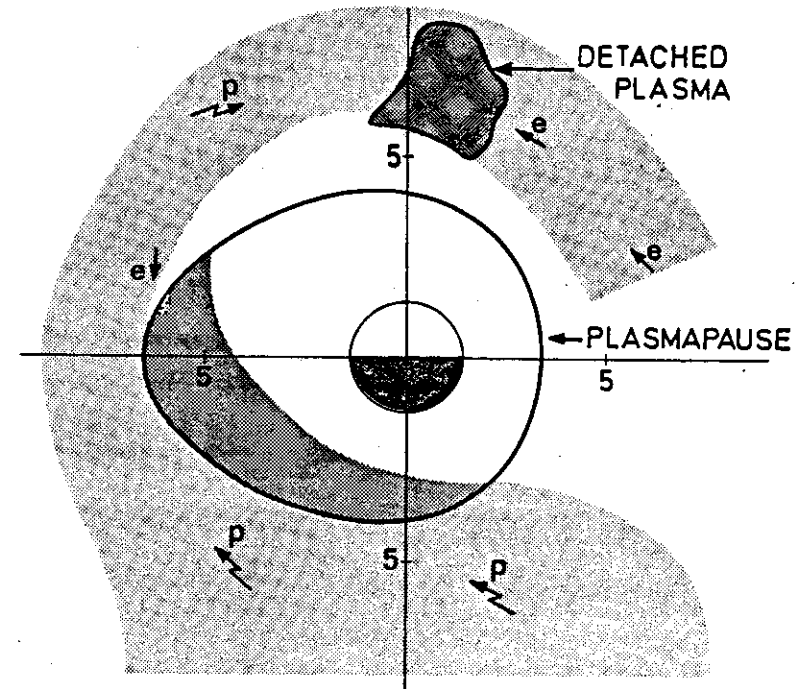


Fig.2.34. A schematic view of an REP event. Protons injected into the nightside magnetosphere during a sub-storm subsequently drift westward towards the dayside. They become subject to ion-cyclotron instability within the plasmasphere and suffer strong diffusion loss which reduces their flux to the stably trapped level for $L < 5$. For $L \geq 5$ the protons are able to reach the dayside without significant flux depletion and there trigger a further zone of intense ion-cyclotron turbulence within a region of detached high density plasma. Relativistic electrons on essentially circular drift orbits are parasitically scattering into the atmosphere on field lines threading both the detached plasma region and the outer edge of the nightside plasmasphere.

R.H. Thorne, *Space Sci. Rev.*, 16, 443, 1974.

He⁺ ions

In the presence of cold He⁺ ions the dispersion characteristics of ICW's are modified (see Section 2.4.1). The dispersion curve has two branches: a 'high frequency' one ($\omega_{cHe^+} < \omega_{co} < \omega < \omega_{cH^+}$) where ω_{co} is the cut-off frequency of the left-hand mode, and a 'low frequency' one ($\omega < \omega_{cHe^+}$). Gyroresonant interactions with magnetospheric thermal He⁺ ions of ionospheric origin may take place in both frequency ranges. They lead to an energization of He⁺ ions up to suprathermal energies (~ 100 eV) and to an increase of their pitch angle, so that these ions become trapped in the equatorial region of the magnetosphere. These effects are discussed in detail in Section 2.4.2.

Thermal electrons

The fourth process listed in Table 2.3 concerns the heating of thermal electrons through Landau damping and subsequent heat transfer to the upper atmosphere where the increase of electron temperature leads to the generation of stable auroral red arcs (SAR arcs). This mechanism is schematically represented on Figure 2.35. (Cornwall *et al.*, 1971). Landau absorption of ICW's by thermal (~ 1 eV) electrons is possible for two reasons:

1. The phase velocity of ICW's is of the order of the thermal velocity of these electrons (for $V_a^+ \sim 1000 \text{ km.s}^{-1}$ which corresponds to $E_p \sim 5 \text{ keV}$, one has $E_e \sim 2.5 \text{ eV}$). Landau resonance ($v_{\parallel} = v_{\phi}$) can therefore occur.
2. During ICW propagation, the wave normal angle rotates with respect to the magnetic field and large values of θ are reached (see Figure 2.9). This is a necessary and sufficient condition for an appreciable Landau resonant energy exchange between ICW's and thermal electrons (Kennel and Wong, 1967).

Computations show that the absorption rate verifies

$$\frac{|Y|}{\omega} = \frac{1}{\pi^{1/2}} \left(\frac{\tan \theta}{\tan \theta_{res}} \right)^2 \cdot \left(\frac{v_{\phi}}{v_{th}} \right) \cdot \exp \left[- \left(\frac{v_{\phi}}{v_{th}} \right)^2 \right] \quad (2.42)$$

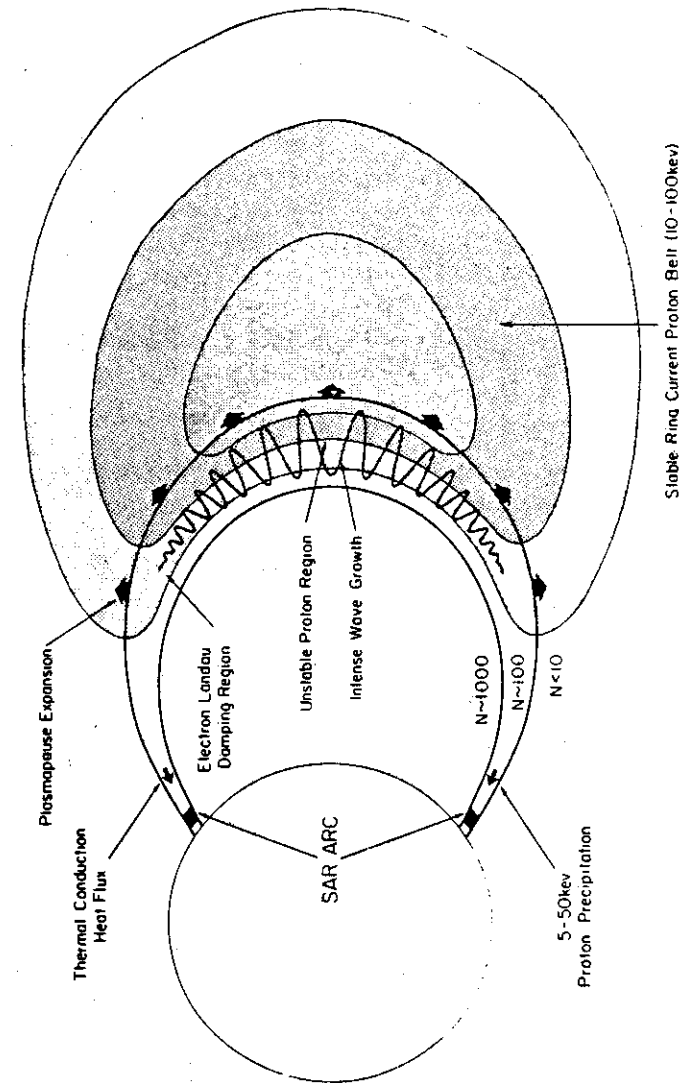


Fig 2.35. A synopsis of the energy transfer processes responsible for SAR arc formation at the plasma-pause (Cornwall *et al.*, 1971). During the recovery phase of major geomagnetic storms the plasma-sphere expands outward and ion-cyclotron turbulence generated within a narrow zone just inside the plasma-pause suffers strong Landau damping by thermal plasmaspheric electrons. The magnetospheric electrons are heated to a few eV and the heat is subsequently conducted along field lines to the ionosphere thus exciting the monochromatic red emissions.

R.M. Thorne, Space Sci. Rev., 16, 443, 1974.

where

$$\theta_{\text{res}} = \tan^{-1} \left[\frac{(\omega_{ci} \omega_{ce})^{1/2}}{\omega} \right] \quad (2.43)$$

is the resonance angle for oblique propagation. The absorption is appreciable for large wave normal angles and it can be shown that between 50 and 80% of the wave energy is transferred to the electrons. Assuming a wave field intensity at the equator equal to 2γ (a rather high value), Cornwall et al. (1971) were able to show that the heat flux at the ionospheric level ($F \sim 7 \times 10^{-5} \text{ W.m}^{-2}$) is sufficient to power a 1-kiloRayleigh SAR arc. The problem is that waves of such a high intensity have not been reported yet to exist in conjunction with SAR arcs and that this energy flux is also equal to the energy flux lost directly at times of SAR arcs by ring current protons (Williams et al., 1976). This leads to the unbelievable conclusion that both conversion processes (wave generation by protons and wave absorption by electrons) have an almost 100% efficiency.

APPENDIX B.

Other interactions involving ICW's and electrons

It has been recently observed that intense ICW's could be at the origin of the generation of field-aligned suprathermal electron fluxes (Cornilleau-Wehrlin, 1981 ; Norris et al., 1982). The large electric field component which is associated with the propagation of ICW's in the presence of cold He^+ ions it at the origin of this phenomenon (see Section 2.4).

THEORY OF GYRORESONANT INTERACTIONS

Finally, some of the auroral luminosity pulsations ($0.05 \leq f \leq 10 \text{ Hz}$) are known to occur in conjunction with ICW's (i.e. Berkey, 1980 ; Hirasawa, 1981). But the links which exist between oscillatory energetic ($\sim 1 - 10 \text{ keV}$) electron precipitation and hydromagnetic fluctuations detected at the ground have not yet been experimentally clarified nor satisfactorily interpreted.

2.4. Spacecraft observations

2.5. Irregular pulsations

These two sections have not yet been written.

APPENDIX B

THEORY OF GYRORESONANT INTERACTIONS

In a collisionless medium, waves and particles can interact coherently over long distances, the phase angle between the particle velocity vector and the wave electric field being able to remain more or less constant, under some conditions. By a cumulative effect, the exchange of energy between the wave and the particle, which is represented by the integral

$$W = q \int \underline{E} \cdot \underline{v} \, dt \quad (B.1)$$

is non zero. If $W > 0$ a fraction of the wave energy is transferred to the particles, the kinetic energy of which increases. If $W < 0$ the wave has taken energy from the particles and its amplitude will grow. Such interactions are called resonant interactions and the conditions which define the phase matching are called the resonance conditions.

Since in the magnetosphere the particle motion exhibits different periodicities, different resonant interactions can occur*. Among those, gyroresonant interactions play a fundamental role in the dynamics of magnetospheric particles, mainly for two reasons. First the gyration motion has the shortest periodicity and interactions involving this motion will be the fastest ones. Second, because they must be circularly polarized in order to interact with the gyrating particles, the waves intervening in this interaction belong to the whistler mode or to the ion cyclotron mode. Waves propagating in these modes are strongly guided by magnetic field lines and they are reflected by the ionosphere. Therefore they come back in the interaction region where they encounter other particles with which they interact again, leading to an increase of their amplification.

* The bounce resonance phenomenon has been already discussed in Chapter I.

This Appendix is devoted to gyroresonant interactions. We will first consider the basic physical principles which lead to the resonance condition (Section B.1). Some useful formulae for interactions between electrons and whistler waves or between protons and ULF waves are given in Section B.2. Growth-rates will then be computed by linearizing the Vlasov-Boltzman equation. The corresponding expressions lead to the concept of critical anisotropy and they show the importance of the cold plasma density value in the amplification process (Section B.3). The reaction of the generated waves upon particles are then studied in the framework of the quasi-linear (QL) theory and the importance of the pitch-angle (p.a.) diffusion is stressed (Section B.4). When gyroresonant interactions are considered as part of a process in which particles are continuously injected and precipitated and waves are continuously generated and reflected, one arrives at the concept of self-consistent equilibrium which is studied in Section B.5. Finally, when the wave amplitude is large, particle velocities are not equipartitioned between the different gyrophase angles and the full equations of movement have to be considered. These non-linear effects are dealt with in Section B.6.

B.1. THE GYRORESONANCE MECHANISM

In order to explain this mechanism in a simple way we will consider waves propagating with a \underline{k} vector strictly parallel or antiparallel to \underline{B} , i.e. to the z axis (Figure B.1). The wave is assumed to have its electric field vector circularly polarized in the x, y plane. The phase angle of this vector (measured positively in the x to y direction) is :

$$\theta = \omega t - kz + \theta_0 \quad (B.2)$$

where ω is positive if the wave is right-handed (RH).

Let us consider a particle whose parallel and perpendicular velocity components are $\underline{v}_{\parallel}$ and \underline{v}_{\perp} . Because of the gyration motion, the phase angle of the velocity vector \underline{v}_{\perp} is

$$\phi = \omega_c t + \phi_0 \quad (B.3)$$

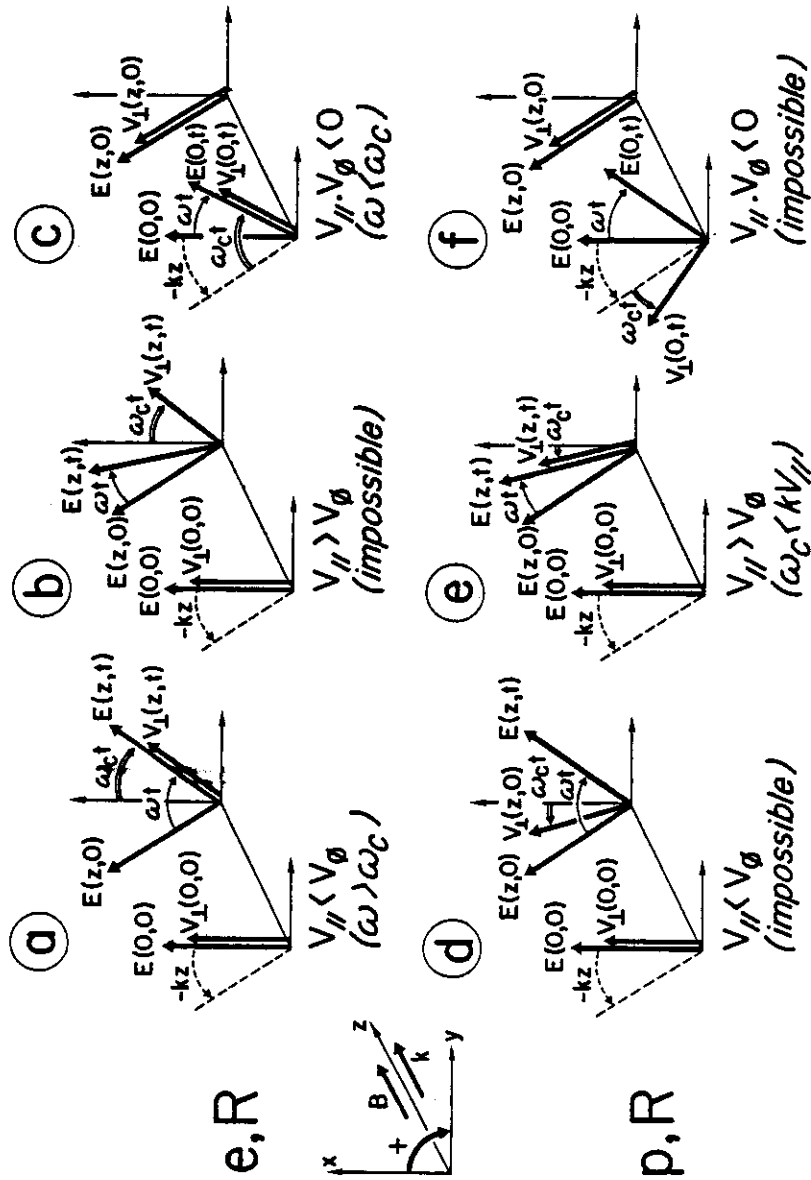


Fig. B.1

Gyroresonant interactions: the polarization fit.

where ω_c , the particle angular gyrofrequency, is positive for electrons and negative for positive ions. Because of the parallel motion $z = v_{||}t$, and the angle between the electric field vector seen by the particle and the instantaneous direction of its perpendicular velocity is

$$\theta - \phi = (\omega - kv_{||} - \omega_c) t + \theta_0 - \phi_0 \quad (B.4)$$

If

$$\omega = \omega_c + kv_{||} \quad (B.5)$$

this angle remains constant. The integral defined by (B.1) is non zero and an exchange of energy between the wave and the particle takes place. For a given $v_{||}$, ω is called the resonance frequency. For a given ω ,

$$v_r = (\omega - \omega_c) / k \quad (B.6)$$

is called the parallel resonant velocity. Equation (B.5) is called the resonance equation. When it is not satisfied the phase angle will take all possible values and the integral $\int \underline{E} \cdot \underline{v} dt$ has no secular term and there is no coherent exchange of energy between the particle and the wave.

The sign convention which has been adopted for deriving equation (B.5) must not be forgotten. Besides its algebraic significance* this equation also contains a condition on the necessary fit between the rotation senses of the two vectors (the polarization fit). The existence or absence of an interaction depends upon :

- the relative 'polarizations' of the wave and the particle. One may define interactions of the same polarity (respectively opposite) as those for which \underline{E} and \underline{v}_\perp rotate in the same (resp. opposite) sense**.

- the relative values of the phase velocity of the wave, v_ϕ and the parallel velocity of the particle, $v_{||}$.

* When written under the form $\omega_c = \omega - kv_{||}$, equation (B.5) expresses the fact that the Doppler shifted frequency seen by the particle is equal to its gyrofrequency.

** For instance interaction between electrons and RH waves or ions and LH waves are interactions of the same polarity.

- the relative values of the wave frequency $\omega/2\pi$ and the particle gyrofrequency $\omega_c/2\pi$.

This is easily demonstrated by considering the orientation change of both \underline{E} and \underline{v}_\perp when the particle moves along the z axis, which is illustrated on Figure 1 where an RH wave propagating in the $+z$ direction is considered. Identical arguments could be developed for an LH wave.

Let us first consider interactions with electrons. Let us assume for reason of simplicity that at time $t = 0$ the particle is at $z = 0$ and that \underline{E} and \underline{v}_\perp are parallel. At the same time the wave electric field at a certain distance z , $\underline{E}(z, 0)$ has the orientation shown on the picture, i.e. its phase angle with respect to the x axis is equal to $-kz$. When time elapses both particles and waves rotate to the right, the wave by an angle ωt , the particle by an angle $\omega_c t$. If a resonance is to occur, $\underline{v}_\perp(z, t)$ and $\underline{E}(z, t)$ where $z = v_{\parallel} t$ must also be parallel. Now one has to consider different cases (letters refer to the cases represented in Figure B.1 :

a) $v_{\parallel} < v_\phi$. $\underline{E}(z, t)$ is on the right of the x axis since the x axis is the position that \underline{E} should have if z were equal to $v_\phi t$. The resonance may exist provided one has $\omega t = kz + \omega_c t$, i.e. provided equation (B.5) is verified. Clearly this is possible only if $\omega_c < \omega$, otherwise the vector \underline{E} will not be able to catch the velocity vector.

b) $v_{\parallel} > v_\phi$. The time z/v_{\parallel} is too short for the wave vector to reach the x axis. $\underline{E}(z, t)$ is on the left of the x axis whereas $\underline{v}_\perp(z, t)$ is on the right. The resonance is impossible.

c) $v_{\parallel} < 0$. In this case one assumes that the particle is at the point z when $t = 0$. $\underline{E}(z, 0)$ and $\underline{v}_\perp(z, 0)$ are also assumed to be parallel. When the particle arrives at $z = 0$, \underline{v}_\perp and \underline{E} have both made a rotation in the positive sense and they can be parallel provided the resonance condition is satisfied, which implies, as seen on the figure, that $\omega < \omega_c$. Such interactions are called 'backward' since waves and particles propagate in opposite directions.

Similar arguments can be used to study the interaction between positive ions and RH waves :

d) $v_{\parallel} < v_\phi$. The interaction is impossible since $\underline{v}_\perp(z, t)$ is on the left of the x axis whereas $\underline{E}(z, t)$ is on the right (the x axis being the position of $\underline{E}(v_\phi t, t)$).

e) $v_{\parallel} > v_\phi$. The particle has such a high speed that the apparent polarization of the wave that it sees is left handed. This is called an 'anomalous' interaction since the particle velocity is larger than the phase velocity of the wave*. However ω_c must be smaller than kv_{\parallel} otherwise $\underline{v}_\perp(z, t)$ would be to the left of $\underline{E}(z, 0)$ whereas $\underline{E}(z, t)$ is on the right.

f) $v_{\parallel} < 0$. The interaction is impossible since $\underline{v}_\perp(0, t)$ is to the left of $\underline{E}(z, 0)$ which itself is to the left of $\underline{E}(0, 0)$ and a fortiori to the left of $\underline{E}(0, t)$.

These considerations are summarized in Table B.1 in which the possible interactions are listed according to their polarity and to the value of the particle velocity with respect to the phase velocity. As far as application to interactions with whistler waves or ion cyclotron waves are concerned, the following comments can be made, according to three cases listed in Table B.1.

1. For whistler waves $|\omega| < |\omega_{ce}|$, so that there is no forward normal e,R interaction. Similarly for ion cyclotron waves $\omega < \omega_{cp}$ where ω_{cp} is the proton gyrofrequency. However if a heavier ion is present, this ion can interact with such a mode since there are frequencies verifying $|\omega_{ci}| < |\omega| < |\omega_{cp}|$. In Section 2.4 we will see the importance of this effect for the heating of He^+ ions in the equatorial magnetosphere.

2. In general the condition $|k| > |\omega_c| / |v_{\parallel}|$ could be unsatisfied for certain values of v_{\parallel} . However whistler waves as well as ion cyclotron waves always present an asymptotic branch with large k values near the gyroresonance frequencies so that there is at least one frequency of interaction of this kind.

* In vacuum such a type of interaction does not exist, since no particle can have a velocity larger than the phase velocity ($v_\phi = c$).

TABLE B.1

Selection rules for gyroresonant interactions

A plus (respectively minus) sign means that the interaction is possible (resp. impossible).

	Case	Type	Same polarity (e,R or i,L)	Opposite polarities (e,L or i,R)
<u>$v_{//} \cdot v_{\phi} > 0$</u>				
$ v_{//} < v_{\phi} $	1	Forward normal	+	- (only if $ \omega > \omega_c $)
$ v_{//} > v_{\phi} $	2	Forward anomalous	-	+ (only if $\omega_c > kv_{//}$)
<u>$v_{//} \cdot v_{\phi} < 0$</u>				
	3	Backward	+	- (only if $ \omega < \omega_c $)

3. The condition $|\omega| < |\omega_c|$ is always satisfied since the waves we are concerned with propagate only in this frequency range.

This rather lengthy discussion has been made in order to clarify the reasons for which waves with different polarizations can resonate with a given particle species depending on the relative values of $v_{//}$ and v_{ϕ} and of ω and ω_c . But all the physics is indeed contained in equations (B.2) and (B.3) with their sign convention. In practical situations one does not have to worry about all the arguments which were developed above. It is sufficient to look at the intersection point(s) in the ω, k plane of the dispersion curve $D(\omega, k) = 0$ with the straight line defined by the resonance condition (B.5). One has just to be careful by assigning the same positive (respectively negative) regions for RH (resp. LH) waves and electrons (resp. ions)*. From Figure B.2 where this construction is made, the conclusions presented in Table B.1 are immediately deduced.

When applied to the practical case of electron or ion cyclotron waves, this construction gives immediately the four possible types of interaction (Figure B.3). These are :

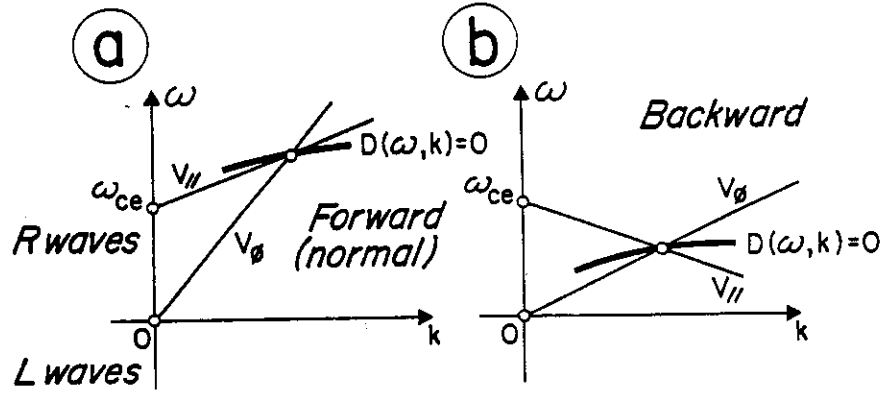
- e,R : this is the classical backward interaction between electrons and whistler waves which are at the origin of magnetospheric hiss and chorus in the VLF range. It will be discussed at length in this Appendix (Section B.5) and in Chapter 3.

- e,L : this is the anomalous (forward) interaction between electrons and ion cyclotron waves. Because of the large value of the ratio ω_{ce}/ω_{ci} , such an interaction implies large electron parallel velocities which correspond to relativistic energies. It has been invoked to interpret the 'parasitic' diffusion of relativistic electrons by ion cyclotron waves (Thorne, 1974).

- p,L : this is the classical backward interaction between protons and ion cyclotron waves which is at the origin of the generation of Pc1 waves (see Chapter 2).

* An opposite (but still coherent) convention may be used as well.

SAME POLARITY



OPPOSITE POLARITIES

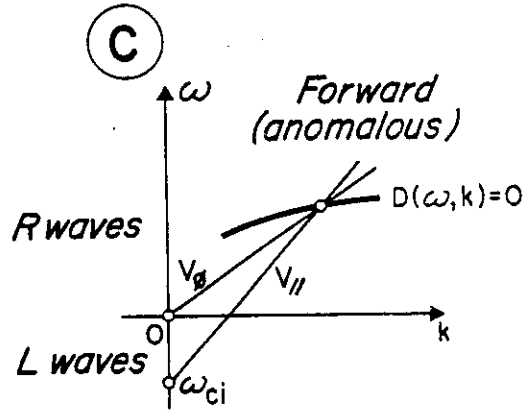


Fig. B2

The three kinds of gyroresonant interactions.

$$F(\omega, k) \equiv c_0^2 k^2 - \omega^2 + \frac{\omega_N^2 \omega}{\omega - \omega_B} + \frac{\Omega_N^2 \omega}{\omega + \Omega_B} = 0, \quad (6.12)$$

$$\omega = \omega_B + ku \quad \text{faisceau d'électrons} \quad (6.13)$$

$$\omega = -\Omega_B + ku \quad \text{faisceau de protons.} \quad (6.14)$$

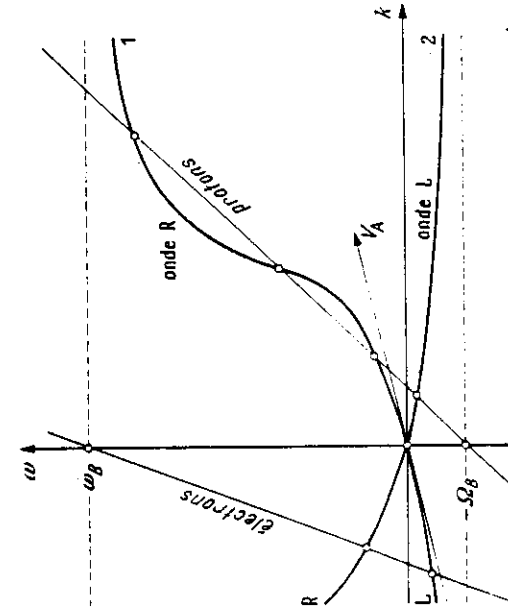


Fig. B3. Représentation graphique dans le plan ω, k des interactions de gyrorésonance. Les courbes continues 1 et 2 représentent dans ce système d'axes l'équation de dispersion pour la propagation longitudinale, dans les deux sens, des ondes T.B.F. et U.B.F. dans un magnétoplasma à un seul constituant ionique. Par convention, les fréquences positives (ou négatives) sont caractéristiques des ondes polarisées à droite (ou à gauche). Les droites représentent l'équation de dispersion des ondes cyclotrons des faisceaux (électrons ou protons); leur pente est proportionnelle à la vitesse longitudinale du faisceau. Une interaction de gyrorésonance est possible pour chacun des points d'intersection. (La partie des fréquences négatives du graphique a été agrandie pour donner plus de clarté au dessin). (D'après GARDNER²⁸.)

- p,R : this is an anomalous interaction between protons and the whistler mode. It may lead to the generation of waves in the magnetosheath region : the 'lion roars' (Smith and Tsurutani, 1976). Contrary to the e, L interaction it does not imply relativistic energies (see below).

Two remarks are worth making. First Figure B.3 does not show any example of a normal forward interaction ($v_{//} < v_\phi$) as represented on Figure B.2.a. In the VLF range this can be understood since there is no wave with $f > f_{ce}$. Indeed such waves exist at higher frequencies $f > f_1$ where

$$f_1 = \frac{1}{2} \left(\sqrt{f_{ce}^2 + 4f_{pe}^2} + f_{ce} \right) \quad (B.7)$$

is the cut-off frequency of the RH mode. But their phase velocity is higher than the velocity of light. In the usual magnetospheric situation for which $f_{pe} \gg f_{ce}$, $f_1 \approx f_{pe}$ so that interactions of this type could take place only with highly relativistic particles which are not present*. But in the ULF range normal forward interactions can exist, but only in multicomponent plasmas (see Section 2.4).

The second remark concerns the nature of the interaction. Having defined the existence of a resonance frequency is not sufficient to know in which direction the exchange of energy will take place. Will the wave be amplified (at the expense of the particles kinetic energy) or will it be damped? The answer to this question can be given only by making the full analytical treatment of the interaction, although in many cases simple geometrical considerations may lead to the correct answer (see Section B.4).

B.2. USEFUL FORMULAE

In practical applications it is interesting to know the value of the resonant frequency as a function of the particle parallel velocity or the resonant velocity which corresponds to a given frequency. This is

* However, when $\alpha = f_{pe}/f_{ce} < 1$ an interaction could occur for reasonable values of the electron velocity since the cut-off frequency is not much higher than the electron gyrofrequency. One has $f_1 = f_{ce} (1 + \alpha^2)$ (Gendrin, 1966). Such an interaction could be envisaged as a possible source for kilometeric radiation.

obtained by combining the dispersion equation $D(\omega, k) = 0$ with the resonance condition, in order to eliminate the wave number k .

Simplified dispersion relations have been given in Appendix A for waves propagating in a medium for which $\alpha^2 = (f_{pe}/f_{ce})^2$ is much larger than unity. For parallel propagation, equation (A.23), which is valid for VLF waves with frequencies higher than the lower hybrid frequency, becomes

$$v_\phi = V_a^- x^{1/2} (1-x)^{1/2} \quad (B.8)$$

where $x = \omega/\omega_{ce}$ and $V_a^- = c/\alpha$ is the 'electron Alfvén velocity'. Equation (A.30) on the other hand is

$$v_\phi = V_a^+ (1-X)^{1/2} \quad (B.9)$$

where $X = \omega/\omega_{ci}$ and $V_a^+ = c/\alpha m^{*1/2}$ is the usual Alfvén velocity. Note that with our conventions, there is only one expression for v_ϕ . But X is positive for LH waves (since both ω and ω_{ci} are negative) and negative for RH waves. By combining these expressions with the relation

$$v_\phi = v_r / (1 - \omega_c/\omega) \quad (B.10)$$

which one deduces from (B.6), one can compute $V_r(\omega)$.

Expressions for the phase velocity, v_ϕ , the group velocity, v_g , and the resonant energy $E_r = mV_r^2/2$ are given in Table B.2 for the two backward interactions, which are the most important ones. Table B.2 also contains some formulae which will be useful in other sections of this Appendix.

The relationships between the interaction frequency and the particle parallel velocity are illustrated on Figure B.4 for e,R and p,R interactions. On the left hand part of Figure B.5, this relationship is represented for the p,R interaction again (but with a linear frequency scale) and for the p,L interaction. The right-hand part of Figure B.5 represents the relationship between v_ϕ and V_r for these two interactions, as given by :

TABLE B.2
Basic formulas

Type of interaction	$x = \omega/ \Omega^\pm $	$V_{\pm} = B_0/(\mu_0 n m^\pm)^{1/2}$	$E_m = (m^\pm V_{\pm}^2)/2 = B_0^2/(2\mu_0 n)$
		e, R	p, L
Wave number $k V_{\pm}/ \Omega^\pm $	$x^{1/2}(1-x)^{-1/2}$		$x(1-x)^{-1/2}$
Phase velocity v_ϕ/V_{\pm}	$x^{1/2}(1-x)^{1/2}$		$(1-x)^{1/2}$
Group velocity V_g/V_{\pm}	$2x^{1/2}(1-x)^{3/2}$		$(1-x)^{3/2}(1-x/2)^{-1}$
Parallel resonant energy E_r/E_m	$x^{-1}(1-x)^3$		$x^{-2}(1-x)^3$
Critical energy E_c/E_m	$A^{-1}(1+A)^{-2}$		$A^{-2}(1+A)^{-1}$
Amplification factor $G(\omega)/ \Omega^\pm V_{\pm} $ (Equation 4)	$2\pi^2 x^{-1/2}(1-x)^{7/2}$		$2\pi^2 x^{-3}(1-x)^{7/2}$
Amplification factor $H(\omega)/ \Omega^\pm $ (Equation 12)	$\pi^2(1-x)^2$		$\pi^2 x^{-2}(1-x)^2$
* Diffusion coefficient $D/(\Omega^\pm)^2$	$x(1+2x)^{-1} (b_t/B_0)^2$		$x(2+x)^{-1} (b_t/B_0)^2$
** Diffusion curve $(v'^2 - v_{\pm}^2)/V_{\pm}^2$	$\frac{2x^2 + 1}{x} - \text{Ln}x$		$\frac{1-x}{x^2} + \text{Ln}x$

* The correct expression for $D[\pi\Omega^2(b_t/B_0)^2(V_{\pm} + |V_t|)^{-1}]$ is taken. Usually, V_{\pm} is neglected with respect to V_t , which is true only if $x \ll 1$.

** In these expressions, x is an implicit function of V_t (see the fifth line); v' is the constant defining the diffusion curve in the $v_{\pm}, v_g = V_t$ plane.

Gendrin, in 'Earth's Magnetospheric Processes', D. Reidel, 1972, pp. 311-328.

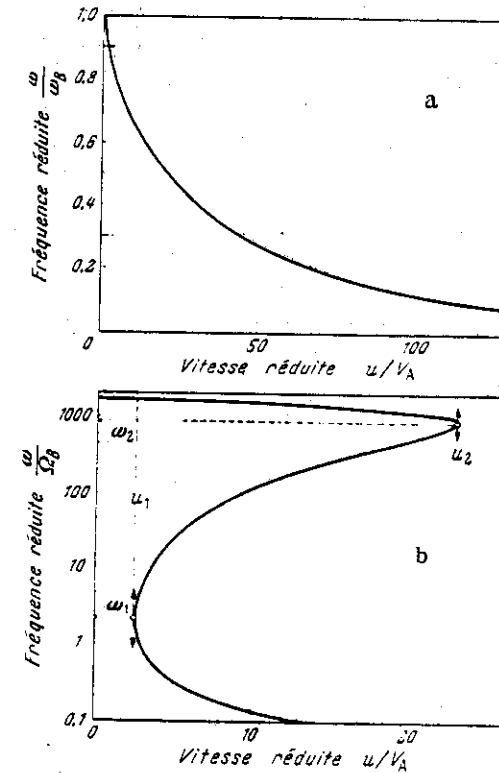


Fig. B.4. Fréquences émises dans une interaction de gyrorésonance donnant naissance à une onde polarisée à droite (mode des sifflements). En abscisse, la vitesse longitudinale du faisceau; en ordonnées, la fréquence émise. (a) cas d'une interaction avec un faisceau d'électrons: la fréquence émise est une fonction continuellement décroissante de la vitesse longitudinale du faisceau (d'après GALLEY [15]). (b) Cas d'une interaction avec un faisceau de protons: pour certaines valeurs de la vitesse longitudinale du faisceau, on peut avoir trois fréquences émises. Les valeurs limites ont pour expressions

$D'après Ginzburg^{(1)}: v_1/V_A \approx 3V_3/2, v_2/V_A \approx 1m^*/2, \omega_1 \approx 2\Omega_B, \omega_2 \approx \frac{1}{2}\Omega_B.$

Gendrin, Handbuch der Physik, Springer, vol. 49/3, 461, 1972

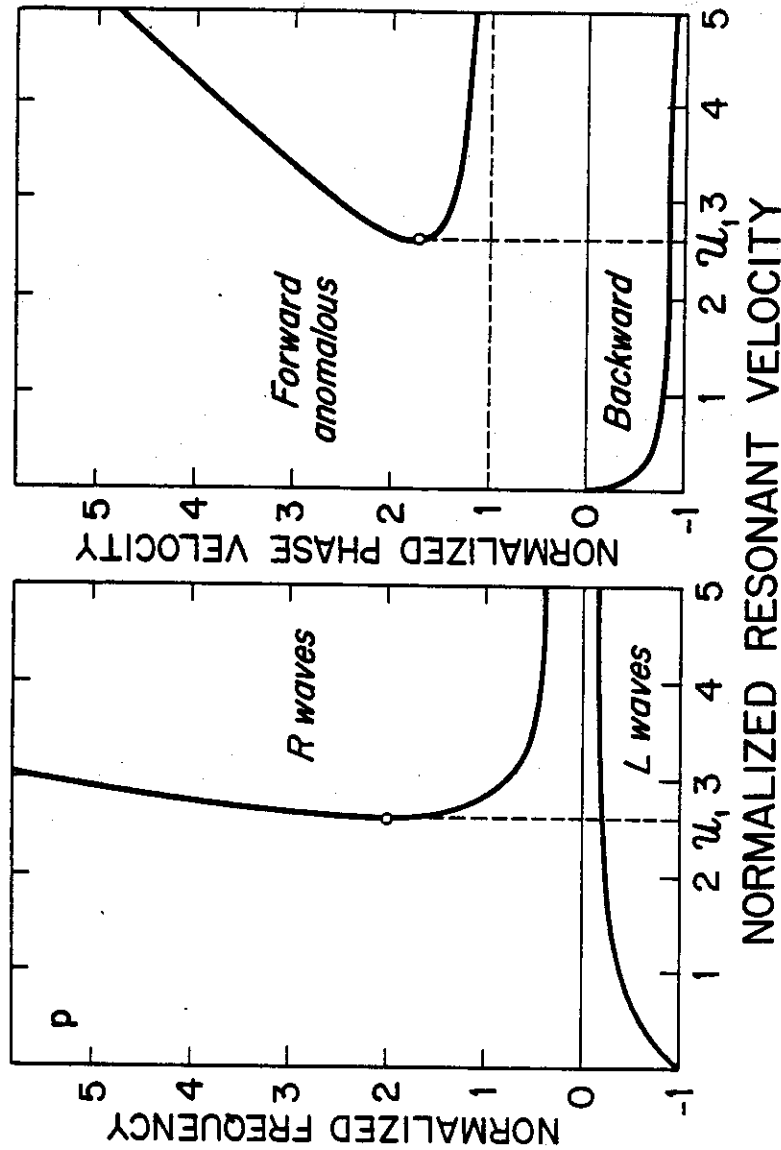


Fig. B5

Relationship between ω , v_ϕ and V_r for gyroresonant interactions with protons

$$V'_r = \frac{v_\phi'^3}{v_\phi'^2 - 1} \quad (B.11)$$

where $V'_r = V_r / V_a^+$ and $v_\phi' = v_\phi / V_a^+$ are normalized values. Equation (B.11) may have one or three roots in v_ϕ . The root which always exist is the one which corresponds to the backward interaction ($v_\phi' < 0$ assuming $V'_r > 0$). The other roots exist only when $v_{||}$ exceeds a certain critical value

$$v_{||} = (3\sqrt{3}/2) \quad (B.12)$$

The parallel energy of the protons must be larger than $(27/2)E_m$ where $E_m = m V_a^2/2$ is the 'magnetic energy per particle' or the 'Alfven energy'. E_m is not a very high energy ; for instance at $L = 6.6$ $E_m \sim 5-10$ keV which means that E must be larger than $\sim 75-150$ keV.

B.3. COMPUTATION OF THE GROWTH RATES

The dispersion relation which was established in Appendix A is valid for propagation of waves in a cold plasma. If one wants to study how this relation is modified by the existence of a finite temperature, one has to introduce the particle distribution function $f_s(v_\perp, v_{||})$ for each species s , which is such that $n_s f_s(v_\perp, v_{||}) v_\perp dv_\perp dv_{||} d\phi$ represents number of particle per unit volume whose velocity vector is contained in the infinitesimal volume $v_\perp dv_\perp dv_{||} d\phi$. Use of cylindrical coordinates is made, n_s is the number of particles per unit volume for species s , integrated over all velocities, and ϕ is the azimuthal angle in the plane perpendicular to B . These distribution functions which satisfy

$$\int_0^{2\pi} d\phi \int_0^\infty v_\perp dv_\perp \int_{-\infty}^\infty dv_{||} f_s(v_\perp, v_{||}) = 1 \quad (B.13)$$

obey the Boltzman-Valsov equation

$$\frac{\partial f_s}{\partial t} + \underline{v} \cdot \underline{\nabla} f_s + \frac{q}{m} \left[\underline{E} + \underline{v} \times (\underline{B} + \underline{b}) \right] \cdot \underline{\nabla} f_s = 0 \quad (B.14)$$

which is deduced from the momentum equation in the absence of collisions. Combining with Maxwell's equations, one arrives at a general dispersion relation (i.e. Sagdeev and Shafranov, 1961^{*}) which, in the case of parallel propagation of electromagnetic waves, is :

$$n_{\pm}^2 = 1 - \sum_s \frac{(\omega_{ps})^2}{\omega} \int_0^{\infty} v_{\perp}^2 dv_{\perp} \int_{-\infty}^{+\infty} dv_{\parallel} \cdot \left[\frac{\partial f_s}{\partial v_{\perp}} \pm \frac{k}{\omega} \left(v_{\parallel} \frac{\partial f_s}{\partial v_{\perp}} - v_{\perp} \frac{\partial f_s}{\partial v_{\parallel}} \right) \right] \cdot \frac{1}{kv_{\parallel} \pm (\omega - \Omega_s)} \quad (B.15)$$

In this equation the summation is made on the different species, the plus (respectively minus) sign corresponds to the L (resp. R) mode, and the sign convention for frequencies is the one we have adopted, i.e. $\omega > 0$ (< 0) for R(L) waves and $\Omega_s > 0$ (< 0) for electrons (ions)^{*}.

When the plasma is supposed to contain only cold particles, whose distribution function is of the form

$$f_c = \frac{1}{2\pi v_{\perp}} \delta(v_{\perp}) \delta(v_{\parallel}) \quad (B.16)$$

the usual dispersion relation is recovered. The problem being to look at the modifications of the dispersion relation when energetic particles are introduced, the plasma is considered to contain two populations : a cold one, of density n_c and whose distribution is given by (B.16) and a hot one, of density n_h and whose distribution is to be specified according to the physical situation under study. Usually only one species of hot particles is introduced at once.

The singularity within the integral (B.15) is avoided by introducing a small imaginary part in the frequency

$$\omega = \omega_r + i\gamma \quad (B.17)$$

^{*} One may also find a demonstration of this equation in Kennel and Petschek (1966), with a different convention for the signs.

where γ , the increment, is such that $\gamma/\omega_r \ll 1$. Because we have assumed that all oscillating quantities vary like $\exp[i(\omega t - kz)]$, $\gamma < 0$ means amplification and $\gamma > 0$ means damping. However it is usual to speak of positive growth rate when there is amplification. Therefore the growth rate is the opposite of the increment (an opposite convection is often used). One uses the Dirac relation

$$\lim_{\gamma \rightarrow 0^-} \int_{-\infty}^{+\infty} \frac{g(v_{\parallel}) dv_{\parallel}}{v_{\parallel} - v_r - i \frac{\gamma}{k}} = \text{pp} \left[\frac{g(v_{\parallel})}{v_{\parallel} - v_r} \right] - i\pi \text{sign}(k) g(v_r) \quad (B.18)$$

where

$$v_r = (\omega_r - \Omega_s) / k \quad (B.19)$$

and

$$\text{pp} \left[\frac{g(v_{\parallel})}{v_{\parallel} - v_r} \right] = \lim_{\epsilon \rightarrow 0^+} \int_{-\infty}^{-\epsilon} \frac{g(v_{\parallel}) dv_{\parallel}}{v_{\parallel} - v_r} + \int_{\epsilon}^{+\infty} \frac{g(v_{\parallel}) dv_{\parallel}}{v_{\parallel} - v_r} \quad (B.20)$$

Then, by equaling the real and imaginary parts of (B.15), the dispersion relation $n(\omega_r)$ and the increment $\gamma(v_r)$ are obtained. When the ratio $n_h/n_c \ll 1$, the dispersion relation is in general identical to the one which prevails in the absence of hot particles. However this is not always the case, as shown for instance by Higuchi and Jacobs (1970), Matsumoto and Kimura (1971) and Gendrin et al. (1971). Expressions which are valid for all the values of n_h/n_c can be found in Perraut (1974), for bi-maxwellian distributions and L waves. Lin and Parks (1974) have also studied this effect in the case of R waves and they have shown that important differences may exist when n_h/n_c exceeds ~ 0.1 . This is demonstrated on Figure B.6 where the value of the resonant velocity (normalized to $\sqrt{2} < v_{\parallel}^2 >$) is plotted as a function of n_h/n_c for different values of ω/ω_{ce} . Within the same constraint ($n_h \ll n_c$) the increment can be expressed as

$$\gamma = - \text{sign} \left(\frac{\omega}{\omega_c} \right) G(\omega) n(v_r) \left[A - (A+1) \frac{\omega}{\omega_c} \right] \quad (B.21)$$

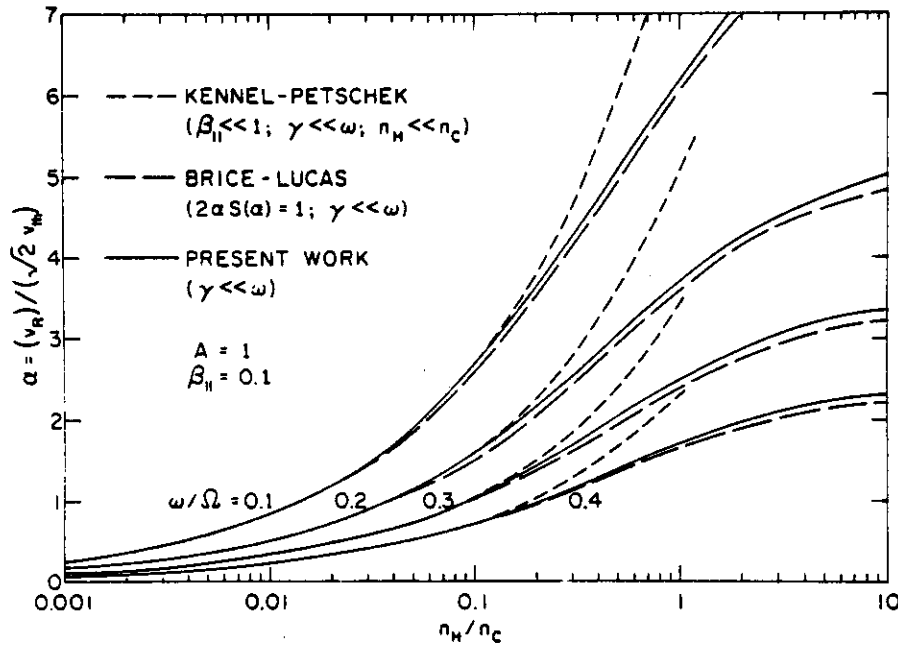


Fig. B.6. Plot of α as a function of n_H/n_C for a plasma of $\beta_{||} = 0.1$ and an anisotropy of $A = 1$. The four curves are for four ω/Ω values.

Lin and Parks, J.G.R., 79, 2894, 1974

where

$$dV_r \eta(V_r) = dV_r n_h v_a \int_0^{+\infty} v_{\perp} dv_{\perp} f_h(v_{\perp}, v_{||} = V_r) \quad (B.22)$$

is the number of particles which resonate with the wave in the frequency range $\omega, \omega + kdV_r$, and where

$$A(V_r) = \frac{\int_0^{+\infty} v_{\perp} dv_{\perp} \left(v_{||} \frac{\partial f_h}{\partial v_{\perp}} - v_{\perp} \frac{\partial f_h}{\partial v_{||}} \right) \frac{v_{\perp}}{v_{||}}}{2 \int_0^{+\infty} v_{\perp} dv_{\perp} f_h} \quad (B.23)$$

defines the anisotropy of the distribution function. Introducing the pitch angle α , i.e. the angle between \underline{v} and \underline{B} , f can be considered as a function of energy and pitch angle: $f \equiv f(v, \alpha)$. Then, by using the relations

$$\begin{aligned} \frac{\partial}{\partial v_{\perp}} &= \sin \alpha \frac{\partial}{\partial v} + \frac{\cos \alpha}{v} \frac{\partial}{\partial \alpha} \\ \frac{\partial}{\partial v} &= \cos \alpha \frac{\partial}{\partial v} - \frac{\sin \alpha}{v} \frac{\partial}{\partial \alpha} \end{aligned} \quad (B.24)$$

one may write

$$A = \frac{\int_0^{+\infty} v_{\perp} dv_{\perp} \tan \alpha \frac{\partial f_h}{\partial \alpha}}{2 \int_0^{+\infty} v_{\perp} dv_{\perp} f_h} \quad (B.25)$$

This expression shows that the amplification (or damping) of the waves is governed by the gradient of the distribution function with respect to pitch angle. If $\partial f / \partial \alpha = 0$ (i.e. if the distribution function is isotropic for all energies, then $A = 0$). A positive anisotropy exists when there are

more particles with large pitch angles than particles with small pitch angles (at a given energy). Because of the existence of a loss-cone, magnetospheric particle distributions generally exhibit a positive anisotropy.

Critical anisotropy

In equation (B.21) the function $G(\omega)$ is positive so that one can immediately find out in which cases there is an amplification. As shown by the last term of (B.21), and as was pointed out by Kennel and Petschek (1966), whether or not an emission can occur depends only on the pitch angle anisotropy (and on the frequency). On the other hand the amplitude of the growth or damping depends on both the anisotropy and the number of resonant particles (and also on the frequency). For p,L and e,R interactions for which ω and ω_c have the same sign, γ is negative (i.e. positive growth rate) if $x = \omega/\omega_c$ verifies

$$x < x_c = \frac{A}{A+1} \quad (B.26)$$

This condition means that, given the anisotropy, amplification is possible only if the frequency is smaller than a certain critical frequency. Conversely, wave amplification can occur at a given frequency only if the anisotropy exceeds a certain value which is called the critical anisotropy

$$A > A_c = \frac{x}{1-x} \quad (B.27)$$

For p,R and e,L interactions $\omega/\omega_c < 0$ so that the conditions on the anisotropy are changed. There still remains, however, a condition on the frequency range over which the instability can occur. These results are summarized in Table B.3.

From now on we restrict ourselves to the most important interactions (i.e. p,L and e,R). In order to progress a specific form for the distribution

* and assuming that the anisotropy is not a function of frequency itself, a point which will be discussed later.

TABLE B.3

Conditions for wave emission for different anisotropy factors and different types of interaction. A plus (respectively minus) sign means amplification (resp. damping). The values of the critical frequencies f_{c1} and f_{c2} are functions of A. For a bi-maxwellian distribution the 3rd case cannot occur as shown by equation (B.30). The Table is adapted from Liemohn (1967) after correction of a slight error.

Anisotropy factor	Type of interaction	
	e,L or p,R	e,R or p,L
$0 < A$	-	+ (if $ f < f_{c1}$)
$-1 < A < 0$	+ (if $ f < f_{c2}$)	-
$A < -1$	+	-

function has to be selected. The bi-maxwellian distribution is one of the most popular since it allows to make analytical computations. Therefore let us assume that

$$f_h = \frac{1}{\pi^{3/2} U_{\perp}^2 U_{\parallel}} \exp \left[-\frac{v_{\perp}^2}{U_{\perp}^2} - \frac{v_{\parallel}^2}{U_{\parallel}^2} \right] \quad (B.28)$$

where $U_{\parallel}^2 = 2\kappa T_{\parallel} / m$ and $U_{\perp}^2 = 2\kappa T_{\perp} / m$ (κ being the Boltzman constant) define the parallel and perpendicular temperatures of the distribution. Note that these temperatures are related to the mean quadratic value of the parallel and perpendicular velocities by the usual thermodynamic relations if one takes into account the fact that v_{\perp} corresponds to two degrees of freedom, whereas v_{\parallel} corresponds to only one. One easily demonstrates that

$$\langle v_{\parallel}^2 \rangle = 2\pi \int_0^{+\infty} v_{\perp} dv_{\perp} \int_{-\infty}^{+\infty} v_{\parallel}^2 dv_{\parallel} f = \frac{U_{\parallel}^2}{2} = \frac{\kappa T_{\parallel}}{m} \quad (B.29)$$

$$\langle v_{\perp}^2 \rangle = 2\pi \int_0^{+\infty} v_{\perp}^3 dv_{\perp} \int_{-\infty}^{+\infty} dv_{\parallel} f = U_{\perp}^2 = \frac{2\kappa T_{\perp}}{m}$$

For such a distribution, it is easily shown that A , as defined by (B.23) is independent of V_r :

$$A = \frac{T_{\perp}}{T_{\parallel}} - 1 \quad (B.30)$$

so that one can speak of the anisotropy of the distribution function. A similar property exists for distributions of the form

$$f(v, \alpha) = g(v) \sin^m \alpha \quad (B.31)$$

which are sometimes used since they are a better approximation to loss-cone distributions (no particles for $\alpha = 0$). Because $\partial f / \partial \alpha = mf / \tan \alpha$, one immediately obtains from (B.25):

$$A = m/2 \quad (B.32)$$

If $T_{\perp} > T_{\parallel}$ or if $m > 0$, examination of Table B.3 shows that the backward interactions between electrons and whistler waves or between protons and ion cyclotron waves lead to an amplification of such waves. This is the basic mechanism by which the generation of hiss or chorus in the VLF range or Pc 1's or IPDP's in the ULF range is explained.

The fact that A is independent of V_r justifies the concepts of critical anisotropy and of critical frequency so successfully introduced by Kennel and Petschek (1966). It can even be demonstrated, by using Lieuvillie's theorem, that for the distributions described by equation (B.31) but not (B.28), A is constant along a magnetic field line if the first invariant is conserved. However for other distributions, A is a function of V_r , i.e. of frequency, and equations like (B.26) or (B.27) have no meaning. The consequences of this effect will be discussed partly in section B.5 of this Appendix and partly in Chapter III.

For bi-maxwellian distributions the precise values of the growth rates are given by (i.e. Kennel and Petschek (1966), Gendrin et al. (1971)):

$$\frac{\gamma_e}{|\omega_{ce}|} = -\sqrt{\pi} \frac{n_h}{n_c} (1-x) \left[A - (A+1)x \right] \sqrt{\gamma_1} \exp(-\gamma_1) \quad (B.33)$$

for e, R interactions and

$$\frac{\gamma_i}{|\omega_{ci}|} = -\sqrt{\pi} \frac{n_h}{n_c} \frac{(1-x)}{x(2-x)} \left[A - (A+1)x \right] \sqrt{\gamma_2} \exp(-\gamma_2) \quad (B.34)$$

for p, L interactions with

$$\left. \begin{aligned} \gamma_1 &= \left(\frac{V_a^-}{U_{\parallel}} \right)^2 \frac{(1-x)^3}{x} \\ \gamma_2 &= \left(\frac{V_a^+}{U_{\parallel}} \right)^2 \frac{(1-x)^3}{x^2} \end{aligned} \right\} \quad (B.35)$$

Application of these formulae will be made in Chapters 2 and 3 where the role of A and of the ratio $U_{//} / V_a$ will be discussed. What we would like to discuss here is the role of the ratio n_h / n_c . Clearly the growth rate increases when the number density of hot particles increases. But what about the effect of increasing n_c ?

Optimum cold plasma density

The idea that increasing the cold plasma density would enhance the wave growth and consequently the particle precipitation was originally brought up by Brice (1970) and Brice and Lucas (1971) for whistler interactions with electrons and by Cornwall et al. (1970) for interactions between ULF waves and protons. The main justification of these ideas is that the exponential term in (B.33) or (B.34) leads to an increase of $|\gamma|$ when n_c is increased since V_a^2 varies like n_c^{-1} . But the other terms in (B.33) or (B.34) cannot be neglected! One has

$$|\gamma| = \frac{k_1}{n_c^{3/2}} \exp\left(-\frac{k_2}{n_c}\right) \quad (\text{B.36})$$

where k_1 and k_2 are constant if one keeps the other parameters (n_h , $U_{//}$, A and ω) constant. Starting from small values of n_c it is clear that $|\gamma|$ increases when n_c increases. However for sufficiently large values of n_c the first term in (B.36) will start to play the dominant role, once the exponential approaches its limit 1. The increment is maximum (Gendrin, 1975a,b) when

$$n_c = 2 k_2 / 3 = (2B^2 / 3\mu_0 m U_{//}^2) F(x) \quad (\text{B.37})$$

where $F(x) = (1-x)^3/x$ for e,R interactions and $(1-x)^3/x^2$ for p,L interactions. In other words there exist an optimum cold plasma density, n_c^* for which the growth rate is maximized. One can write

$$\frac{n_c^*}{n_h} = \frac{1}{3\beta_{//}} F(x) \quad (\text{B.38})$$

where $\beta_{//} = \mu_0 n_h \kappa T_{//} / B^2$ is the ratio of the parallel kinetic pressure of the hot particles to the magnetic pressure. Since the assumption has been made, in the derivation of (B.33) and (B.34), that $n_h \ll n_c$, equation (B.38) is not valid for too large value of $\beta_{//}$. A correct computation of this effect was made by Lin and Parks (1974) who dropped the assumption that $n_h \ll n_c$. Independently they found an expression which is equivalent to (B.38) and they showed that it was valid as long as $\beta_{//} < 0.1$.

But in all these computations, the intrinsic frequency dependence of γ was ignored. In order to find the optimum optimum value of n_c one must first compute the value of γ , say γ_m for which $\partial\gamma/\partial\omega = 0$ and then find the values of the parameters which lead to the largest values of γ_m (Gendrin, 1972). In other words one must compute $\partial\gamma_m/\partial n_c$ and not $\partial\gamma/\partial n_c$.

This has been done both analytically (Cuperman and Landau, 1974) and numerically (Cuperman and Salu, 1974). The two results agree and the optimum optimum cold plasma density is given by

$$1 + \frac{n_c^*}{n_h} = \frac{C}{\beta} F(\omega_c) \quad (\text{B.39})$$

where $C = 1$ for e,R interactions and where $\omega_c/2\pi$ is the critical frequency defined by (B.26). These results are shown on Figure B.7. Assuming a hot plasma density of 1 cm^{-3} , we see that the optimum cold plasma density is very low ($\sim 10 \text{ cm}^{-3}$ for $A = 0.5$ and $\sim 1 \text{ cm}^{-3}$ for $A = 1$). From the sole consideration of this effect, the plasmasphere does not seem to be the region where maximum growth rate will occur, contrary to a widely spread idea. However, taking into account the variation of n_h , A, $U_{//}$ which are associated with the inward convection of hot particles may drastically change this picture.

Similar computations have been made by Perraut and Roux (1974) for p,L interactions. The results are presented on Figure B.8. Vertical sections through this figure would give curves similar to the ones presented on Figure B.7. Let x_{opt} be the normalized frequency for which $\gamma = \gamma_{\text{max}}$ when

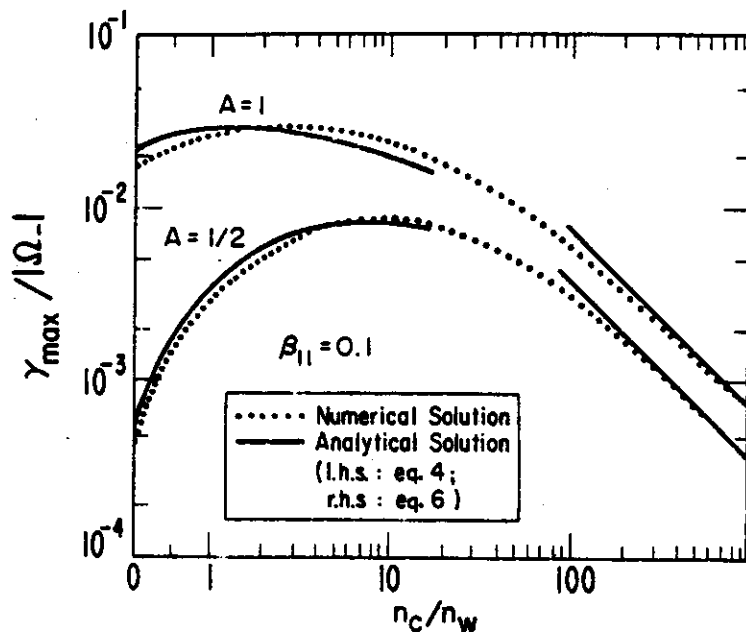


Fig. B7. Comparison of analytical and numerical predictions for the maximum growth rate $\gamma_{\max}/|\Omega_{-}|$ as a function of the ratio of cold to warm plasma density for the parameters $\beta = 0.1$ and $A = \frac{1}{2}$ and 1. Note that the horizontal scale is linear for $n_c/n_w < 1$ in order to show more effectively the cold plasma enhancement of the growth rate.

Superman and Salu, J.G.R., 79, 135, 1974.

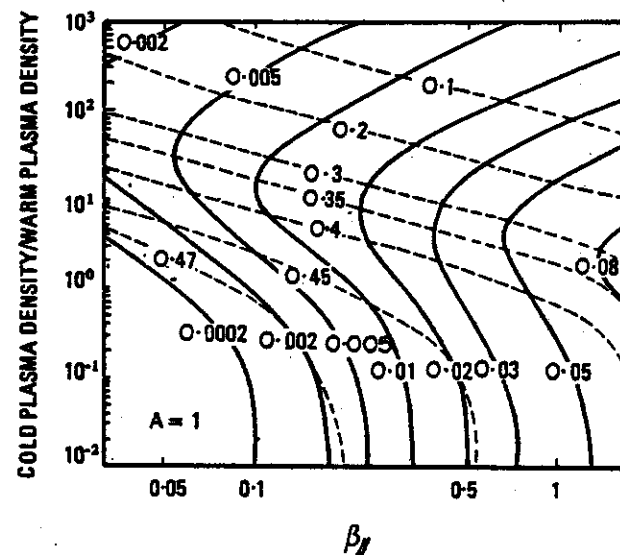


Fig. B8. Each curve represents the optimized growth rates (solid line) and the corresponding frequency (dashed line) for any set of parameters $\beta_{||}$ or n_c/n_w . Frequencies and growth rates are normalized to the proton gyrofrequency. Note that increasing β increases the growth rate. For a given $\beta_{||}$, the largest maximum growth rate corresponds to a particular value of n_c/n_w . The frequency which gives the largest maximum growth rate is found to be almost independent of the value of $\beta_{||}$ (or n_c/n_w) and of the order of $\sim 0.7A/(A+1)$.

Perraut and Roux, J.A.T.P., 37, 407, 1975.

the cold plasma density is equal to its optimum value n_c^* . For $A = \text{constant}$ Figure 2.28 shows that x_{opt} is almost constant for a wide range of variation of both n_h and n_c . For $A = 1$ one has $x_{\text{opt}} \sim 0.35 \sim 0.7 x_c$. Solomon (1974, 1975) has demonstrated that indeed x_{opt} verifies the following relation, which is valid for a wide range of n_h/n_c and B_{\parallel} :

$$x_{\text{opt}} \sim \frac{x_c}{2 - x_c} = \frac{A}{A + 2} \quad (\text{B.40})$$

The concept of optimum cold plasma density plays an important role in the design of active cold plasma injections (see discussion by Gendrin, 1975 a and references therein)

B.4. QUASI-LINEAR DIFFUSION

As said in the general introduction, waves play a negligible role in the overall energy budget of the solar wind - magnetosphere - ionosphere system, but they play a fundamental role in modifying the dynamics of particles. Under the influence of the electric and magnetic fields of the wave, the direction and (to less an extent) the amplitude of the particle velocity are changed. Since this reaction of the wave on particles depends on the phase angle of the velocity vector and since this phase is in general randomly distributed, the net result is a diffusion in both pitch angle and energy. The purpose of this section is to study these diffusion effects and to show that they are intimately related with the generation mechanism itself.

B.4.1. The diffusion curves

Let \underline{b} and \underline{E} be the magnetic and electric components of the wave. The force which is exerted on the particle is

$$\underline{F} = q \left[\underline{E} + \underline{v} \times (\underline{B} + \underline{b}) \right] \quad (\text{B.41})$$

By making use of the relation $\underline{k} \times \underline{E} = -\omega \underline{b}$ (which is valid for sinusoidal plane waves) and by considering a frame of reference moving with the wave phase velocity, equation (B.41) becomes :

$$\underline{F} = q \underline{u} \times (\underline{B} + \underline{b}) \quad (\text{B.42})$$

where $\underline{u} = \underline{v} - \underline{v}_\phi$. Since the force is orthogonal to the particle displacement, the particle energy is constant in this frame of reference (Brice, 1964). Coming back to the laboratory frame, one gets the differential equation

$$v_\perp dv_\perp + (v_\parallel - v_\phi) dv_\parallel = 0 \quad (\text{B.43})$$

The integration of (B.43), which must be done keeping in mind that v_ϕ is a function of v_\parallel , should yield the equation of the diffusion curve, D :

$$D(v_\parallel, v_\perp) = R \quad (\text{B.44})$$

Locally, equation (B.43) means that the infinitesimal variation of the velocity, $d\underline{v}$ is orthogonal to the vector \underline{WP} , W being the extremity of the phase velocity vector and P being the extremity of the particle velocity vector (Figure B.9). When $B \gg b$, it is easily seen that \underline{F} is situated in the plane defined by \underline{B} and \underline{u} , so that the diffusion proceeds along curves which are situated in the $\underline{v}_\parallel, \underline{v}_\perp$ plane. The figure has been drawn in the case of a backward interaction. The constant energy curve, E , is a circle centered at the origin. Therefore when the particle loses energy (i.e. when the wave is amplified) its pitch angle decreases ; when it gains energy (i.e. when the wave is damped) its pitch angle increases. This effect will be discussed in more detail later. Let us for the moment integrate equation (B.43), which can be written

$$v_\perp dv_\perp + (v_\parallel - v_\phi) d(v_\parallel - v_\phi) + (v_\parallel - v_\phi) dv_\phi = 0 \quad (\text{B.45})$$

This form has been chosen in order to demonstrate that the integration of (B.43) does not yield $v_\perp^2 + (v_\parallel - v_\phi)^2 = \text{constant}$ as a simplistic interpretation of the sentence "the particle energy remains constant in a frame of reference moving with the wave phase velocity" could suggest.

* In this figure and in all what follows, we assume that $\underline{k} \parallel \underline{B}$.

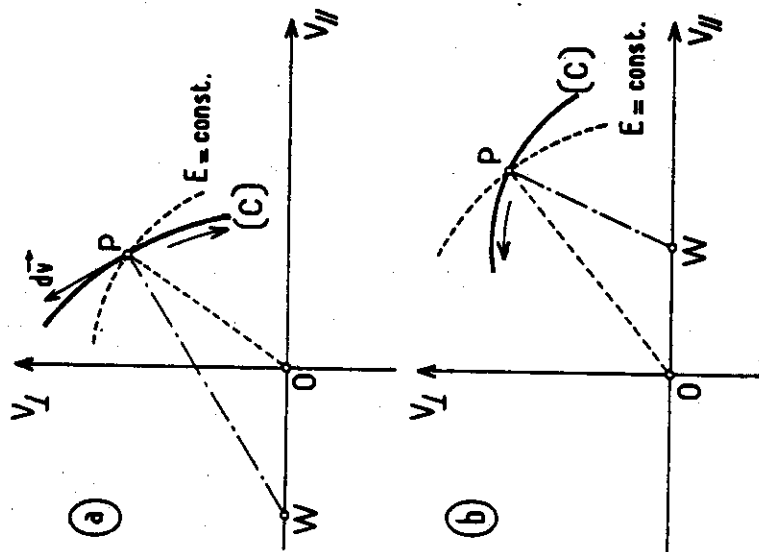


Fig. B9. Movement in velocity space of a gyroresonant particle. (a) (p, L) interaction. v_{\parallel} and v_{\perp} are opposite in sign. The pitch angle of the particle must decrease if it is to lose energy.

(b) (p, R) interaction. v_{\parallel} and v_{\perp} have the same direction. If the particle radiates energy, its pitch angle increases.

Gendrin, J. Atmosph. Terr. Phys., 30, 1313/1968.

Both v_{\parallel} and v_{\perp} being known functions of the frequency, it is possible to obtain D under the parametric form $v_{\perp} = f(\omega)$, $v_{\parallel} = g(\omega)$. The integration of (B.45) is an easy task in the case of interactions occurring in a one-component plasma and it is done below. It is more difficult in the case of multi-component plasmas (see Chapter II, section 2.4).

Let us introduce normalized quantities : $v' = v/V_a$ and $x = \omega/\omega_c$ where $V_a = V_a^+$ and $\omega_c = \omega_{ci}$ (respectively V_a^- and $|\omega_{ce}|$) when low-frequency (resp. high-frequency) waves are considered. Let us also assume that both v_{\perp} and ω are positive. From the resonance condition, one easily demonstrate that

$$v'_{\parallel} - v'_{\perp} = \epsilon v'_{\perp} / x \quad (\text{B.46})$$

where $\epsilon = -1$ for backward interactions and $\epsilon = +1$ for forward (anomalous) interactions. The wave phase velocities are expressed as (see Appendix A)* :

$$\begin{aligned} \text{L-wave, low-frequency} : v_{\perp}'^2 &= 1 - x \\ \text{R-wave, low-frequency} : v_{\perp}'^2 &= 1 + x \\ \text{R-wave, high-frequency} : v_{\perp}'^2 &= x(1 - x) \end{aligned} \quad (\text{B.47})$$

Equation (B.45) is then easily integrated and gives v_{\perp}^2 as a function of frequency. Together with (B.46) and the relevant equation (B.47) it constitutes the two parametric equations which define the diffusion curve. The formulae are given in Table B.4.

As an example, the diffusion curves obtained for p,L and p,R interactions in the low-frequency limit are represented on Figure B.10 (Gendrin, 1968). As expected, interactions with R waves exist only for $v_{\parallel} > v_{\perp} = 3/3 V_a^+/2$, a value for which the diffusion curves exhibit turning points. For interactions with L-waves, the diffusion curves noticeably differ from constant energy circles. They are more elongated along the v_{\perp} axis. This effect is more important than in the case of interaction between electrons and whistler waves. It has been invoked by Eather and Carovillano (1971)

* low-frequency means $f \lesssim 10 f_{ci}$, high-frequency means $f_{thr} < f < f_{ce}$

Table B.4

Parametric equations of the diffusion curves. Frequencies are positive

Frequency range	Normalization	Wave polarization	Interacting particles	Equations
Low ($f \leq 10 f_{ci}$)	$v' = v/V_a^+$	L	p	$v_L'^2 = C - \frac{1-x}{x^2} - L n x$
	$x = \omega/\omega_{ci}$			$v_{//}'^2 = 1 - x$
		R	p	$v_L'^2 = C - \frac{1+x}{x^2} - L n x$
				$v_{//}'^2 = 1 + x$
High ($f_{ghr} < f$)		L	e	$v_L'^2 = C - \frac{1-x}{x^2} + L n x$
				$v_{//}'^2 = 1 - x$
	$v' = v/V_a^-$ $x = \omega/ \omega_{ce} $	R	e	$v_L'^2 = C - \frac{2x^2+1}{x} + L n x$
				$v_{//}'^2 = x(1-x)$

R. GENDRIN
J. Atmosph. Terr. Phys., 30, 1313, 1968.

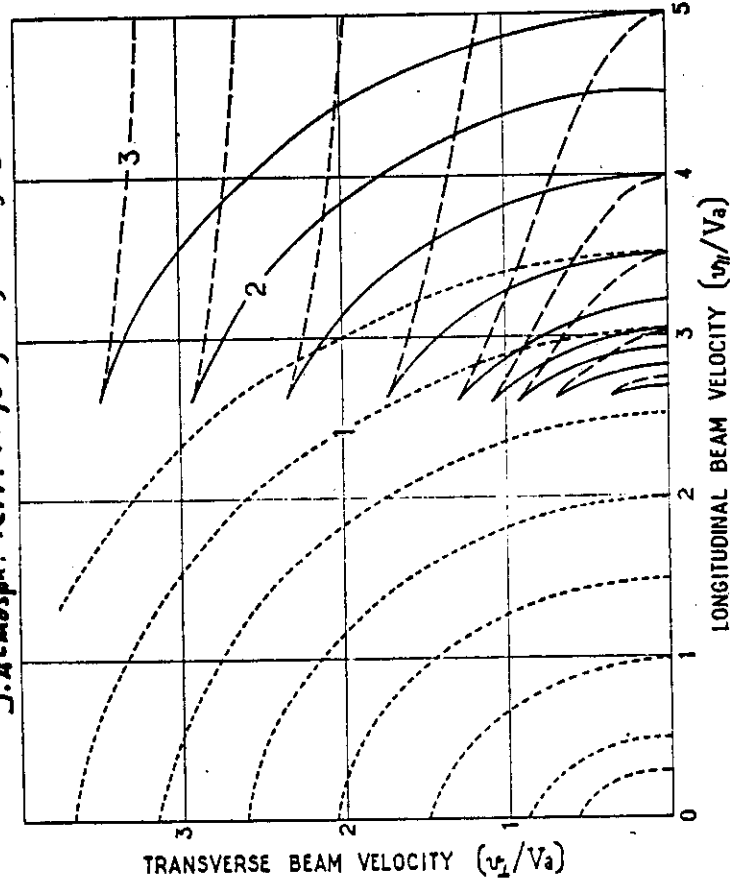


Fig. B10. Trajectories of the particles in velocity space. 1: (p, L) interactions. 2: (p, R) interactions in which the emitted frequency is less than $2F_B$. 3: (p, R) interactions in which the emitted frequency is greater than $2F_B$.

to explain the lowering of the characteristic energy of precipitated protons at auroral altitudes with respect to the characteristic energy measured in the equatorial plane.

B.4.2. Relationship between amplification and diffusion

We just showed that given the sense of the energy exchange between the wave and the particle (the wave is amplified or damped) the sense of the particle pitch angle variation is determined (and vice-versa). We will now demonstrate that, given the shape of the distribution function ($T_{\perp} > T_{\parallel}$ or $T_{\parallel} < T_{\perp}$ for instance) the sense of the particle pitch angle variation is determined. The direction in which the energy is converted (from the particle to the wave or from the wave to the particle) is therefore deduced. The demonstration of this property will be done first. Then it will be applied to the study of interactions for different types of distribution functions.

Let us introduce the iso-density curves, that is curves in the v_{\parallel}, v_{\perp} plane along which the distribution function $f(v_{\parallel}, v_{\perp})$ is constant. Let us consider three of these curves (F_1, F_2 and F_3) and, for the purpose of illustration, let us assume that the density in the phase space is smaller for higher values of the velocity (Figure B.11).

The diffusion which is induced by the wavefield is a stochastic process. If the wave has a finite spectrum, corresponding to a finite range of Δv_{\parallel} , particles will diffuse in both directions along the diffusion curve D . But because there are more particles in A_1 than in A_2 the integrated result (over Δv_{\parallel}) corresponds to a net displacement in the direction of the lower density region. In other words, given the iso-density curves (and the direction of their gradient, which is generally inward) and the diffusion curve, it is possible to know the direction in which particles move as a consequence of their quasi-linear interactions with the wave. One immediately sees that depending on the relative positions of the curves F and D , the particle pitch angle will decrease (Figure B11b) or increase (Figure B11c) as is shown by the arrows.

Knowing the direction of the displacement along D , one can see if the particle gains or loses energy by introducing the constant-energy curve,

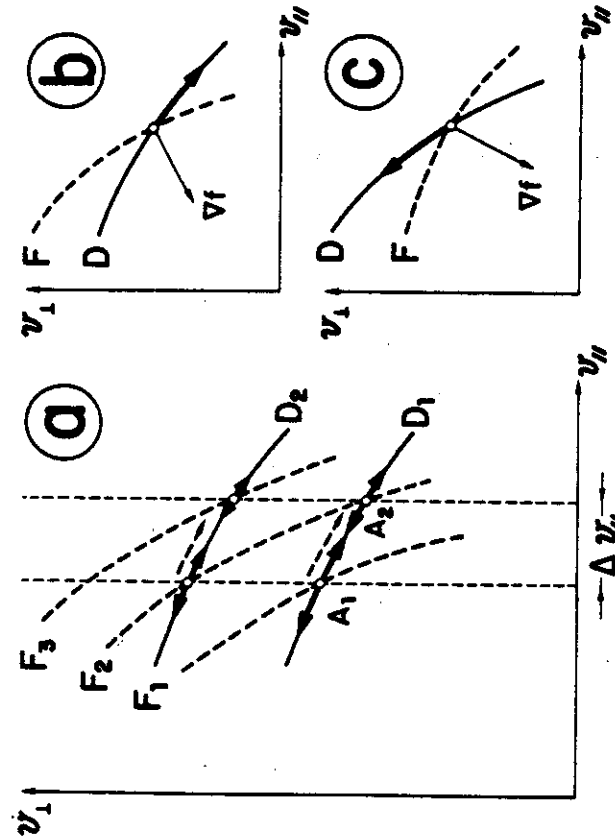


Fig. B.11. Pitch angle variation during a wave-particle interaction (WPI). The particle distribution function is assumed to be 'regular' (i.e., with an inward gradient ∇f). (a) Since there are more particles in A_1 than in A_2 , the diffusion in the velocity range Δv_{\parallel} is equivalent to a net displacement toward lower pitch angles. (b) WPI leading to a pitch angle decrease. (c) WPI leading to a pitch angle increase.

Gendrin, *Rev. Geophys. Space Phys.*, 19, 171, 1981

E, which is a circle centered at the origin. Therefore the nature of the interaction ($\gamma > 0$ or $\gamma < 0$) can be determined if the relative position in the v_{\parallel}, v_{\perp} plane of

- the iso-density curve, F
- the diffusion curve, D
- the constant-energy curve, E

is known (Gendrin, 1981). For 'regular' distributions, i.e. distributions for which F is concave around the origin, waves are amplified if the D curve is situated inside the area delineated by the F and E curves. The eight possible configurations which may occur for that kind of distributions are described on Figure B.12 (on this figure, $\gamma > 0$ means that waves are amplified). This figure provides a simple physical definition of the critical anisotropy. A_c is the anisotropy of a distribution for which the iso-density curve is locally coincident with the diffusion curve. The growth rate γ is then equal to zero. However in order that $\gamma = 0$ at the frequency which corresponds to a given v_{\parallel} , this property must be satisfied for all v_{\perp} associated with this v_{\parallel} (see below). Figure B.12 also shows that the forward interaction ($v_{\phi} > v_{\parallel}$) always leads to wave absorption. In Figure B.12 the anisotropy is defined qualitatively, the limit $A = A_c$ being the one for which $F \equiv D$ (locally) and the limit $A = 0$ being the one for which $F \equiv E$ (locally). The consequences of, and conditions for, wave amplification and wave diffusion are summarized in Table B.5.

It is worth noticing that the diffusion mechanism proceeds in such a way that it tends to suppress the cause of the emission. For instance in backward interactions waves are generated when, at a given energy, there are more particles with large pitch angles than particles with small pitch angles: $A > A_{c1} > 0$. Because of the diffusion the pitch angle α decreases so that A decreases. In the absence of particle injection and of wave absorption the process will stop when A will reach the critical anisotropy A_{c1} . A similar argument can be developed for forward (anomalous) interactions: initially $A < A_{c2}$, but α increases so that A increases until it reaches the critical value for which $\gamma = 0$.

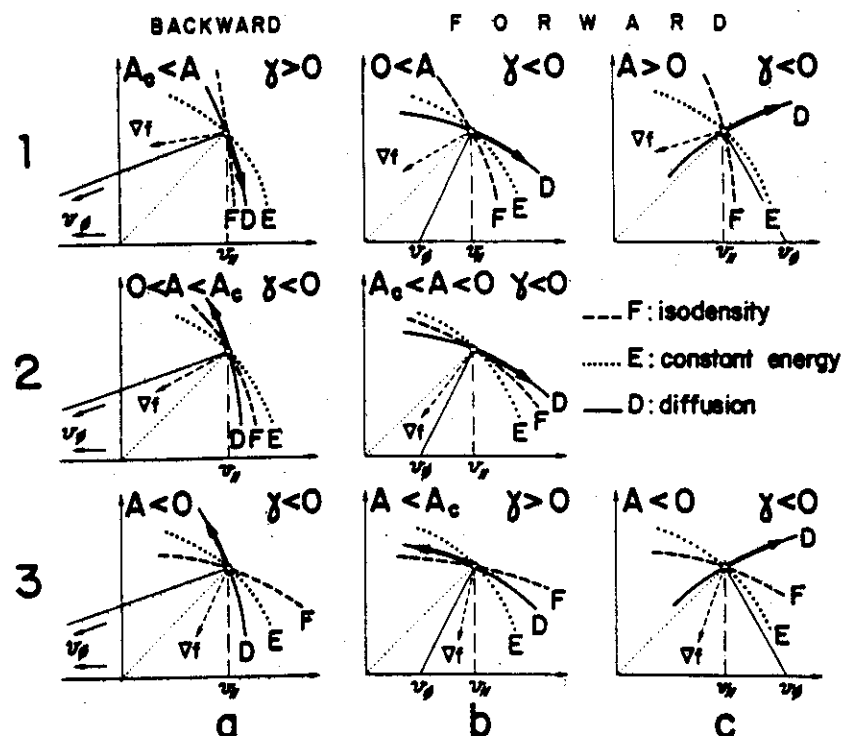


Fig. B.12. The eight possible configurations for an interaction involving a 'regular' distribution. (a) Backward interaction ($v_{\parallel} \cdot v_{\phi} < 0$). (b) Forward interaction with $v_{\phi} < v_{\parallel}$. (c) Forward interaction with $v_{\parallel} < v_{\phi}$. Cases 1, 2, and 3 correspond to different values of the 'anisotropy,' that is, to different relative configurations of curves D, E, and F; $\gamma > 0$ corresponds to an amplification, and $\gamma < 0$ to an absorption.

Gendrin, *Rev. Geophys. Space Phys.*, 19, 171, 1981.

Table B.5

Consequences of, and conditions for wave amplification or absorption ('Regular' distributions only). α is the particle pitch angle

INTERACTION	AMPLIFICATION		ABSORPTION	
	CONSEQUENCE	CONDITION	CONSEQUENCE	CONDITION
Backward	$\alpha \searrow$	$A > A_{C1} > 0$	$\alpha \searrow$	$A < A_{C1}$
Forward (normal)		amplification is impossible	$v_{\perp}^2 < v_{\parallel} (v_{\phi} - v_{\parallel}) : \alpha$ $v_{\perp}^2 > v_{\parallel} (v_{\phi} - v_{\parallel}) : \alpha$	no condition for regular distributions
Forward (anomalous)	$\alpha \searrow$	$A < A_{C2} < 0$	$\alpha \searrow$	$A > A_{C2}$

The criteria concerning the relative configuration of curves D, E and F is easily transformed into criteria involving the relative position on the v_{\parallel} axis of three characteristic points : 1) the origin, which is the center of curve E ; 2) the extremity of the phase velocity vector, which is the instantaneous center of the curve D ; 3) the point where the normal to the curve F cuts the v_{\parallel} axis. Let X be the abscissa of this last point. For bi-maxwellian distributions it is easily shown that

$$X = -A v_{\parallel} \quad (B.48)$$

where $A = U_{\perp}/U_{\parallel} - 1$, so that X does not depend on v_{\perp} : if γ is positive (or negative) for a specific value of $v_{\parallel 0}$, $v_{\perp 0}$, it remains so for all values $v_{\parallel 0}$, v_{\perp} . Assuming $v_{\phi} < 0$ and $v_{\parallel} > 0$, examination of Figure B.12 (1a) shows that amplification occurs if

$$X < v_{\phi} \quad (B.49)$$

Since, for backward interactions $v_{\parallel} = v_{\phi} (x-1) / x$ (equation (B.46)), condition (B.49) is equivalent to

$$A > A_c = \frac{x}{1-x} \quad (B.50)$$

which is identical to (B.27). Therefore geometrical considerations not only yield a simple physical definitions of the critical anisotropy, they also yield the concept of critical frequency. However, this demonstration of the existence of a critical frequency is based upon an assumption on the shape of the distribution function, whereas Kennel and Petschek's (1966) demonstration of equation (B.50) is valid for all types of distributions.

The same geometrical method may be applied to beams of particles, defined by

$$f(v_{\parallel}, v_{\perp}) \equiv \frac{n}{\pi^{3/2} U_{\perp}^2 U_{\parallel}} \exp \left[-\frac{v_{\perp}^2}{U_{\perp}^2} - \frac{(v_{\parallel} - U_0)^2}{U_{\parallel}^2} \right] \quad (B.51)$$

or to rings of particles, defined by

$$f(v_{\parallel}, v_{\perp}) \equiv \frac{n}{\pi^{3/2} U_{\perp}^2 U_{\parallel}} \exp \left[- \frac{(v_{\perp} - V_0)^2}{U_{\perp}^2} - \frac{v_{\parallel}^2}{U_{\parallel}^2} \right] \quad (B.52)$$

The case of beams is illustrated on Figure (B.13) where $\gamma > 0$ means amplification. Depending on the value of the anisotropy and of the ratio U_0 / U_{\parallel} , waves are amplified or absorbed. Emission may even occur in both modes (backward and forward) simultaneously. This has been demonstrated quantitatively (Perraut, 1974) by computing analytically the growth rate coefficient γ for proton interactions (Figure B.14). Simultaneous generation of LH and RH waves can occur, a point which is discussed in Chapter II (Section 2.2.3).

For ring distributions, the problem is more complex and, generally, it cannot be solved by geometry (Gendrin, 1981 a).

B.4.3. Analytical formulation

The above geometrical consideration show that amplification or absorption are related with the sign of the variation of f with energy, along the diffusion curve. This can be demonstrated analytically, the starting equation for computing both the wave amplification and the particle diffusion being the Boltzman - Vlasov equation

$$\left[\frac{\partial}{\partial t} + \underline{v} \cdot \underline{\nabla}_x + \frac{\underline{F}}{m} \cdot \underline{\nabla}_v \right] f = 0 \quad (B.53)$$

The last term of this equation can be written

$$\left[\underline{u} \times (\underline{B} + \underline{b}) \right] \cdot \underline{\nabla}_v f = \left[\underline{\nabla}_v f \times \underline{u} \right] \cdot (\underline{B} + \underline{b}) \quad (B.54)$$

which means that the quantity that plays a role is the derivative of f along the diffusion curve D (since \underline{u} is orthogonal to D). Taking into account equation (B.43) which defines D , one introduces the operator

$$\mathcal{Q} \equiv \frac{\underline{\nabla}_v \times \underline{u}}{|\underline{u}|} = (v_{\parallel} - v_{\phi}) \frac{\partial}{\partial v_{\perp}} - v_{\perp} \frac{\partial}{\partial v_{\parallel}} \quad (B.55)$$

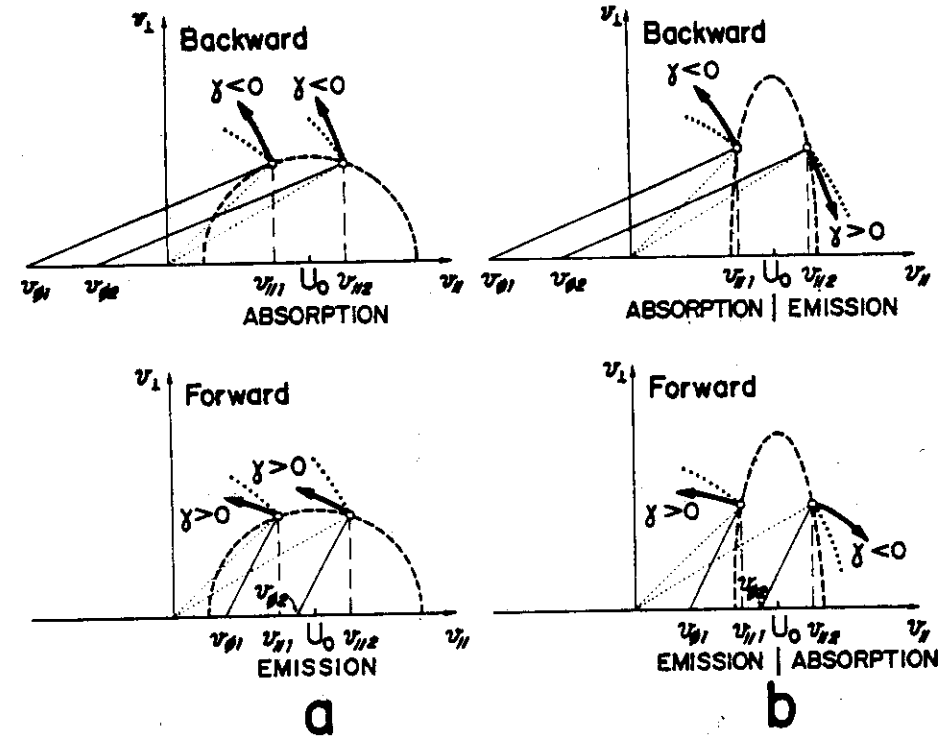
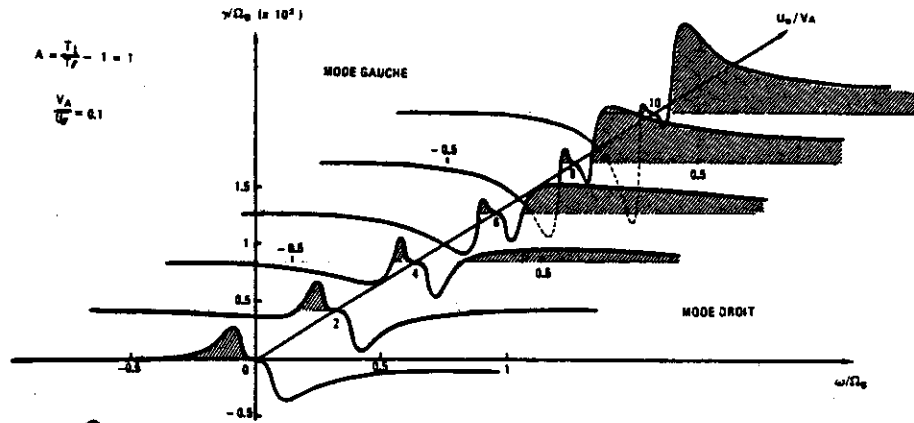
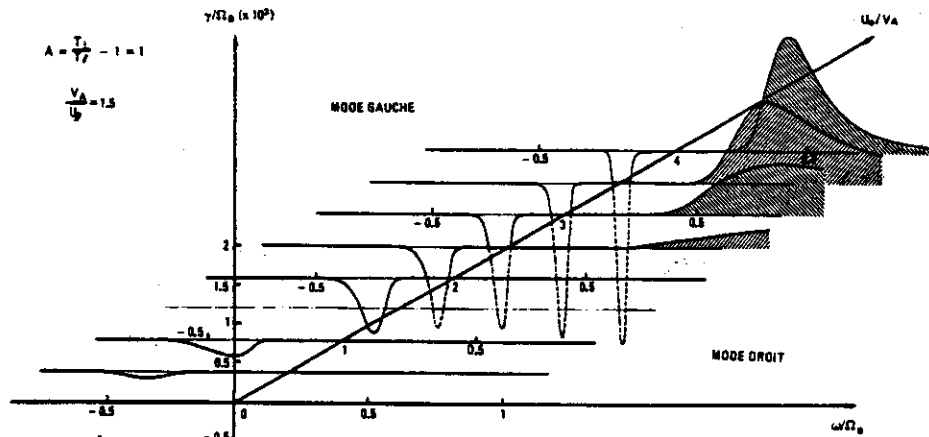


Fig.B13. Interaction properties of a field-aligned beam. The dashed, dotted, and solid curves correspond to the isodensity, constant energy, and diffusion curves, respectively. (a) The ratios U_0/U_{\parallel} and $A = U_{\perp}/U_{\parallel}$ are not too large. We have an absorption for a backward interaction and an emission for a forward interaction. (b) The ratios U_0/U_{\parallel} and $A = U_{\perp}/U_{\parallel}$ are not too small. It is possible to have an emission on both modes simultaneously: low frequencies (large v_{\parallel}) are excited in the backward interaction, and high frequencies (low v_{\parallel}) in the forward interaction.

Gendrin, Rev. Geophys. Space Phys., 19, 171, 1981



a. Variation of the amplification coefficient (normalized to the proton gyropulsation) as a function of the normalized frequency for different values of the ratio U_0/V_e . The right-hand (left-hand) part of the figure corresponds to right-hand (left-hand) waves. When U_0/V_e is not too large or too small, significant amplification may occur in both modes. The ratio of the beam density to the cold plasma density is equal to 10^{-3} [after *Perraut*, 1974].



b. Same as a except that U_0/V_e has been decreased. Significant amplification occurs only in the right-hand mode for large values of the ratio U_0/V_e . Note that since the scales are linear, a very small amplification or absorption is not visible [after *Perraut*, 1974].

Fig. B 14

which appears in the formula giving γ (see the term in brackets in equation (B.15)). For instance it can be shown (*Gendrin*, 1981) that for p,L interactions one has

$$\gamma' = -\pi^2 \frac{\omega_{pi}^2}{\omega^2} \cdot \frac{v_g v_\phi}{2c^2} \int_0^\infty v_\perp^2 dv_\perp Qf \Big|_{v_\parallel = v_r} \quad (B.56)$$

where ω_{pi} is the ion angular plasma frequency and v_g is the wave group velocity. It is clear that the physical variables are not v_\parallel and v_\perp but

- R , which defines the diffusion curves (equation (B.44)),

- $E = v_\perp^2 + v_\parallel^2$, which defines the energy.

Therefore one introduces

$$F(E, R) \equiv f[v_\parallel(R, E), v_\perp(R, E)] \quad (B.57)$$

Since

$$\left. \begin{aligned} \partial E / \partial v_\perp &= 2v_\perp & \partial E / \partial v_\parallel &= 2v_\parallel \\ \partial R / \partial v_\perp &= v_\perp & \partial R / \partial v_\parallel &= v_\parallel - v_\phi \end{aligned} \right\} \quad (B.58)$$

one has

$$Qf \equiv -2v_\perp v_\phi \partial F / \partial E \quad (B.59)$$

from which one deduces

$$\gamma' = -\pi^2 \omega_{pi}^2 \frac{(1-x)}{x} v_g \int_0^\infty dv_\perp v_\perp^3 \frac{\partial F}{\partial E} \Big|_{v_\parallel = v_r} \quad (B.60)$$

For backward interactions $v_g < 0$ when $v_\parallel > 0$. Therefore the necessary condition for amplification to occur ($\gamma' > 0$) is that $\partial F / \partial E$ be positive, at least for some range of v_\perp values. This is exactly the conclusion which we arrived at in the previous section. Let us for instance consider the case which is represented on Figure B.12.a.1. When R is kept constant (i.e. when

the particle moves along the D curve) $\partial F/\partial E$ is positive since F decreases when E decreases (or it increases when E increases). On the contrary, in the situations represented by cases a.2 or a.3 for which γ' is negative, $(\partial F/\partial E)_R$ is negative.

Equation (B.60) looks very simple, but it has no practical application since it is not possible to compute $(\partial F/\partial E)_R$, the diffusion curves being obtained in parametric form only. Equation (B.56) is the only one which can be used in practice.

B.4.4. Diffusion coefficients

The displacement of the velocity vector in the $v_{//}$, v_{\perp} plane being known for all particles, it is possible to compute the temporal change of the distribution function $f(v_{//}, v_{\perp})$. By analogy with spatial (not velocity) diffusion processes in inhomogeneous media, one has $\partial f/\partial t = -\nabla \cdot \underline{j}$ where \underline{j} is the flow induced by diffusion in the presence of a density gradient: $\underline{j} = -D \nabla f$ where D is the diffusion coefficient. So that one expects an equation of the form:

$$\frac{\partial f}{\partial t} = \nabla \cdot (D \nabla f) \quad (B.61)$$

Indeed it is possible to develop the Boltzman - Vlasov equation (B.53) up to the first order in the wave field, assuming that $f = f_0 + f_1$ with f_0 homogeneous and f_1 , the perturbation of the distribution function, being small with respect to f_0 . This leads to the following set of equations

$$\left[\frac{\partial}{\partial t} + \underline{v} \cdot \nabla + \frac{q}{m} (\underline{v} \times \underline{B}) \cdot \frac{\partial}{\partial \underline{v}} \right] f_1 = -\frac{q}{m} \left[\underline{E} + \underline{v} \times \underline{b} \right] \cdot \frac{\partial f_0}{\partial \underline{v}} \quad (B.62)$$

$$\left[\frac{\partial}{\partial t} + \frac{q}{m} (\underline{v} \times \underline{B}) \cdot \frac{\partial}{\partial \underline{v}} \right] f_0 = -\frac{q}{m} \left[\underline{E}^* + \underline{v} \times \underline{b}^* \right] \cdot \frac{\partial f_1}{\partial \underline{v}}$$

The first equation is the one which gives the dispersion relation (including the imaginary terms associated with wave amplification) whereas the second ones, in which appear the complex conjugates \underline{E}^* and \underline{b}^* , gives the diffusion equation. The mathematical procedure is described in detail for gyroresonant interactions by Gendrin (1968). One obtains:

$$\frac{\partial f}{\partial t} = \frac{1}{v_{\perp}} \mathcal{Q} [v_{\perp} D \mathcal{Q} f] \quad (B.63)$$

where \mathcal{Q} is the operator defined by equation (B.55) and where

$$D = \pi \cdot \frac{\omega_c^2}{|v_{//} - v_g|} \frac{b_k^2}{B^2} \quad (B.64)$$

In this expression $b_k^2 = v_g b_p^2/2\pi$ is the power density per unit wave number (b_p^2 is the usual power spectral density per unit frequency)*. As expected the diffusion coefficient is proportional to the power density. It is also inversely proportional to $v_{//} - v_g$. Sometimes v_g is omitted. Such an approximation is justified for e,R interactions, but only in the low frequency part of the spectrum ($\omega \ll \omega_c$). For $\omega = |\omega_{ce}|/2$ for instance $v_g = v_{//} = v_a^-/2$ (see Table B.2). For p,L interactions, v_g cannot be neglected since $v_g \sim v_a^+$ and $U_{//} \sim v_a^+$.

Except for numerical errors, neglecting v_g with respect to $v_{//}$ has no fundamental consequences in the case of backward interactions since v_g and $v_{//}$ have opposite signs. The situation is different in the case of forward interactions since the denominator of (B.64) may become equal to zero. This is the case for instance for p,R interactions when $|\omega| \sim 2\omega_{ci}$ and $v_{//} = u_1$ as defined by (B.12). This is also the case for interactions involving He^+ ions and proton cyclotron waves (see Chapter II, Section 2.4). In both cases, $v_{//} = v_g$ defines the turning points of the diffusion curves. The diffusion coefficient becomes very large, the infinity being removed when inhomogeneity effects are taken into account.

* Formulae in Gendrin (1968) have been corrected for some numerical factors.

When $v_{\perp} \ll v_{\parallel}$ the diffusion in energy can be neglected. In that case equations (B.24) and (B.55) show that Q reduces to

$$Q = \frac{\partial}{\partial \alpha} \quad (B.65)$$

so that the diffusion equation corresponds to a pure pitch angle diffusion equation

$$\frac{\partial f}{\partial t} = \frac{1}{\sin \alpha} \frac{\partial}{\partial \alpha} \left(D \sin \alpha \frac{\partial f}{\partial \alpha} \right) \quad (B.66)$$

which is the equation first introduced by Kennel and Petschek (1966) in the field of magnetospheric physics. Such a situation occurs for e, R interactions involving low frequencies $\omega \ll |\omega_{ce}|$, as stated above. In the case of p, R interactions the diffusion in energy cannot be neglected (Gendrin, 1968; Eather and Carovillano, 1971).

The above formulae were obtained by assuming a strictly parallel propagation for the wave. But when the wave normal angle θ is not equal to zero, all possible resonances $\omega = n\omega_c + kv_{\parallel}$ where $n = 0, \pm 1, \pm 2, \dots$ must be taken into account. This has been done by Lyons (1974) who has introduced four diffusion coefficients. Indeed, equation (B.61) becomes in a spherical coordinate system :

$$\begin{aligned} \frac{\partial f}{\partial t} = & \frac{1}{v \sin \alpha} \frac{\partial}{\partial \alpha} \left(D_{\alpha\alpha} \cdot \frac{1}{v} \frac{\partial f}{\partial \alpha} + D_{\alpha v} \frac{\partial f}{\partial v} \right) \\ & + \frac{1}{v^2} \frac{\partial}{\partial v} \left(v^2 \left(D_{v\alpha} \cdot \frac{1}{v} \frac{\partial f}{\partial \alpha} + D_{vv} \frac{\partial f}{\partial v} \right) \right) \end{aligned} \quad (B.67)$$

It is easily shown that $D_{\alpha v} = D_{v\alpha}$. Lyons (1974) has computed $D_{\alpha\alpha}$, $D_{\alpha v}$ and D_{vv} for both e, R and p, L interactions, for different values of the plasma parameters and for different wave normal distributions. He has shown that in general $D_{\alpha\alpha} > |D_{\alpha v}| > D_{vv}$, the ratio $D_{\alpha\alpha} / D_{vv}$ being of the order of 10^3 for e, R interactions. $D_{\alpha v}$ is often positive but it may be negative for some ranges of wave normal directions. The different modes $n = \pm 1, \pm 2, \dots$ contribute for $\sim 10\%$ to the total value of D .

In practice the exact computation of the diffusion coefficients is difficult and rough approximations are used. One way of proceeding is to use the equivalence between the diffusion equation and the Fokker-Planck equation (Kennel and Petschek, 1966). In doing so one obtains

$$D_{\alpha\alpha} = \frac{\langle (\Delta\alpha)^2 \rangle}{2\Delta t} \quad (B.68)$$

where $\langle (\Delta\alpha)^2 \rangle$ is the mean quadratic excursion in pitch angle over the time Δt . To the lowest order $\langle \Delta\alpha \rangle = 0$ since the particle velocity vectors are randomly distributed in phase with respect to the wave field. Since $\tan \alpha = v_{\perp}/v_{\parallel}$ and $v^2 = v_{\perp}^2 + v_{\parallel}^2$ one gets

$$d\alpha = - \frac{dv_{\parallel}}{v_{\perp}} - \tan \alpha \frac{dv}{v} \quad (B.69)$$

which reduces to

$$d\alpha = - \frac{dv_{\parallel}}{v_{\perp}} \quad (B.70)$$

when the energy variation is neglected (e, R interactions with $\omega < |\omega_{ce}|$). In a homogeneous medium ($\partial B/\partial z = 0$) there is no adiabatic effect since $E_{\parallel} = 0$. The variation of v_{\parallel} is solely due to the action of the magnetic field of the wave :

$$dv_{\parallel} = \frac{q v_{\perp} b}{m} dt \quad (B.71)$$

which can be written

$$dv_{\parallel} = \omega_c \left(\frac{b}{B} \right) dt \quad (B.72)$$

so that

$$D_{\alpha\alpha} = \frac{\omega_c^2}{2} \left(\frac{b}{B} \right)^2 \Delta t \quad (B.73)$$

The time Δt can be evaluated as the time during which particles which resonate with a wave defined by ω and k remains in resonance with

wave defined by ω and k remains in resonance with waves having a slightly different frequency or wave number. The end of resonance is evaluated when $\delta\phi = 2\pi$ with

$$\delta\phi = \delta(\omega - \omega_c - kv_{\parallel}) \Delta t = (\delta\omega - v_{\parallel} \delta k) \Delta t \quad (B.74)$$

But $\delta\omega = v_g \delta k$ so that

$$|\Delta t| = 2\pi / |v_g - v_{\parallel}| \delta k \quad (B.75)$$

and

$$D_{\alpha\alpha} \sim \frac{\pi \omega_c^2}{|v_{\parallel} - v_g|} \left(\frac{b_k}{B} \right)^2 \quad (B.76)$$

in which $b^2 = b_k^2 \delta k$ is the wave energy contained within the wave number range δk and b_k^2 is the wave power density per unit wave number*. Neglecting v_g as compared with v_{\parallel} , one gets the Kennel and Petschek's (1966) evaluation.

$$D_{\alpha\alpha} \sim \pi \omega_c k^* \left(\frac{b_k}{B} \right)^2 \quad (B.77)$$

where $k^* = \omega_c / v_{\parallel}$ is a characteristic wave number associated with the particle parallel velocity. The comparison between equations (B.64) and (B.76) shows that the rough evaluation gives a correct insight within the physical process of pitch angle diffusion.

Orders of magnitude for $L = 6.6$ can be evaluated. At $L = 6.6$, $B \sim 100\gamma$, $f_{ci} \sim 1.5$ Hz, $f_{ce} \sim 3$ kHz, $V_a^+ \sim 10^6$ m.s⁻¹, $V_a^- \sim 4 \times 10^7$ m.s⁻¹. Let us assume an interaction taking place at $\omega = \omega_c/2$ so that $v_{\parallel} = -v_g$. Equation (B.76) becomes

$$D \sim (\pi f_c b_f / B)^2$$

In the ULF range, a typical value for the spectral density observed at the geostationary orbit is $1\gamma \cdot \text{Hz}^{-1/2}$, so that $D \sim 2 \times 10^{-3} \text{ s}^{-1}$. In the VLF range, $b_f \sim 1 \text{ m}\gamma \cdot \text{Hz}^{-1/2}$ so that $D \sim 10^{-2} \text{ s}^{-1}$. These values are sufficient to put the particles in the strong diffusion limit (see next section).

* For a practical evaluation of D , one uses the power spectral density (the power per unit frequency bandwidth) $b_f^2 = 2\pi b_k^2 / v_g$, since this is the experimentally measured quantity.

B.4.5. The self consistent equilibrium

If the particle distribution function is such that the amplification is positive (for instance if $A > A_c$ for backward interaction) and if there is no loss mechanism for the wave (infinite medium) the wave will grow. But the quasi-linear effects act in such a way that the difference between A and A_c decreases, as explained in Section B.4.2. In the absence of a particle source, A will tend towards A_c , γ will tend towards zero and the wave field reach a final intensity which can be computed as a function of the initial anisotropy and of the ratio U_{\parallel} / V_a (i.e. Rowlands et al., 1966).

But the magnetospheric situation is different. Waves can escape from the region where they are generated and new particles can be injected continuously. The following set of equations must be solved

$$\frac{\partial f}{\partial t} = \frac{1}{v_{\perp}} Q [v_{\perp} D Q f] + S - L \quad (B.78)$$

$$\frac{\partial b_k^2}{\partial t} + v_g \frac{\partial b_k^2}{\partial z} = 2\gamma b_k^2 \quad (B.79)$$

where D is expressed as a function of the wavefield intensity b_k (equation (B.64)) and where γ is expressed as a function of the distribution function f (equation (B.21) et seq.)*. S and L are particle source and loss terms. The complexity of the coupling between the two equations is obvious, even if one works the time-independent problem ($\partial/\partial t = 0$), i.e. the equilibrium configuration. The first attempt to solve this system of two equations was made by Kennel and Petschek (1966) in the case of e,R interactions. In this attempt the basis physical processes are described and important concepts are introduced so that it is worth spending some time to explain it.

First, equation (B.78) is simplified by neglecting the diffusion in energy, so that the expression (B.65) may be used :

$$\frac{1}{\sin\alpha} \frac{\partial}{\partial\alpha} \left[\sin\alpha D \frac{\partial f}{\partial\alpha} \right] + S - L = 0 \quad (B.80)$$

* In this section, $\gamma > 0$ means amplification so that the sign of eq. (B.21) has to be changed.

Second, equation (B.79) is also replaced by an equilibrium equation : it is assumed that a fraction of the wave energy is reflected by the ionosphere and comes back into the interaction region. Let R be the ionospheric reflexion coefficient and τ the time that the wave spend in the interaction region :

$$\tau = \mathcal{L}/v_g \quad (\text{B.81})$$

where \mathcal{L} is the length of the interaction region, usually a fraction of the field line length. The equilibrium is reached when

$$R e^{Y\tau} = 1 \quad (\text{B.82})$$

Let us compute the value of γ which is needed to maintain such an equilibrium configuration. Usually one assumes that $\mathcal{L} = L R_e$ (that is half the length of the field line) and $R = 0.1$. Assuming that $v_g \sim 1000 \text{ km.s}^{-1}$ in the ULF range and $L = 4$, one gets $\tau \sim 20 \text{ s}$ and $\gamma_{eq.} \sim 0.1 \text{ s}^{-1}$ which corresponds to $\gamma/\omega_{ci} \sim 2 \times 10^{-3}$ for $f_{ci} \sim 10 \text{ Hz}$. This is a rather high value in the ULF range (see for instance Figures 2.19 and 2.20 in Chapter II). In the VLF range, the equilibrium value of γ/ω_{ce} is much smaller since v_g is only $\sqrt{m^*} \sim 40$ times larger whereas ω_c is m^* times larger (m^* being the mass ratio between protons and electrons). One has $\gamma/\omega_{ce} \sim 5 \times 10^{-5}$ which is easily achieved (see for instance Figure 2.21 in Chapter II).

In any case these values of γ have to be maintained. In the absence of particle injection this would not be possible since by quasilinear processes γ would revert to zero. Consequently a source of particles has to be assumed. The problem is still simplified by assuming that the source exists only for high pitch angles, whereas the losses operate only for low pitch angles. Equation (B.80) is divided into two equations, one of which is valid outside the loss cone, the other one inside the loss cone. Let us consider that one first and let us introduce the particle escaping time

$$T_e \sim L R_e / v_{||} \quad (\text{B.83})$$

which corresponds to a quarter bounce period. The losses are equal to f/T_e so that, inside the loss cone which is defined by $\alpha_0 \ll 1$, one has :

$$\frac{1}{\alpha} \frac{\partial}{\partial \alpha} \left(D \alpha \frac{\partial f}{\partial \alpha} \right) - \frac{f}{T_e} = 0 \quad (\text{B.84})$$

If the wave spectrum is independent of frequency D is a constant and the solution of this equation is

$$f(\alpha, v) = H(v) I_0(z) \quad (\text{B.85})$$

where $z = \alpha / \sqrt{DT_e}$, I_0 is the modified Bessel function of the first kind and where $H(v)$ is an arbitrary function which will be fixed by matching the solution outside the loss cone for $\alpha = \alpha_0$. Outside the loss cone losses are negligible and one has

$$\frac{1}{\sin \alpha} \frac{\partial}{\partial \alpha} \left(D \sin \alpha \frac{\partial f}{\partial \alpha} \right) = s(\alpha, v) \quad (\text{B.86})$$

where $s(\alpha, v)$ is the source term. Assuming that $s = \delta(\alpha - \pi/2)$ i.e. that particles are injected only at 90° pitch angles, Kennel and Petschek (1966) obtained the solution inside and outside the loss cone

$$\left. \begin{aligned} f_i &= \frac{s(v)}{D} \cdot \frac{I_0(z)}{z_0 I_1(z_0)} \\ f_o &= \frac{S(v)}{D} \cdot \left\{ \frac{I_0(z_0)}{z_0 I_1(z_0)} + \text{Ln} \frac{\sin \alpha}{\sin \alpha_0} \right\} \end{aligned} \right\} \quad (\text{B.87})$$

In these equations $S(v)$ is the rate at which particles are injected and is therefore the precipitation flux (at equilibrium). The life time T_L is the ratio of the total number of trapped particles (i.e. the integral of $f_o \sin \alpha d\alpha$ between α_0 and $\pi/2$) to $S(v)$:

$$T_L \sim \frac{1}{D} \left[\frac{I_0(z_0)}{z_0 I_1(z_0)} - \text{Ln} \left(e \tan \frac{\alpha_0}{2} \right) \right] \quad (\text{B.88})$$

The parameter

$$z_0 = \alpha_0 / \sqrt{DT_e} \quad (\text{B.89})$$

defines the strength of the diffusion. Weak diffusion corresponds to $z_0 \gg 1$. In that case, because of the exponential factor in the asymptotic expansion ($I_0(z) \sim I_1(z) \sim (2\pi z)^{-1/2} \exp[z]$ when $z \rightarrow \infty$), the distribution function f_1 increases exponentially in the vicinity of the loss cone. The corresponding lifetime is

$$T_{LW} \sim \frac{1}{D \ln(2/e\alpha_0)} \quad (B.90)$$

when $\alpha_0 \ll 1$. In this regime the lifetime depends primarily on wave intensity and only logarithmically on the size of the loss cone.

In the strong diffusion limit ($z_0 \ll 1$), $I_0(z_0) \sim 1$ and $I_1(z_0) \sim z_0/2$, so that the pitch angle distribution is isotropic within the loss cone and almost isotropic outside. The lifetime is independent of the wave intensity and depends only on the size of the loss cone. It is equal to the minimum lifetime

$$T_{LS} \sim T_m = \frac{2T_e}{\alpha_0^2} \quad (B.91)$$

The lifetime can be related to the ratio of the mean directional intensity of the particle flux outside the loss cone, $\langle J_T \rangle$ (i.e. the trapped particles) to the mean directional intensity within the loss cone $\langle J_p \rangle$ (i.e. the precipitated particles). The total flux of trapped particles, within one hemisphere, is $N = 2\pi \langle J_T \rangle$. The total flux of precipitated particles, within one hemisphere, is $\pi\alpha_0^2 \langle J_p \rangle$. Since the lifetime of particles within the loss cone is T_e , the flux of particles with crosses the loss cone boundary per unit time because of diffusion is $j = \pi\alpha_0^2 \langle J_p \rangle / T_e$. By definition

$$T_L = N/j \quad (B.92)$$

so that

$$\frac{\langle J_p \rangle}{\langle J_T \rangle} = \frac{T_m}{T_L} \quad (B.93)$$

which shows that in strong diffusion ($T_L \rightarrow T_m$) there is complete isotropy in the particle distribution (Coroniti and Kennel, 1970).

The two equations (B.87) allow to compute all the characteristics of the distribution function provided a specific form for the energy dependence of $S(v)$ is assumed. In particular, the anisotropy can be computed. One finds

$$A \sim (-2 \ln \alpha_0)^{-1} \quad (B.94)$$

which is of the order of 0.15 for auroral field lines. The growth rate for the waves can be evaluated. Assuming that the waves are in equilibrium, i.e. that equation (B.82) is satisfied, one gets an expression for the absolute values of the trapped particle flux. Under certain assumption, Kennel and Petschek (1966) have found an expression for the integral flux

$$J^* (> E_r) \sim \frac{(1 - E_c/E_r)}{(A - E_c/E_r)} \cdot 10^{10} \frac{B \ln(1/R)}{L R_e} \quad (B.95)$$

where J^* is in $(\text{cm}^2 \cdot \text{s})^{-1}$, B in Gauss and R_e in cm. J^* is called the limiting flux. If the actual value of J is smaller than J^* , there are not enough particles to sustain the waves. If on the contrary the source is sufficiently strong, J may reach J^* but it cannot trespass it : as soon as $J > J^*$ waves will grow above their equilibrium value and all the extraparticles will be precipitated.

One may note the inconsistencies of equation (B.95) : for large values of E_r , J^* is independent of energy, whereas high energy particles are those which interact with the waves. At low energies, J^* may become negative which has no physical meaning. These inconsistencies are the consequence of the assumption that the wave spectrum was flat (so that D could be kept constant). But the wave field can in fact be computed self-consistently. This was done by Etcheto et al. (1973).

The source term was assumed to be of the form :

$$s(\alpha, v) = C \cdot \frac{1}{n_c} \frac{dn_h}{dt} \cdot \sin^{2m} \alpha \exp \left[- \left(\frac{v}{v_0} \right)^2 \right] \quad (B.96)$$

where C is a normalization constant, n_c is the cold plasma density and dn_h/dt describes the density of particles injected per unit time. The practical choice for the source anisotropy, m has no importance on the results, the anisotropy of the final distribution being determined by the quasi-linear diffusion equilibrium. By integrating twice equation (B.80) and by making use of the equation which defines the growth rate and of the equilibrium equation (B.82), the equilibrium wave spectrum can be computed (Figure B.15). It almost does not depend on the initial anisotropy of the source as explained above, but it depends on its characteristic energy $mV_0^2/2$. The frequency which corresponds to the maximum spectral density is given by

$$\chi_{\max} \sim u^2/2 \quad (\text{B.97})$$

where $u = V_a^- / V_0$. The corresponding value of b_f^2 is

$$b_{f^2 \max} = \frac{2\pi^{1/2} \mu_0^2 e^2}{\exp(2)} \cdot \frac{n_c L R_e V_0^3}{\omega_{ce}^3 \ln(1/R)} \cdot \frac{dn_h}{dt} \quad (\text{B.98})$$

and it increases when either n_c or dn_h/dt increases. Therefore the source intensity is what defines the strength of the diffusion ($DT_e > \alpha_0^2$).

Etcheto et al. also computed the equilibrium particle distribution function. They found analytical expressions for both weak and strong diffusion. They confirmed the idea that in strong diffusion (strong source) the distribution function is almost isotropic, whereas in weak diffusion (weak source) the flux decreases exponentially within the loss cone (Figure B.16). However, contrary to Kennell and Petschek's (1966) conclusion, the total flux also increases with the source strength: strictly speaking there is no limiting flux. Indeed in an equilibrium configuration all injected particles are precipitated. If dn_h/dt increases, $\langle J_p \rangle$ increases. But since there is a non zero minimum lifetime, $\langle J_T \rangle$ cannot be smaller than $\langle J_p \rangle$. Consequently in the strong diffusion limit, $\langle J_T \rangle$ increases proportionally to the source strength. A schematic variation of the integral flux of trapped particles as a function of the source intensity is represented on Figure B.17. The 'critical' value of the source strength which separates the two regimes of strong and weak diffusion (point B) is given by

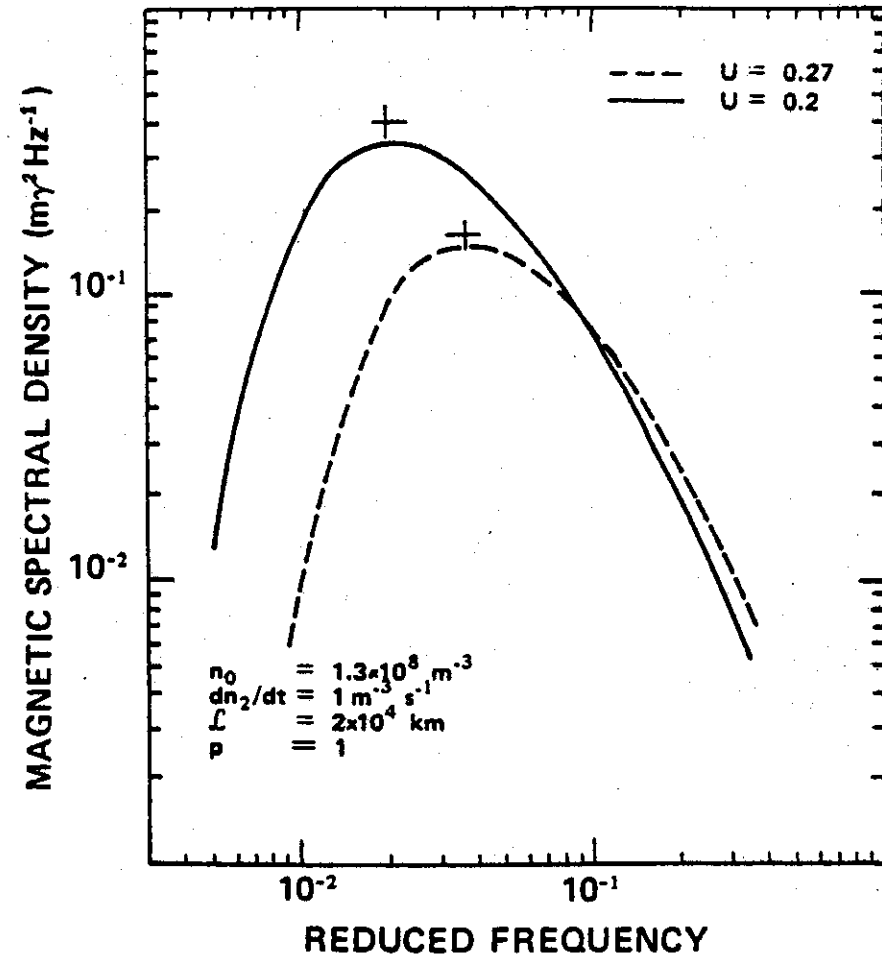


Fig.B.15.Wave spectra for different values of the characteristic energy parameter; $U = V_a/V_0$. For comparison, the analytical values for $p = 0$ are also represented (crosses).

Etcheto et al., J.G.R., 78, 8150, 1973

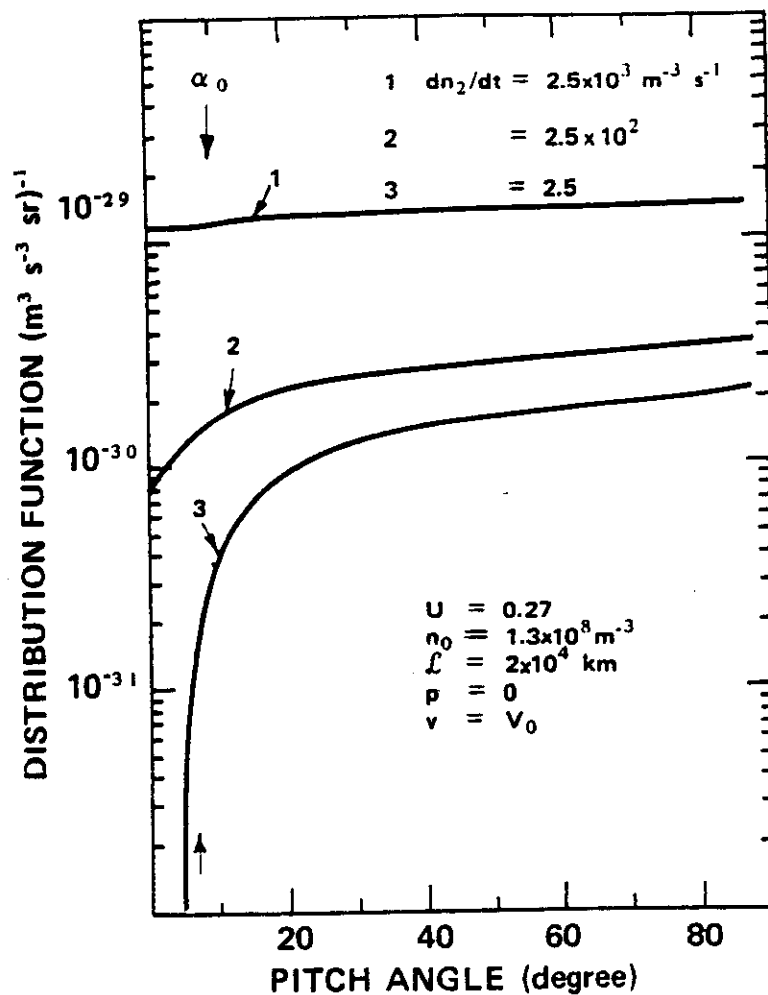


Fig. B.16. Variation of the angular distribution function with the source intensity. The curves have been computed for an energy E equal to the characteristic energy of the source E_0 . Increasing the source intensity not only changes the angular distribution but also increases the total flux.

Etcheto et al., J.G.R., 78, 8150, 1973.

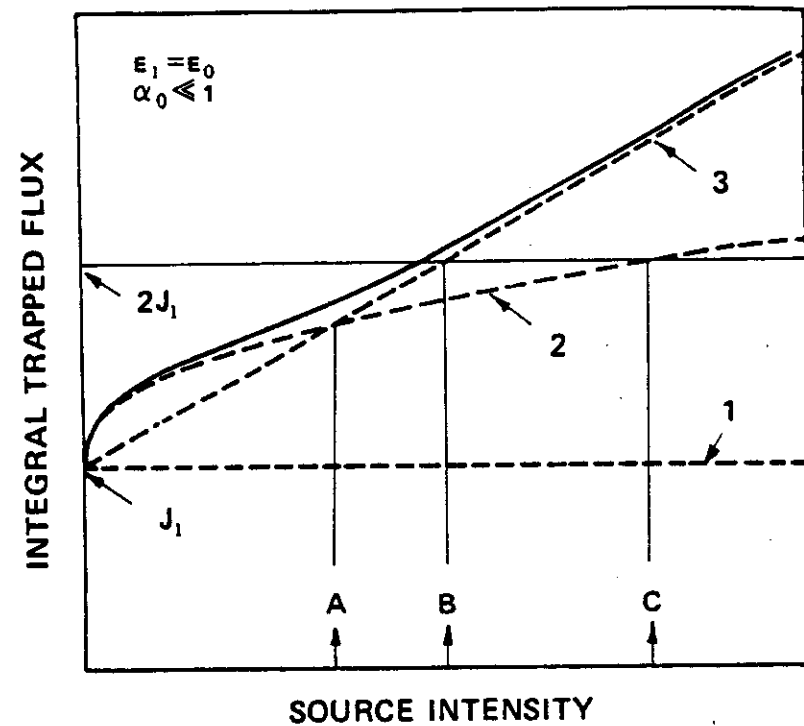


Fig. B.17. Schematic representation of the equilibrium trapped flux as a function of source intensity. The solid curve represents the true variation of $J(>E_1)$ as a function of dn_2/dt . The dashed curves are approximations: 1, zero-order approximation J_1 [Kennel and Petschek, 1966]; 2, weak diffusion approximation J_{2w} ; 3, strong diffusion approximation J_{2s} . The relative values of A, B, and C depend on the value of α_0 ; here $\alpha_0 \ll 1$. The scales are linear.

Etcheto et al., J.G.R., 78, 8150, 1973

$$\left(\frac{dn_h}{dt}\right)^* = 4.7 \times 10^{-2} \left(\frac{m}{\mu_0 e^2}\right) \frac{\omega_c \ln(1/R)}{1.4 (LR_e)^2} \quad (B.99)$$

which, for $R = 0.1$, reduces to $\sim 3 \times 10^5 / L^5 \text{ (m}^3\text{s)}^{-1}$.

There is no experimental method for measuring the source strength : one can detect the particles which are present, not the new ones which 'enter' the volume where the measurements are made. On the contrary it is possible to measure the wave field intensity. By using (B.64), (B.83) and (B.89) it is possible to determine if particles are in strong or weak diffusion. This depends on the field intensity (which defines D), on the particle energy (which defines T_e) and of the L -value which defines all the other parameters. The expressions which are given in Table B.2 allow to compute

$$D = \left(\frac{\omega_{ce} b_f}{B}\right)^2 \cdot x(1+x) \quad (B.100)$$

$$T_e \sim \frac{LR_e}{V_a} \cdot \frac{x^{1/2}}{(1-x)^{3/2}}$$

for e,R interactions and

$$D = \left(\frac{\omega_{ci} b_f}{B}\right)^2 \cdot \frac{x}{(2+x)} \quad (B.101)$$

$$T_e \sim \frac{LR_e}{V_a} \cdot \frac{x}{(1-x)^{3/2}}$$

for p,L interactions. Writing

$$DT_e = \alpha_0^2 \quad (B.102)$$

defines the critical power density $(b_f^2)^*$ above which particles are in strong diffusion. This value depends on the frequency and therefore on the

parallel energy of the particles. The relationship is very cumbersome. Besides, the exact computation of $(b_f^2)^*$ is of not much practical interest. Orders of magnitude are sufficient. These were computed by Thorne and Andreoli (1980) and the results are reported on Figure B.18 where B' is the total intensity in mV of the wave field ($B'^2 = b_f^2 + \omega_c^2$). These values have been obtained by neglecting the factor $v_g / |v_{||} - v_g|$, by assuming a wave spectrum independent of frequency and a frequency band equal to the gyrofrequency. These approximations are very crude and the numerical results must be considered cautiously. But they allow to compute B' as a function of the particle energy. One gets :

$$B' \sim 10^2 (\gamma^2 - 1)^{1/4} L^{-7/2} \quad (B.103)$$

for e,R interactions* and

$$B' \sim 3 \times 10^2 E^{1/4} L^{-7/2} \quad (B.104)$$

for p,L interactions. In these equations B' is expressed in gammas and the approximation

$$\alpha_0^2 \sim L^{-3/2} \quad (B.105)$$

has been used. It is worth comparing these approximate values with the result of exact computations. Let us take as an example the two cases which were discussed at the end of the previous section.

For $E = 5 \text{ keV}$ and $L = 6.6$, we have found $D \sim 2 \times 10^{-3} \text{ s}^{-1}$ for $b_f = 1 \gamma \cdot \text{Hz}^{-1/2}$ in the ULF range and $D \sim 10^{-2} \text{ s}^{-1}$ for $b_f = 1 \text{ m}\gamma \cdot \text{Hz}^{-1/2}$ in the VLF range. Assuming that $\Delta f \sim 0.2 \text{ Hz}$ in the first case and that $\Delta f \sim 500 \text{ Hz}$ in the second one, one gets $B' = 0.5 \gamma$ (ULF) and $B' = 25 \text{ m}\gamma$ (VLF). Since for $E = 5 \text{ keV}$ $T_e \sim 40 \text{ s}$ for protons and $T_e \sim 1 \text{ s}$ for electrons, $DT_e / \alpha_0^2 \sim 60$ for ULF and $DT_e / \alpha_0^2 \sim 7$ for VLF. The values of B' which would give $DT_e / \alpha_0^2 = 1$ are respectively $60 \text{ m}\gamma$ and $10 \text{ m}\gamma$ whereas one reads on Figure B.18 $500 \text{ m}\gamma$ and $50 \text{ m}\gamma$. In other words, for the values which are plotted on Figure B.18, the particles have already exceeded the transition between weak and strong diffusion. In this approximation, the variation of DT_e with E merely reflects the

* $\gamma = (1 - v^2/c^2)^{-1/2}$ is the relativistic factor.

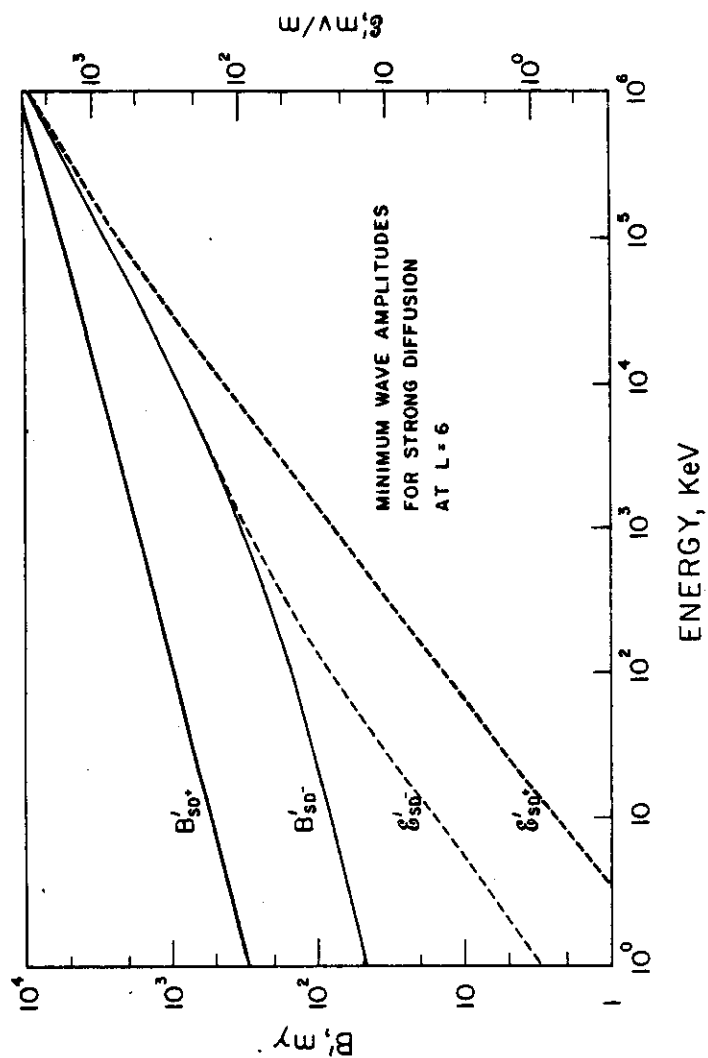


Figure B.18. Minimum fluctuating electric or magnetic wave amplitudes required to scatter protons (+) or electrons (-) on strong diffusion at $L = 6$. At other locations the required amplitudes scale as $L^{-1/2}$.

Thorne and Andreoli, in "Exploration of the Polar Upper Atmosphere", D. Reidel, 1980, 391.

variation of $T_e \sim E^{-1/2}$ so that B' varies like $E^{1/4}$. However for high energies $D \propto b^2_f x$ and $x \propto E^{-1}$ for VLF or $x \propto E^{-1/2}$ for ULF, so that the correct variation of B' at high energies is

$$B' \propto (\gamma^2 - 1)^{3/4} \quad (B.105)$$

for VLF and

$$B' \propto E^{1/2} \quad (B.106)$$

for ULF. The advantage of Figure B.18 is that it gives also (with similar limitations) a rough estimation of the field intensities which are needed bring particles into the strong diffusion regime by interactions with electrostatic waves.

Recent progress in the study of the self-consistent equilibrium has been made in two directions. For p,L interactions the theory has been improved by considering charge exchange processes between protons and neutral hydrogen atoms (Cornwall, 1977 ; Solomon and Picon, 1981). Because the magnetospheric hydrogen density is larger at low altitudes the charge exchange loss rate is larger for protons of small pitch angles. This process, which operate not only within the loss cone but outside of it, is indeed a source of positive anisotropy since it removes low pitch angle particles. The growth rate can be sustained if the source strength is larger than a certain critical value. In the presence of charge exchange, the wave spectrum is narrowed.

In the case of e,R interactions, the detailed experimental results obtained with the european geostationary spacecraft GEOS have allowed to improve the theory and to model the electron distribution function at equilibrium. The experiment demonstrates, and the theory justifies, that this distribution function cannot be factorized : the pitch angle distribution is actually a function of energy. Within the frequency band where the interaction take place, the anisotropy follows very accurately the variation of the critical anisotropy with frequency (Cornilleau-Wehrlin et al., 1983). These effects are discussed in Chapter III.

Before closing this Section it is worth giving an approximate expression for the ratio between the characteristic times for energy diffusion, τ_E and pitch angle diffusion, τ_α . From simple geometrical considerations, it is easily deduced that the velocity variation dv associated with a pitch angle variation $d\alpha$ verifies

$$\frac{dv}{v d\alpha} = - \frac{\sin \alpha v_\phi}{v - v_\phi \cos \alpha} \quad (B.107)$$

from the definitions $D_{vv} = \langle \Delta v^2 \rangle / 2\Delta t$ and $D_{\alpha\alpha} = \langle (\Delta \alpha)^2 \rangle / 2\Delta t$ one gets

$$\frac{D_{vv}}{D_{\alpha\alpha}} = \frac{\sin^2 \alpha v_\phi^2 v^2}{(v - v_\phi \cos \alpha)^2} \quad (B.108)$$

the characteristic times τ_E and τ_α are defined by

$$\left. \begin{aligned} D_{vv} &= \frac{v^2}{2\tau_E} \\ D_{\alpha\alpha} &= \frac{(\pi/2)^2}{2\tau_\alpha} \end{aligned} \right\} \quad (B.109)$$

so that

$$\frac{\tau_E}{\tau_\alpha} = \frac{1}{(\pi/2)^2} \left(\frac{v - v_\phi \cos \alpha}{\sin \alpha v_\phi} \right)^2 \quad (B.110)$$

If $v_\phi \ll v_{\parallel}$ and for medium values of the pitch angle, one gets

$$\frac{\tau_E}{\tau_\alpha} \sim \left(\frac{v_{\parallel}}{v_\phi} \right)^2 \quad (B.111)$$

but it must be noted that this rough approximation is not valid for small pitch angles ($\tau_E/\tau_\alpha \rightarrow \infty$ whereas v_{\parallel}/v_ϕ remains finite) nor for large pitch angles ($\tau_E/\tau_\alpha \rightarrow (v/v_\phi)^2$ whereas $(v_{\parallel}/v_\phi)^2 \rightarrow 0$).

8.5. NONLINEAR EFFECTS

This part of the Appendix is not yet written.

REFERENCES

TO CHAPTER II and APPENDIX B

BOOKS

- BUDDEN, K.G., *Radiowaves in the ionosphere*, Cambridge Univ. Press, 1961.
 JACOBS, J.A., *Geomagnetic Micropulsations*, Springer-Verlag, New-York, 1970.
 QUEMADA, D., *Ondes dans les plasmas*, Hermann, Paris, 1968.
 RATCLIFFE, J.A., *The magneto-ionic theory and its application to the ionosphere*, Cambridge Univ. Press, 1959.
 SCHULZ, M., and J.L. LANZEROTTI, *Particle diffusion in the radiation belts*, Springer-Verlag, New-York, 1974.
 STIX, T.H., *Theory of Plasma Waves*, McGraw-Hill, New-York, 1962.

REVIEWS

- FRASER-SMITH, A.C., ULF/Lower-ELF electromagnetic field measurements in the polar caps, *Rev. Geophys. Space Phys.*, **20**, 497-512, 1982.
 GALLET, R.M., Whistler mode and theory of VLF emissions, in '*Natural Electromagnetic Phenomena below 30 kc/s*', D.S. Bleil ed., Plenum Press, New-York, 1964, pp. 167-204.
 GENDRIN, R., Propagation longitudinale des ondes électromagnétiques dans un milieu ionisé en présence d'un champ magnétique, avec application aux phénomènes TBF et UBF rencontrés en géophysique externe, *Revue du CETHEDC*, **7**, 1-50, 1966.
 GENDRIN, R., Progrès récents dans l'étude des ondes TBF et UBF, *Space Sci. Rev.*, **7**, 314-395, 1967a.
 GENDRIN, R., Substorm aspects of magnetic pulsations, *Space Sci. Rev.*, **11**, 54-130, 1970.
 GENDRIN, R., Changes in the distribution function of magnetospheric particles associated with gyroresonant interactions, in '*Earth's Magnetospheric Processes*', B.M. McCormac ed., D. Reidel, Dordrecht, 1972, pp. 311-328.

- GENDRIN, R., Changes in the distribution function of magnetospheric particles associated with gyroresonant interactions, in 'Earth's Magnetospheric Processes', B.M. McCormac ed., D. Reidel, Dordrecht, 1972, pp. 311-328.
- GENDRIN, R., Waves and wave-particle interactions in the magnetosphere : a review, Space Sci. Rev., 18, 145-200, 1975a.
- GENDRIN, R., General relationships between wave amplification and particle diffusion in a magnetoplasma, Rev. Geophys. Space Phys., 19, 171-184, 1981a.
- GINZBURG, M.A., and A.A. RUHADZE, Waves and resonances in magneto-active plasmas, Hendbuch der Physik, vol. 49/4, K. Rawer ed., Springer Verlag, Heidelberg, 1970, pp. 395-560.
- MCPHERRON, R.L., C.T. RUSSELL, and P.J. COLEMAN, Jr., Fluctuating magnetic fields in the magnetosphere, Space Sci. Rev., 13, 411-455, 1972.
- PERRAUT, S., Wave-particle interactions in the ULF range : GEOS-1 and -2 results, Planet. Space Sci., to be published, 1982.
- THORNE, R.M., The consequences of micropulsations on geomagnetically trapped particles, Space Sci. Rev., 16, 443-458, 1974b.
- THORNE, R.M., and L.J. ANDREOLI, Mechanisms for intense relativistic electron precipitation, in 'Exploration of the Polar Upper Atmosphere', C.S. Deehr and J.A. Hoit et eds., D. Reidel, Amsterdam, 1980, pp. 381-394.
- TROITSKAYA, V.A., Micropulsations and the state of the magnetosphere, in 'Solar-Terrestrial Physics', J.W. King and W.S. Newman eds., Academic Press, New-York, 1967, pp. 213-274.

OTHER REFERENCES CITED IN THE TEXT

- AKASOFU, S.I., Attenuation of hydromagnetic waves in the ionosphere, Radio Sci., 69D, 361-366, 1965.
- ALTMAN, C., and E. FIJALKOW, The transmission of electromagnetic waves through the ionosphere at micropulsations frequencies, Alta Freq., 38, 183-188, 1969.
- ALTMAN, C., and H. CORY, The simple thin-film optical method in electro-magnetic wave propagation, Radio Sci., 4, 449-457, 1969a.

- ALTMAN, C., and H. CORY, The generalized thin-film optical method in electro-magnetic wave propagation, Radio Sci., 4, 459-470, 1969b.
- ANTONOVA, A.E., D.S. FLIEGEL, and B.V. DOVBNJA, The influence of the magnetic field and plasma structures in the earth magnetosphere on some properties of the hydromagnetic waves in the 0.1 - 1.0 Hz frequency band, Adv. Space Res., 1, 381-385, 1981.
- BARANSKY, L.N., Yu. GOLIKOV, F.Z. FEIGIN, I. HARCHENKO, J. KANGAS, and T. PIKKARAINEN, Role of the plasmopause and ionosphere in the generation and propagation of pearl pulsations, J. Atmos. Terr. Phys., 43, 875-881, 1981.
- BERKEY, F.T., Temporal fluctuations in the luminosity of diffuse auroras, J. Geophys. Res., 85, 6075-6079, 1980.
- BOOKER, H.G., and R.B. DYCE, Dispersion of waves in a cold magneto-plasma from hydromagnetic to whistler frequencies, Radio Sci., 69D, 463-492, 1965.
- BRICE, N.M., Fundamentals of very low frequency emission generation mechanisms, J. Geophys. Res., 69, 4515-4522, 1964.
- BRICE, N., Artificial enhancement of energetic particle precipitation through cold plasma injection : a technique for seeding substorms ? J. Geophys. Res., 75, 4890-4892, 1970.
- BRICE, N.M., and C. LUCAS, Influence of magnetospheric convection and polar wind on loss of electrons from the outer radiation belt, J. Geophys. Res., 76, 900-908, 1971.
- CAMPBELL, W., Low attenuation of hydromagnetic waves in the ionosphere and implied characteristics in the magnetosphere for Pcl events, J. Geophys. Res., 72, 3429-3445, 1967.
- CORNILLEAU-WEHLIN, N., A new ULF-modulated electrostatic wave detected in the extremely low frequency range onboard GEOS, J. Geophys. Res., 86, 1365-1373, 1981.
- CORNILLEAU-WEHLIN, N., J. SOLOMON, A. KORTH, and G. KREMSER, Experimental relationships between energetic electron anisotropy and ELF wave spectra onboard GEOS : a support to quasilinear theory, J. Geophys. Res., submitted to, 1983.
- CORNWALL, J.M., On the role of charge exchange in generating unstable waves in the ring current, J. Geophys. Res., 82, 1188-1196, 1977.

- CORNWALL, J.M., F.V. CORONITI, and R.M. THORNE, Turbulent loss of ring current protons, J. Geophys. Res., 75, 4699-4709, 1970.
- CORNWALL, J.M., F.V. CORONITI, and R.M. THORNE, Unified theory of SAR arc formation at the plasmopause, J. Geophys. Res., 76, 4428-4445, 1971a.
- CORNWALL, J.M., H.H. HILTON, and P.F. MIZERA, Observations of precipitating protons in the energy range $2.5 \text{ keV} \leq E \leq 200 \text{ keV}$, J. Geophys. Res., 76, 5220-5234, 1971b.
- CORONITI, F.V., and C.F. KENNEL, Electron precipitation pulsations, J. Geophys. Res., 75, 1279-1289, 1970.
- COWLEY, S.W.H., and M. ASHOUR-ABDALLA, Adiabatic plasma convection in a dipole field : variation of plasma bulk parameters with L, Planet. Space Sci., 23, 1527-1549, 1975.
- CRISWELL, D.R., Pcl micropulsation activity and magnetospheric amplification of 0.2 to 5.0 Hz hydromagnetic waves, J. Geophys. Res., 74, 205-224, 1969.
- CUPERMAN, S., and R.W. LANDAU, On the enhancement of the whistler mode instability in the magnetosphere by cold plasma injection, J. Geophys. Res., 79, 128-134, 1974.
- CUPERMAN, S., and Y. SALU, Optimum cold plasma density for maximum whistler instability : numerical versus analytical, J. Geophys. Res., 79, 135-137, 1974.
- DOWDEN, R.L., Micropulsation modes, propagation in the magnetosphere, Planet. Space Sci., 13, 773-779, 1965.
- EATHER, R.H., and R.L. CAROVILLANO, The ring current as the source region for proton auroras, Cosmic Electrodyn., 2, 105-132, 1971.
- FIELD, E., and C. GREIFINGER, Transmission of geomagnetic micropulsations through the ionosphere and lower exosphere, J. Geophys. Res., 70, 4885-4899, 1965.
- FUKUNISHI, H., T. TOYA, K. KOIKE, M. KUMASHIMA, and K. KAWAMURA, Classification of hydromagnetic emissions based on frequency-time spectra, J. Geophys. Res., 86, 9029-9039, 1981.
- GENDRIN, R., Sur une théorie des pulsations rapides structurées, Ann. Geophys., 19, 197-214, 1963.
- GENDRIN, R., E.B.F. et micropulsations, 2. Structure, polarisation et propagation des oscillations hydromagnétiques, Ann. Geophys., 23, 153-171, 1967b.
- GENDRIN, R., Pitch-angle diffusion of low energy protons due to gyroresonant interaction with hydromagnetic waves, J. Atmos. Terr. Phys., 30, 1313-1330, 1968.
- Erratum : J. Atmosph. Terr. Phys., 31, 617-618, 1969.
- GENDRIN, R., Is the plasmopause a preferential region for proton precipitation ? Ann. Geophys., 31, 127-136, 1975b.
- GENDRIN, R., and V.A. TROITSKAYA, Preliminary results of a micropulsation experiment at conjugate points, Radio Sci., 69D, 1107-1116, 1965.
- GENDRIN, R., S. LACOURLY, M.V. GOKHBERG, P. MALEVSKAYA, et V.A. TROITSKAYA, Polarisation des oscillations hydromagnétiques de type Pcl observées en deux stations géomagnétiquement conjuguées, Ann. Geophys., 22, 329-337, 1966.
- GENDRIN, R., et J. VIGNERON, Relations entre l'apparition des émissions de très basse fréquence et l'agitation magnétique, C.R. Acad. Sci., Paris, 263B, 1147-1150, 1966.
- GENDRIN, R., S. LACOURLY, A. ROUX, J. SOLOMON, F.Z. FEIGIN, M.V. GOKHBERG, V.A. TROITSKAYA, and V.L. YAKIMENKO, Wave-packet propagation in an amplifying medium and its application to the dispersion characteristics and to the generation mechanisms of Pcl events, Planet. Space Sci., 19, 165-194, 1971.
- GENDRIN, R., S. PERRAUT, H. FARGETTON, F. GLANGEAUD, and J.L. LACOUME, ULF waves : conjugated ground-satellite relationships, Space Sci. Rev., 22, 433-442, 1978.
- GENDRIN, R., and A. ROUX, Energization of Helium ions by proton-induced hydromagnetic waves, J. Geophys. Res., 85, 4577-4586, 1980.
- GINZBURG, M.A., Electromagnetic radiation from solar corpuscular streams, Phys. Rev. Lett., 7, 399-401, 1961.
- GLANGEAUD, F., and J.L. LACOUME, Etude de la propagation des Pcl en présence de gradients d'ionisation alignés sur le champ magnétique terrestre, C.R. Acad. Sci., Paris, 272, 397-400, 1971.
- GLANGEAUD, F., J.L. LACOUME, H. FARGETTON, R. GENDRIN, S. PERRAUT, and V.A. TROITSKAYA, Cross-spectral analysis of Pcl emissions recorded at different stations, J. Geophys. Res., 85, 4115-4124, 1980.

- HIGUCHI, Y., and J.A. JACOBS, Plasma densities in the thermal magnetosphere determined by using hydromagnetic whistlers, J. Geophys. Res., 75, 7195-7116, 1970.
- HIRASAWA, T., Rapid auroral pulsations with frequencies of 0.05 - 40 Hz, Memoirs of the National Institute of Polar Research, Special Issue Nr. 16, Tokyo, Sept. 1980, pp. 17-24
- HIRASAWA, T., Effects of magnetospheric compression and expansion on spectral structure of ULF emissions, Memoirs of the National Institute of Polar Research, Special Issue Nr. 18, Tokyo, March 1981, pp. 127-151.
- IMHOF, W.L., J.B. REAGAN, and E.E. GAINES, Fine-scale spatial structure in the pitch angle distributions of energetic particles near the midnight trapping boundary, J. Geophys. Res., 82, 5215-5221.
- JACOBS, J.A., and T. WATANABE, Micropulsation whistlers, J. Atmos. Terr. Phys., 26, 825-829, 1964.
- JACOBS, J.A., and T. WATANABE, Propagation of hydromagnetic waves in the lower exosphere and the origin of short period geomagnetic micropulsations, J. Atmos. Terr. Phys., 24, 413-434, 1962.
- JOSELYN, J.A., and L.R. LYONS, Ion cyclotron wave growth calculated from satellite observations of the ring current during storm recovery, J. Geophys. Res., 81, 2275-2282, 1976.
- KARPLUS, R., W.E. FRANCIS, and A.J. DRAGT, The attenuation of hydromagnetic waves in the ionosphere, Planet. Space Sci., 9, 771-785, 1962.
- KAYE, S.M., M.G. KIVELSON, and D.J. SOUTHWOOD, Evolution of ion cyclotron instability in the plasma convection system of the magnetosphere, J. Geophys. Res., 84, 6397-6406, 1979.
- KENNEL, C.F., and H.E. PETSCHKE, Limit on stably trapped particle fluxes, J. Geophys. Res., 71, 1-28, 1966.
- KENNEL, C.F., and H.V. WONG, Resonantly unstable off-angle hydromagnetic waves, J. Plasma Phys., 1, 81-104, 1967.
- LACOURLY, S., Evaluation de certains paramètres de la magnétosphère à partir des propriétés des pulsations hydromagnétiques irrégulières (SIP et IPDP), Ann. Geophys., 25, 651-657, 1969.
- LIEMOHN, H.B., Cyclotron-resonance amplification of VLF and ULF whistlers, J. Geophys. Res., 72, 39-55, 1967.
- LIN, C.S., and G.K. PARKS, Further discussion of the cyclotron instability, J. Geophys. Res., 79, 2894-2897, 1974.
- LIN, C.S., and G.K. PARKS, Ion cyclotron instability of drifting plasma clouds, J. Geophys. Res., 81, 3919-3922, 1976.
- LYONS, L.R., Pitch angle and energy diffusion coefficients from resonant interactions with ion-cyclotron and whistler waves, J. Plasma Phys., 12, 417-432, 1974.
- MAUK, B.H., C.E. MCILWAIN, and R.L. MCPHERRON, Helium cyclotron resonance within the earth's magnetosphere, Geophys. Res. Lett., 8, 103-106, 1981.
- NORRIS, A.J., J.F.E. JOHNSON, J.J. SOJKA, G.L. WRENN, N. CORNILLEAU-WEHLIN, S. PERRAUT, and A. ROUX, Experimental evidence for the acceleration of thermal electrons by ion cyclotron waves in the magnetosphere, J. Geophys. Res., to be published, 1982.
- OBAYASHI, T., Hydromagnetic whistlers, J. Geophys. Res., 70, 1069-1078, 1965.
- PERRAUT, S., Détermination des paramètres magnétosphériques à partir de l'analyse des pulsations magnétiques rapides, Thesis, Paris, 1974.
- PERRAUT, S., and A. ROUX, Respective role of the cold and warm plasma densities on the generation mechanism of ULF waves in the magnetosphere, J. Atmos. Terr. Phys., 37, 407-418, 1975.
- PERRAUT, S., R. GENDRIN, and A. ROUX, Amplification of ion-cyclotron waves for various typical radial profiles of magnetospheric parameters, J. Atmos. Terr. Phys., 38, 1191-1199, 1976.
- RAUCH, J.L., Etude des ondes d'ultra basse fréquence (UBF) observées à bord des satellites européens GEOS-1 et GEOS-2. Tracé de rayons dans un magnétoplasma à trois composantes (e^- , H^+ , He^+), Thesis, Paris, 1981.
- RAUCH, J.L., and A. ROUX, Ray tracing of ultra low frequency waves in a multi-component magnetospheric plasma. Consequences on the generation mechanism of ion cyclotron waves, J. Geophys. Res., 87, 8191-8198, 1982.

- ROUX, A., N. CORNILLEAU-WEHLIN, and J.L. RAUCH, Acceleration of thermal electrons by quasi-electrostatic ULF waves, J. Geophys. Res., submitted to, 1983.
- ROWLANDS, J., V.D. SHAPIRO, and V.I. SCHEVCHENKO, Quasilinear theory of plasma cyclotron instability, Sov. Phys. JETP, Engl. Transl., 23, 651-660, 1966.
- RUSSELL, C.T., and R.M. THORNE, On the structure of the inner magnetosphere, Cosmic Electrodyn., 1, 67-89, 1970.
- SAGDEEV, R.Z., and V.D. SHAFRANOV, On the instability of a plasma with an anisotropic distribution of velocities in a magnetic field, Soviet. Phys. JETP, 12, 130-132, 1961.
- SINGH, N., W.J. RAITT, and F. YASUHARA, Low-energy ion distribution functions on a magnetically quiet day at geostationary altitude ($L = 7$), J. Geophys. Res., 87, 681-694, 1982.
- SMITH, R.L., and N. BRICE, Propagation in multi-component plasmas, J. Geophys. Res., 69, 5029-5040, 1964.
- SMITH, E.J., and B.T. TSURUTANI, Magnetosheath ion roars, J. Geophys. Res., 81, 2261-2266, 1976.
- SOLOMON, J., Drift of particles and wave-particle interactions, in "The Magnetospheres of the Earth and Jupiter", ed. by V. Formisano, D. Reidel, Dordrecht, 1975, pp. 153-159.
- SOLOMON, J., Injections de particules énergétiques dans la magnétosphère. Conséquences sur les déformations de fonctions de distribution et sur les interactions de gyrorésonance, Thesis, Paris-11, 1977.
- SOLOMON, J., and O. PICON, Charge exchange and wave-particle interaction in the proton ring current, J. Geophys. Res., 86, 3335-3344, 1981.
- STOREY, L.R.O., A method for measuring local electron density from an artificial satellite, J. Res. N.B.S., 63D, 325-340, 1959.
- TEPLEY, L., Low-latitude observations of fine-structure hydromagnetic emissions, J. Geophys. Res., 69, 2273-2290, 1964.
- TEPLEY, L.R., Regular oscillations near Ω_{He^+} observed at middle and low latitudes, Radio Sci., 69D, 1089-1105, 1965.
- THORNE, R.M., A possible cause of dayside relativistic electron precipitation events, J. Atmos. Terr. Phys., 36, 635-645, 1974a.
- THORNE, R.M., and C.F. KENNEL, Relativistic electron precipitation during magnetic storm main phase, J. Geophys. Res., 76, 4446-4453, 1971.
- TROITSKAYA, V.A., Pulsations of the Earth's electromagnetic field with periods of 1 to 15 seconds and their connection with phenomena in the high atmosphere, J. Geophys. Res., 66, 5-18, 1961.
- WILLIAMS, D.J., T.A. FRITZ, and A. KONRADI, Observations of proton spectra ($1.0 \geq E_p \leq 300$ keV) and fluxes at the plasmopause, J. Geophys. Res., 78, 4751-4755, 1973.
- WILLIAMS, D.J., and L.R. LYONS, The proton ring current and its interaction with the plasmopause storm recovery phase, J. Geophys. Res., 79, 4195-4207, 1974.
- WILLIAMS, D.J., G. HERNANDEZ, and L.R. LYONS, Simultaneous observations of the proton ring current and stable auroral red arcs, J. Geophys. Res., 81, 608-616, 1976.
- YOUNG, D.T., S. PERRAUT, A. ROUX, C. de VILLEDARY, R. GENDRIN, A. KORTH, G. KREMSER, and D. JONES, Wave-particle interactions near Ω_{He^+} observed on GEOS-1 and -2. 1. Propagation of ion cyclotron waves in He^+ -rich plasma, J. Geophys. Res., 86, 6755-6772, 1981.



INTERNATIONAL ATOMIC ENERGY AGENCY
UNITED NATIONS EDUCATIONAL, SCIENTIFIC AND CULTURAL ORGANIZATION



INTERNATIONAL CENTRE FOR THEORETICAL PHYSICS
34100 TRIESTE (ITALY) - P.O. B. 586 - MIRAMARE - STRADA COSTIERA 11 - TELEPHONES: 224281/23456
CABLE: CENTRATOM - TELEX 460392-1

SMR/98 - 40

AUTUMN COURSE ON GEOMAGNETISM, THE IONOSPHERE
AND MAGNETOSPHERE

(21 September - 12 November 1982)

Booker's Mode Theory of Guidance of Electromagnetic Waves
in the Magnetosphere.

M. DOBROWOLNY
Istituto Fisica Spazio Interplanetario
C.N.R.
C.P. 27
00044 Frascati (Roma)
ITALY

These are preliminary lecture notes, intended only for distribution to participants.
Additional or extra copies are available from Room 230.

8. BOOKER'S MODE THEORY OF GUIDANCE OF ELECTROMAGNETIC WAVES IN THE MAGNETOSPHERE

8.1 Introduction

In Sect. 6 I have presented the ray theory of Smith et al. (1960) for whistler trapping in field aligned ducts of density ionization. This theory, which gives the critical fractional density gradients for ray trapping as a function of initial wave normal angle with respect to the magnetic field and as a function of frequency, is based on the whistler dispersion equation (6.1) and hence refers to the FMS branch in the frequency region

$$\omega_{Bi} \ll \omega < |\omega_{Be}|$$

A quite different theory of guidance in ducts was developed in 1962 by H. Booker and is the object of the present section. Booker's theory is different from the work of Smith et al. (1960) in several respects. First of all it is a mode theory (and not a ray theory) of wave guidance. The duct is modelled by Booker as a thin field aligned density discontinuity which is contrary to the ray theory of Smith et al. where the thickness of the duct must exceed the wavelength of the waves whose propagation is considered. We will come back later to the physical meaning of the discontinuity model of Booker. More important, Booker's theory is done using the dispersion relation for purely longitudinal propagation and thus, in fact, ignores the anisotropic properties of the medium. The point of view here is that of deciding under which conditions a ray which, at a given point in the magnetosphere is field aligned, continues to stay so during propagation. The use of the longitudinal dispersion relation (eqs. (1.21) (1.22))

which is exact for all frequencies, implies that Booker's theory of guidance covers all possible electromagnetic waves from hydromagnetic to radio frequencies. Finally, curvature of the Earth's magnetic field (which was neglected in the whistler theory of Smith et al. (1960) but has been later included by Walker (1966b) in a study also directed to whistler waves), plays, as we will see, a crucial role in Booker's theory.

8.2. Magnetospheric model

The magnetic field of the Earth is, in the simplest approximation, assumed to be that of a central dipole (see Fig. 36) and a particular line of flux is conveniently identified by the latitude λ at which it intersects the surface of the Earth. With s we denote the distance, measured along a line of flux of a given point P on that line from the point A where the line intersects the equatorial plane; r will denote the distance of P from the center of the Earth and the angle AOP will be indicated by θ . Then, if a is the radius of the Earth, the equation of the line of flux of latitude λ is

$$r = a \frac{\omega s^2 \theta}{\omega s^2 \wedge} \quad (8.1)$$

The variation of the radial distance r with θ for specified lines of flux is illustrated in Fig. 37. For most purposes, it is convenient to identify position on a line of flux of latitude λ by means of the angular distance θ from the equatorial plane. In some cases, however, it may be necessary to refer to the actual distance s along the line. It is easy to see that the relation between the two is given by the equation

$$\frac{1}{s} \frac{ds}{d\theta} = \frac{\omega s \theta}{\omega s^2 \Lambda} (4 - 3 \cos^2 \theta)^{1/2} \quad (8.2)$$

Let us indicate with f_{MO} the value of the electron gyrofrequency at the equator of the Earth. In terms of this, the gyrofrequency at the point r, θ of the ionosphere or magnetosphere will be given, for the assumed dipole field of the Earth, by

$$f_M = f_{MO} (a/r)^3 (4 - 3 \cos^2 \theta)^{1/2} \quad (8.3)$$

For the line of latitude Λ , we obtain the variation with θ of f_M by substituting (8.1) into (8.3). The result is

$$f_M = f_{MO} \frac{\omega s^2 \Lambda}{\omega s^2 \theta} (4 - 3 \cos^2 \theta)^{1/2} \quad (8.4)$$

This variation (and the analogous for the proton gyrofrequency) is illustrated in Fig. 38 for a number of lines of flux (and for $f_{MO} = 0.87$ Mc/s).

Going now to the density variations, Booker assumes the following model for the smooth density variations of the magnetospheric plasma

$$N = N_0 (a/r)^p \cos^q \theta \quad (8.5)$$

with p and q positive. Correspondingly, one obtains for the electron plasma frequency

$$f_{pe} = f_{Po} (a/r)^{1/2p} \cos^{1/2q} \theta \quad (8.6)$$

Using eq. (8.1) for the line of flux corresponding to latitude Λ , we obtain, for the variation of the electron plasma frequency along a given line of flux

$$f_{pe} = f_{Po} \frac{\omega s^2 \Lambda}{\omega s^{p-1/2} \theta} \quad (8.7)$$

The variation of this frequency with θ along several lines of flux is given in Fig. 39 corresponding to the following parameter values

$$p = 4, \quad q = 0, \quad f_{Po} = 1 \text{ Mc/s}$$

Notice that the plasma distribution assumed by Booker refers really to the magnetosphere and would have to be modified at levels below ~ 1000 km.

8.3 Inner and outer zones of longitudinal propagation

As already mentioned in Sect. 8.1, Booker's theory of guidance refers to electromagnetic waves for longitudinal propagation. The two refractive indices are then given (see Sect. 1) by

$$n_{\pm}^2 = 1 - \frac{\omega_{pi}^2}{\omega(\omega \mp \omega_{Bi})} - \frac{\omega_{pe}^2}{\omega(\omega \pm \omega_{Be})} \quad (8.8)$$

Here, as we saw in Sect. 1.3, the upper sign refers to L waves (singularity at $\omega = \omega_{Bi}$) and the lower to R waves (singularity at $\omega = \omega_{Be}$). We recall that the two waves are also commonly denoted, especially at radio frequencies, as ordinary (L) and extraordinary (R) waves. In the range of frequencies $\omega < \omega_{Be}$ (and for the ionospheric and magnetospheric plasmas for which $\omega_{Be} < \omega_{pe}$), the extraordinary (R) wave, which is the FMS branch using Shafranov's notation (see Sect. 1), becomes the parallel electron whistler for $\omega > \omega_{Bi}$ and the hydromagnetic magnetoacoustic mode for $\omega < \omega_{Bi}$. The ordinary (L) wave, on the other hand, is the Alfvén

5

6

branch for $\omega < \omega_{Bi}$ going over to the ion cyclotron wave at frequencies ω close to ω_{Bi} and then essentially it propagates (SE branch of Fig. 1) only at frequencies above the cut-off frequency $\omega_o^{(3)} \sim (\omega_{pe}^2 + 1/4\omega_{Be}^2)^{1/2} - \frac{1}{2}|\omega_{Be}|$ (which, for the ionosphere magnetospheric plasma, are in general above ω_{Be}).

It is important now to point out that, given the refractive index (8.8), for any fixed wave frequency, the magnetosphere can be divided into zones where longitudinal propagation is possible and zones where it is forbidden. The transition between the two regions occurs, as we know, when n^2 passes through either of the values 0 or ∞ .

Referring to the R wave, a resonance occurs when

$$\omega = \omega_{Be} \quad (8.9)$$

Thus, for this wave, at a given frequency, one boundary of the forbidden zone for longitudinal propagation occurs at the level in the magnetosphere where the local electron gyrofrequency is equal to the frequency under consideration. For a frequency of 100 kc, this gives the inner surface of the stapled area of Fig. 40a (corresponding to the magnetospheric model of Sect. 8.2). The outer surface corresponds to the condition $n^2=0$. This is the frequency $\omega_o^{(3)}$ of Shafranov given by

$$\omega_o^{(3)} = (\omega_{pe}^2 + \frac{1}{4}\omega_{Be}^2)^{1/2} - \frac{1}{2}|\omega_{Be}| \quad (8.10)$$

above which we have propagation of the SE branch (see Fig. 1). Thus, in the stapled region in Fig. 40a propagation is not possible and the two conditions $n^2=\infty$, $n^2=0$ separate the magnetosphere into an inner region and an outer region of propagation. In the outer zone a wave supposed to be guided along the lines of flux of the Earth's magnetic field is returned when it encounters the outer surface of the forbidden

zone (where $n^2=0$). On the other hand, a wave travelling in the inner zone (and also supposed to be guided), when it intersects the $n^2=\infty$ surface is not reflected but rather it dissipates there causing some heating of the magnetosphere.

Fig. 40a refers to the R wave at 100 Kc. The forbidden magnetospheric zone will of course vary with frequency. The variation of its location in the equatorial plane, as a function of frequency, is indicated by the horizontal shading in Fig. 41. From this we see clearly that, at frequencies below ~ 1 Kc the inner zone for propagation for the R wave occupies virtually the entire magnetosphere. These are frequencies typical of whistlers which can in general propagate from one to the other hemisphere without encountering zones of forbidden propagation. On the other hand, we see from the same figure that high frequencies do essentially propagate only in the outer zone.

The same type of reasoning can be applied to the n_- wave (L wave). There, it is $n_-^2=\infty$ when

$$\omega = \omega_{Bi} \quad (8.11)$$

and $n_-^2=0$ at the frequency

$$\omega_o^{(2)} \sim \omega_{pe} \quad (8.12)$$

which give the boundaries of the inner and outer zones of longitudinal propagation for this wave. In the inner region we have therefore propagation of the A branch and in the outer region of the FE branch. At the same frequency $\omega=100$ Kc (considered before for the R wave), we see now for the L wave, from Fig. 40b, that there is an outer zone of propagation for the L wave but no inner zone (except below the ionosphere). On the other hand, at the very low frequency of 10 c/s, Fig.

40c, always referring to the L wave (which is now the Alfvén wave) indicates that there is essentially no outer zone of propagation but instead there is a substantial inner zone of longitudinal propagation. It is in this inner zone that Alfvén waves possibly propagate between conjugate hemispheres of the Earth.

The location of the forbidden zone of propagation for the L wave is shown, at the equator and as a function of frequency, in Fig. 41, denoted with a vertical shading. As the external boundary of the inner region of propagation for the L wave occurs at $\omega = \omega_{Bi}$, whereas it occurs at $\omega = \omega_{Be}$ for the R wave, we see that the forbidden zone of propagation of the L wave is enormously thicker than that of the R wave. At audio frequencies (the whistler's frequencies) this forbidden zone occupies virtually the all magnetosphere (and it is only the R mode whistlers that propagate). It is only for the very low frequencies that we have an almost entirely inner zone of propagation, as seen in Fig. 40c.

Fig. 40a-c, giving the inner and outer zone of magnetospheric propagation, indicate also that, for a given wave frequency, there is a maximum latitude of line of flux for which longitudinal propagation entirely within the inner zone is possible between conjugate hemispheres. Conversely, for a given latitude of a flux line, there is a maximum frequency ^{below} ~~above~~ which longitudinal propagation entirely within the inner zone is possible between conjugate hemispheres. These important features of magnetospheric propagation are presented in Fig. 42 which gives in fact the maximum frequencies for interhemispheric propagation (within the inner zone) as a function of latitude of the line of flux, both for the R (dashed line) and the L waves (solid line). In this same figure one finds indicated both the whistler and the Alfvén wave regimes.

8.4 Field curvature

An important quantity which must be computed is the curvature of the Earth's magnetic field. The condition for guiding of electromagnetic waves that will be later imposed will be that the curvature of a given ray follows the curvature of magnetic field lines.

With reference to Fig. 43, let MN and M'N' be two adjacent magnetic lines of force of any curvature. Consider then two equipotential lines AB and A'B' of length dr separated by a small distance and inclined by an angle α . If OA=OA'=r and the magnetic fields along AA' and BB' and H + dH respectively, we can write

$$(H+dH)(r+dr)d\alpha = Hr d\alpha$$

from which

$$H dr + r dH = 0 \quad (8.13)$$

Then the local curvature $1/r$ of Fig. 43 will be given by

$$K_F \equiv \frac{1}{r} = -\frac{1}{H} \frac{dH}{dr} = -\frac{1}{f_M} \frac{df_M}{dr} \quad (8.14)$$

where, in the last expression, f_M is the cyclotron frequency. More generally it is advisable to write

$$K_F = -\frac{1}{H} \nabla_{\perp} H = -\frac{1}{f_M} \nabla_{\perp} f_M \quad (8.15)$$

to recall that the gradient which enters is that along the local normal to the magnetic field line. Eq. (8.15) is general and can be applied to a variety of field patterns. Let us see, in particular, the results

it gives for the magnetic field of the Earth. We want the field curvature at the point θ on the line of latitude Λ . An easy calculation, using for example (8.4), leads to

$$\frac{K_F}{K_E} = 3 \omega^2 \Lambda \frac{2 - \omega^2 \theta}{\omega \theta (4 - 3 \omega^2 \theta)^{1/2}} \quad (8.16)$$

where, as it is convenient, the field curvature has been normalized to the curvature of the Earth

$$K_E = 1.57 \times 10^{-7} \text{ rad/meter} \quad (8.17)$$

The θ dependence of the ratio K_F/K_E is reported in Fig. 44 for various values of Λ . For low latitude lines, the field curvature exceeds the Earth's curvature while the opposite is true for high latitude lines. Note, however, that, apart from special cases, the field curvature is not of a different order of magnitude with respect to the Earth's curvature.

8.5 Ray curvature and excess field curvature

Consider a curved magnetic field and an electromagnetic wave, considered as a ray, bent into a curve owing to refractive effects and inclined at a small angle ϕ at P and $\phi + d\phi$ at Q, as shown in Fig. 45, PQ being ds , an element of the ray path. For simplicity, let the field line and the ray be in the same plane. Let the normal distance from Q to the field line through P be dr . If n is the refractive index for the ray, by Snell's law, the curvature of the ray can be expressed as

$$K_R = - \frac{d\phi}{ds} = - \frac{1}{n} \frac{dn}{dr} \omega s \phi \quad (8.18)$$

For small values of ϕ , we have

$$K_R = - \frac{1}{n} \nabla_{\perp} n \quad (8.19)$$

i.e. the ray curvature is given by the fractional downward gradient of refractive index in the outward principal normal direction to the magnetic field line.

Using now the expression (8.8) for longitudinal refractive index, we obtain

$$K_R = \frac{1-n^2}{n^2} \frac{1}{N} \nabla_{\perp} N + \frac{K_F}{2n^2} \left[\frac{1}{\omega \omega_{Bi}} \frac{\omega_{pi}^2}{(1 \pm \omega/\omega_{Bi})} \pm \frac{\omega_{pe}^2}{\omega \omega_{Be} (1 \pm \omega/\omega_{Be})} \right] \quad (8.20)$$

with K_F given by (8.15). There are therefore two separate contributions to the ray curvature, one arising from the fractional gradient of the magnetic field and the other from the fractional gradient of the ionization density.

The condition for guiding of electromagnetic rays along the curved magnetic field line is clearly

$$\frac{K_R}{K_F} = 1 \quad (8.21)$$

In relation to guiding it is important to introduce the quantity

$$K = K_F - K_R \quad (8.22)$$

which is the excess of field over ray curvature, (or briefly excess field curvature). It is this quantity, as we will see, which enters the notion of modified refractive index (see Sect. 8.7) and it is the

consequences of this curvature differential that have to be overcome by means of field aligned irregularities of ionization, if guiding along the lines of flux of the Earth's magnetic field is to take place. Using the model of magnetic field and density described in Sect. 8.2, Booker derives the variation of the differential curvature along a number of lines of flux and for a number of wave frequencies. His results are shown in Figs. 46a-d where the excess curvature on the ordinate axes is normalized to Earth's curvature. We see from these results that the curvature differential between the rays and the lines of flux is, broadly speaking, of the order of magnitude of the Earth's curvatures. Furthermore K is always positive. This means that, for the magnetic field and density models assumed, additional downward curvature is required at all places and all frequencies to produce guiding along the lines of flux.

8.6 Model for field aligned irregularities of ionization

The model assumed by Booker to study guided propagation in field aligned ducts is the following. Take a particular line of flux of the Earth's magnetic field and rotate it around the magnetic axis, thereby forming a geometrical surface in the magnetosphere. Booker assumes that, upon crossing this surface from inside to outside there is a discontinuous increase in electron density ΔN , either positive or negative. Inside the surface the ionization density is assumed to be given by eq. (8.5). Outside, the density variation is still represented by (8.5) but with a slightly different value of the constant ($N_0 + \Delta N$). Thus, with respect to the ray theory of Smith et al. (1960) for guiding of whistlers in ducts which was requiring density variation across the field containing many wavelengths, Booker's approach is quite different in that it refers to a thin field aligned discontinuity.

As will be seen, following Booker's treatment such a surface of discontinuity is capable of acting as a guide for transmission between conjugate points in the northern and southern hemispheres. A ray on the inside of the surface of discontinuity can, under suitable conditions, suffer successive internal reflections from the interface and thus convey energy along a line of flux.

8.7 Modified refractive index

The method of modified refractive index to study ray propagation with account taken of the curvature of the Earth's magnetic field was first introduced by Booker and Walkinslaw (1946) in a study of tropospheric propagation.

In the free space between the Earth and the ionosphere a ray travels in a straight line. An observer who thought that the Earth was flat would say that this line is not straight but has an upward curvature which he might ascribe to a variation of refractive index with height. If the actual refractive index is n , let us call $n'(z)$ the fictitious refractive index (a function of the vertical) which one would have to imagine with a flat earth and let us derive what is the form of $n'(z)$. Suppose then that, in this fictitious medium, the ray is inclined at an angle ψ to the horizontal and let s be the distance measured along the ray. From Snell's law we have that $n' \cos \psi = \text{const}$ so that

$$\frac{dn'}{d\psi} = n' \tan \psi$$

As a consequence, the curvature of the ray is

$$\frac{d\psi}{ds} = \frac{dn'}{ds} / \frac{dn'}{d\psi} = \frac{dn'}{dz} \sin \psi / n' \tan \psi = \frac{1}{n'} \frac{dn'}{dz} \cos \psi \quad (8.23)$$

Now, again referring to free space, an observer who thinks that the earth is flat will think that the ray has an upper curvature $\cos\psi/R_E$, with R_E the Earth's radius. Hence, equating this to (8.23) we obtain

$$\frac{1}{n'} \frac{dn'}{dz} = \frac{1}{R_E} \quad (8.24)$$

$$n' = \exp\left(\frac{z-h}{R_E}\right)$$

where h is a constant. For example h can be the level of the ionosphere so that, just below, $n'=1$. Now, as in practice $z-h$ is always much smaller than R_E we can expand (8.24) and obtain

$$n'^2 = 1 + \frac{2(z-h)}{R_E} \quad (8.25)$$

This formula, as already mentioned, applies to the free space below the ionosphere. However the trick of substituting the actual refractive index with one containing a linear variation in z to simulate curvature ~~of the Earth's line~~ can be applied more generally and, in fact, was applied by Booker to study the guiding of rays along a density discontinuity. Then, in studying nearly longitudinal propagation near a particular point of a particular line of magnetic flux, the line of flux and the associated field aligned density irregularity are considered to be straight but, instead of the actual refractive index n , a modified index n' is employed to study propagation, given by

$$n' = n(1 + Kz) \quad (8.26)$$

Here z is a coordinate measured transverse to the field in the outward direction and K is the differential curvature defined in (8.22). The modified refractive index (8.26) has therefore an additional transverse

gradient across the magnetic field not possessed by the actual refractive index and actually proportional to the differential curvature K . As a consequence, the curvature of wave rays with respect to the straight line of flux in this model is the same as the curvature of the actual rays relative to the bent lines of force in the real world. This technique requires that the radius of curvature of the rays and of the lines of magnetic flux to be large compared with the local wavelength in the medium. After the line of flux has been straightened out in accordance with the concept of modified refractive index, a ray which is successively reflected at the interface has the form shown in Fig. 47. Each segment of the ray has now the differential curvature K calculated from (8.22) and plotted in Fig. 47. As we move along the guide, the curvature K of the ray segments in Fig. 47 changes slowly in accordance with the variations shown in Figs. 46.

In conclusion it should be pointed out that, as clear from Fig. 47, the linear z variation of the modified refractive index (8.26) refers to the width of the wave guide.

8.8 Phase integral condition in Booker's theory

Let α be the elevation angle of a wave at the plasma interface, as shown in Fig. 47. We shall assume this angle to be small so that use can be made of the longitudinal expression (8.8) for the refractive index n . We will investigate a posteriori to which extent this is justified. Corresponding to the discontinuity in density (from N_0 to $N_0 + \Delta N$) at the interface of Fig. 47 we will have a discontinuity in refractive index. Reflection at the interface is described by Fresnel's formulae. The critical value α_c of α below which total internal reflection occurs is found (see Appendix B) to be given by

$$\alpha_c^2 = \frac{1-n^2}{n^2} \frac{\Delta N}{N} \quad (8.27)$$

The phase change ϕ_1 of the waves at this reflection, corresponding to the value α of the inclination angle is given approximately (see Appendix B) by

$$\phi_1 = 2 \arctg \left(\frac{\alpha_c^2}{\alpha^2} - 1 \right) \quad (8.28)$$

From this formula we see that, when $\alpha > \alpha_c$, ϕ_1 is complex corresponding to imperfect reflection.

We will now write the phase integral condition of mode theory (see Sect. 7) for the wave guide of Fig. 47. There, one of the boundaries of the wave guide is the interface across which there is the density jump. The other edge is the caustic surface indicated in Fig. 47 which corresponds to reflection at a zero of q (the z projection of the refractive index vector). We have already calculated in Sect. 7 the change in phase of a wave while crossing twice the wave guide in the case of a linear variation of refractive index (see eq. 7.10). For the Booker's case ($\alpha \ll 1$) this becomes

$$2 \frac{2\pi\alpha^3}{3K\lambda} - \frac{\pi}{2} - \phi_1 = 2\pi(p-1) \quad (8.29)$$

where $p=1$ is now the lowest order mode and the term $-\pi/2$ is the phase change at the caustic. Substituting eq. (8.28) for ϕ_1 , we rewrite (8.29) as

$$\frac{2\pi\alpha^3}{3K\lambda} - \arctg \left(\frac{\alpha_c^2}{\alpha^2} - 1 \right)^{1/2} = \left(p - \frac{3}{4} \right) \pi \quad (8.30)$$

At a given point of a line of flux of the Earth's field, and for a given frequency, the differential curvature K of eq. (8.22) can be

obtained from Figs. 46. Also, for a given fractional density change $\Delta N/N$ across the interface, the critical angle α_c is obtained from (8.27). When all this is used, one determines, from (8.30), the angle of elevation α of the p -th mode.

8.9 Minimum fractional density gradient for trapping and track width

It is important to derive the minimum fractional density change $\Delta N/N$ that produces reasonable good guiding of one mode. This occurs when the mode changes from leaky to trapped behaviour and, therefore, when the mode angle α is close to α_c . In these conditions, the second term on the left hand side of eq. (8.30) (the phase change at the interface) can be neglected and, referring to the lowest order mode $p=1$, the equation reduces to

$$\frac{2\pi\alpha^3}{3K\lambda} = \frac{1}{4} \pi \quad (8.31)$$

of which we must impose, for minimum guiding, the solution to be

$$\alpha = \alpha_c \quad (8.32)$$

Thus the condition for the lowest mode to be guided becomes

$$\alpha_c = (3/8 K\lambda)^{1/3} \quad (8.33)$$

Using now eq. (8.27) for α_c , it follows that the minimum fractional change in ionization density necessary to guide the lowest order mode is given by

$$\frac{\Delta N}{N} = \frac{n^2}{1-n^2} \left(\frac{3}{8} K\lambda \right)^{2/3} \quad (8.34)$$

necessary for guiding as a function of position (θ) along different magnetic flux lines.

Fig. 48a refers to the frequency $f=1\text{Kc/s}$. At this frequency, the lines of magnetic flux for latitudes $\Lambda=15^\circ, 30^\circ, 45^\circ, 60^\circ, 75^\circ$ which are reported in the figure, lie entirely in the inner zone of longitudinal propagation for the FMS (R) wave and in the forbidden zone for the L wave (see Sect. 8.3). Thus all the curves in Fig. 48a refer to R waves (whistlers). It is seen that, at 1Kc/s , guidance can be produced by fractional variations of ionization density of the order of 1%.

The track width of the lowest order mode, for the same frequency, is plotted as a function of θ , for different latitudes Λ , in Fig. 49a and, as it can be seen, varies from ~ 10 to ~ 100 km.

Going now to a low frequency, of 10 c/s , Fig. 48b gives the minimum $\Delta N/N$ required for guiding. In this case inner zone longitudinal propagation is possible not only for the R but also for the L wave (correspondingly different curves, dashed and not dashed respectively are given in the Figure). Here we see that guidance of such waves round the lines of flux of the Earth requires higher values of $\Delta N/N$, from 10% to 25%, than in the case of the 1Kc/s wave, the smaller values being adequate for the higher latitude lines. The track width at this frequency, given in Fig. 49b is also much higher than for the 1Kc/s wave and ranges roughly from 100 to 1000 km.

On the other hand, moving to much higher frequencies and, for example, for $f=10\text{Mc/s}$, we see from Fig. 48c that we need $\Delta N/N \sim 10\%$ to ensure guiding for low latitude lines (and guiding takes place now in the outer zone). For high latitudes and near the equatorial plane, guiding becomes impossible. The track width, given in Fig. 49c, is, for this frequency, much smaller than at the lower frequencies and, in general, below 1 km.

Thus, the overall impression that we get from these (and other)

numerical results, is that guidance disappears as we go to high frequencies, of the order of 10 Mc/s , and also going to low frequencies, of the order of 10 c/s or smaller. On the other hand, guidance is most easily obtained for whistler waves, in the inner zone of propagation, at intermediate frequencies (Kc/s). For a given mode, at a given frequency and on a given flux line, the variations of $\Delta N/N$ with position (θ) along the line are not very remarkable but, in any case, one gets somewhat larger values of $\Delta N/N$ when the line crosses the equatorial plane.

A very convenient way of looking globally at these results is that of fixing θ , at the position of crossing of the equatorial plane for any given line, and there plot the values of $\Delta N/N$ required for guiding and the corresponding track width as a function of frequency. This is done in Figs. 50a-d where the left hand ordinate scale refers to $\Delta N/N$ and the right hand scale to the width w and the successive figures (a-d) refers to lines of different latitude. The curves for $\Delta N/N$ show strikingly the disappearance of guiding both as we go to high radio frequencies and as we go to low hydromagnetic frequencies. The low frequency branches refer, as it is explicitly indicated, to inner zone of propagation and the high frequency branches to outer zone of propagation. These curves show that, for the R waves, there are about 5 decades in frequency where guidance is possible for relatively small values of $\Delta N/N$. From the sequence a-d of the figures, it is also seen that this frequency range slides down by about 3 decades as we move from low latitude to high latitude lines of flux. In other words, guidance of radio waves in the outer zone is easier at low latitudes than at high latitudes, while the opposite is true for guidance of hydromagnetic waves in the inner zone (easier at high than at low latitudes).

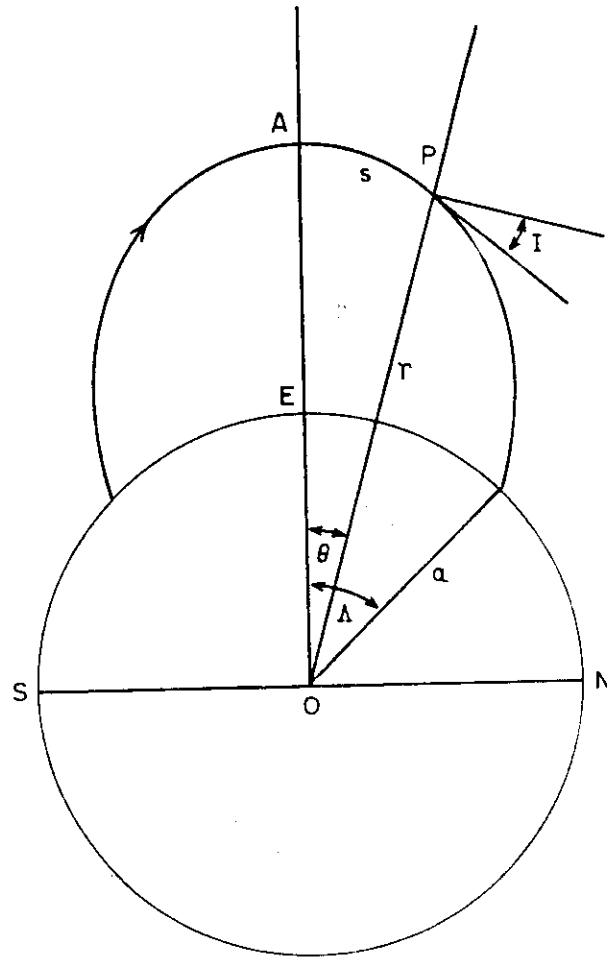
To explain in physical terms, at least in a qualitative way, these numerical results we must give some comments on the meaning of the track width of the modes. As commented by H. Booker, the model taken of a discontinuity in density at an interface parallel to a flux line, must be interpreted in the sense that the results obtained are valid for any continuous density variation across the magnetic flux line of scale somewhat less than the track width w obtained by the calculations (*). It follows then that the track width obtained may be also interpreted as the (maximum) lateral extension of the field aligned density irregularity. Let us look now from this point of view at the results shown in Figs. 50a-d. The values of w reported in these figures can be interpreted as the maximum transverse scale of the density irregularity for which (under the calculated value of $\Delta N/N$) trapped propagation (of the lowest order mode) is obtained. For the intermediate frequencies (Kc's), where guiding is obtained for relatively small values of $\Delta N/N$ (down to 1%), we see that the transverse scale runs from ~ 2 km to ~ 100 km for the 15° line of flux and from 50 km to ~ 1000 km for the 75° line of flux.

For $f=10$ Mc/s the transverse scale is less than 1 km. Most likely inhomogeneities on this scale are present in the magnetosphere. However, what inhibits guidance at these radio frequencies, are the higher values of $\Delta N/N$ required.

On the other hand, at hydromagnetic frequencies, the transverse scale w becomes exceedingly large (as it is also seen in Fig. 50) and, in fact, it approaches, at the low frequency limit, the radius of the Earth. Such large scale inhomogeneities are at least unlikely. It is seen therefore that guidance at very low hydromagnetic frequencies in the magnetosphere may be impossible because such large scale inhomogeneities are simply not accommodated.

(*) On the other hand, being the calculation based on the use of the plane integral condition, such track width must large in comparison with the wavelength of the mode considered. Thus we see that, in the end, the Booker's discontinuous model is not very different from the duct models used in the ray theory of guided whistlers by Smith et al. (1960).

FIG. 36



$$Z = a \frac{\omega^2 \theta}{\omega^2 \Lambda}$$

FIG 37

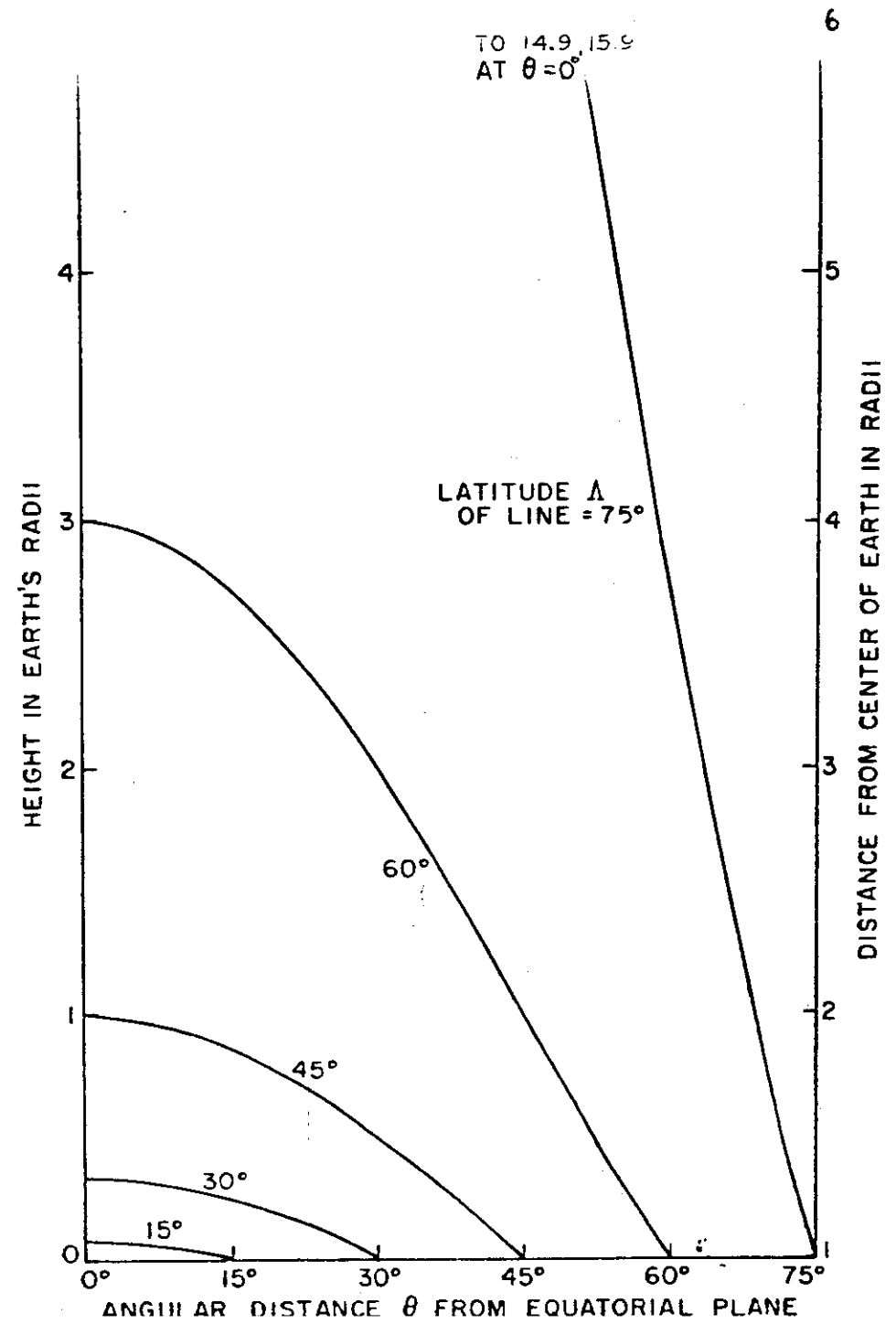
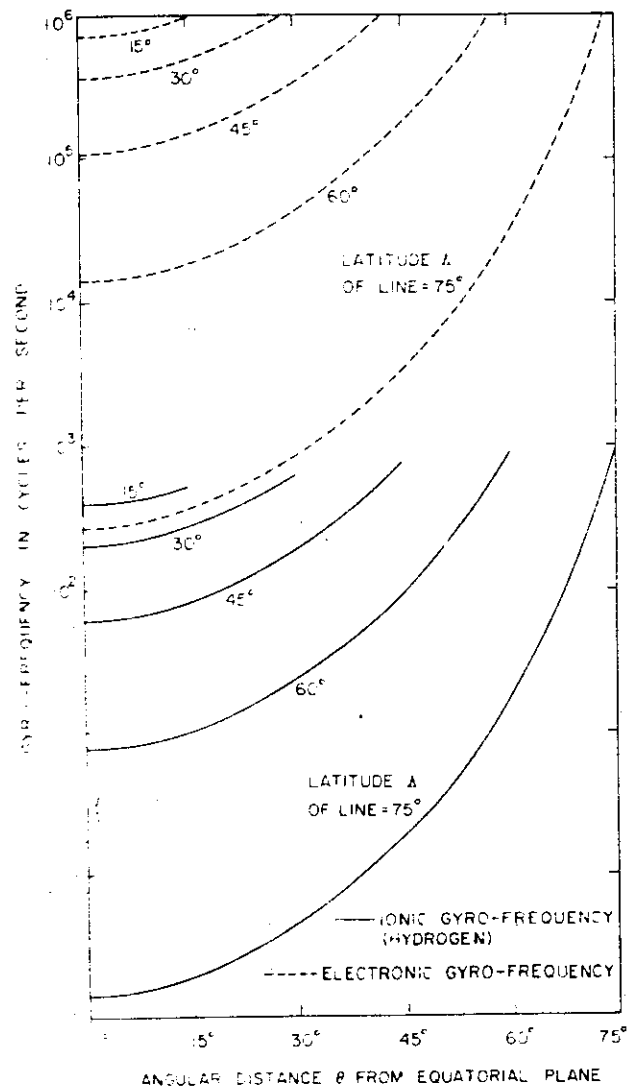


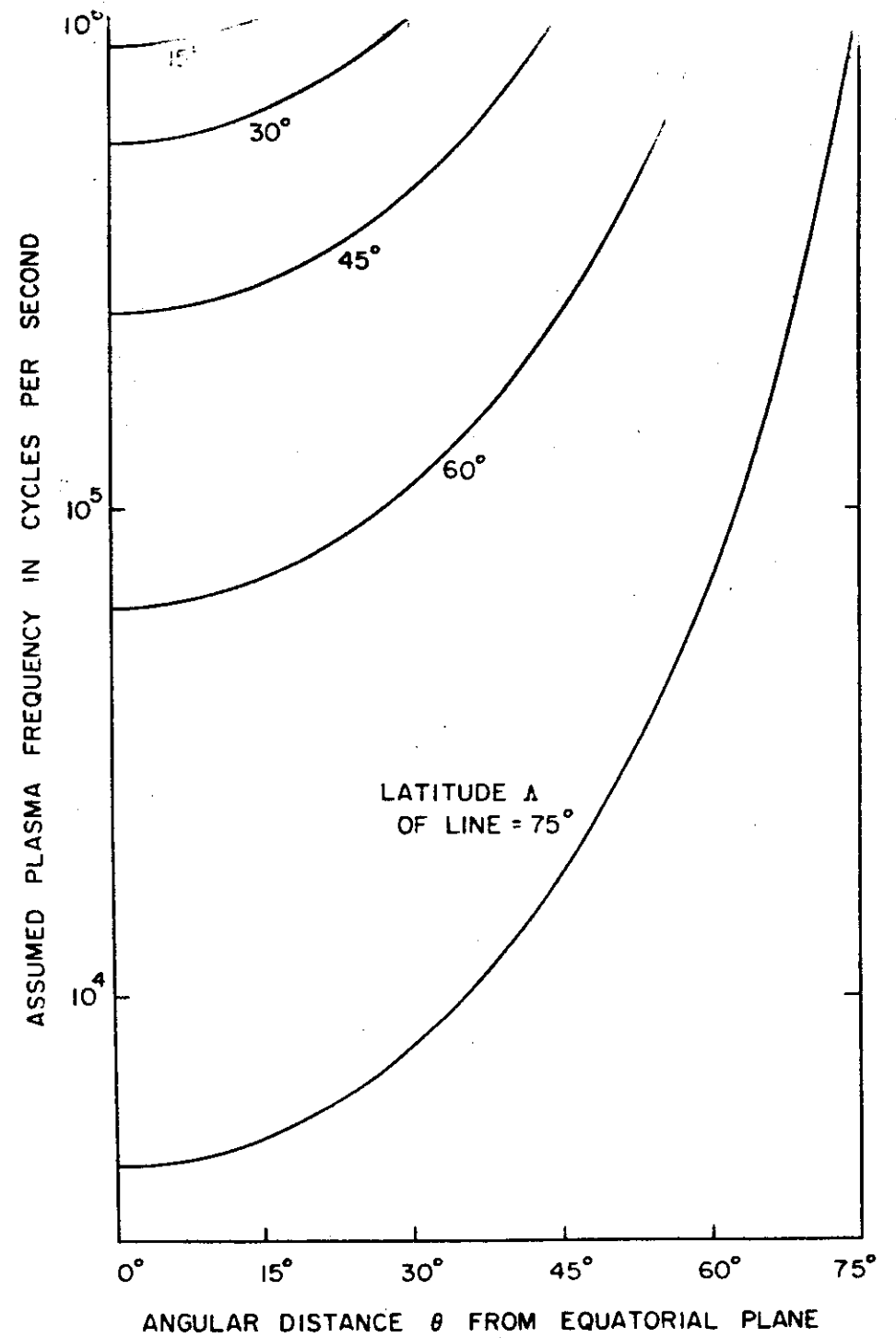
FIG 38



(23)

FIG-39

(24)



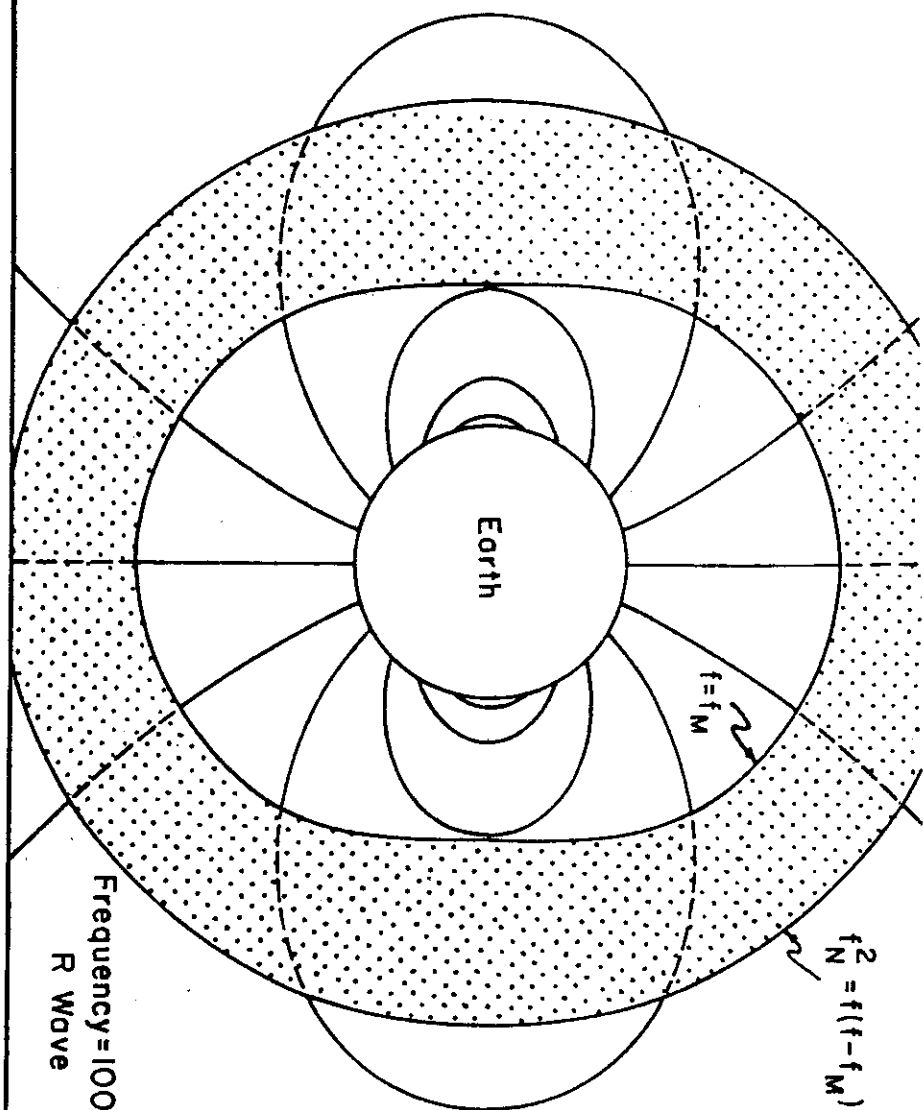


FIG. 10.

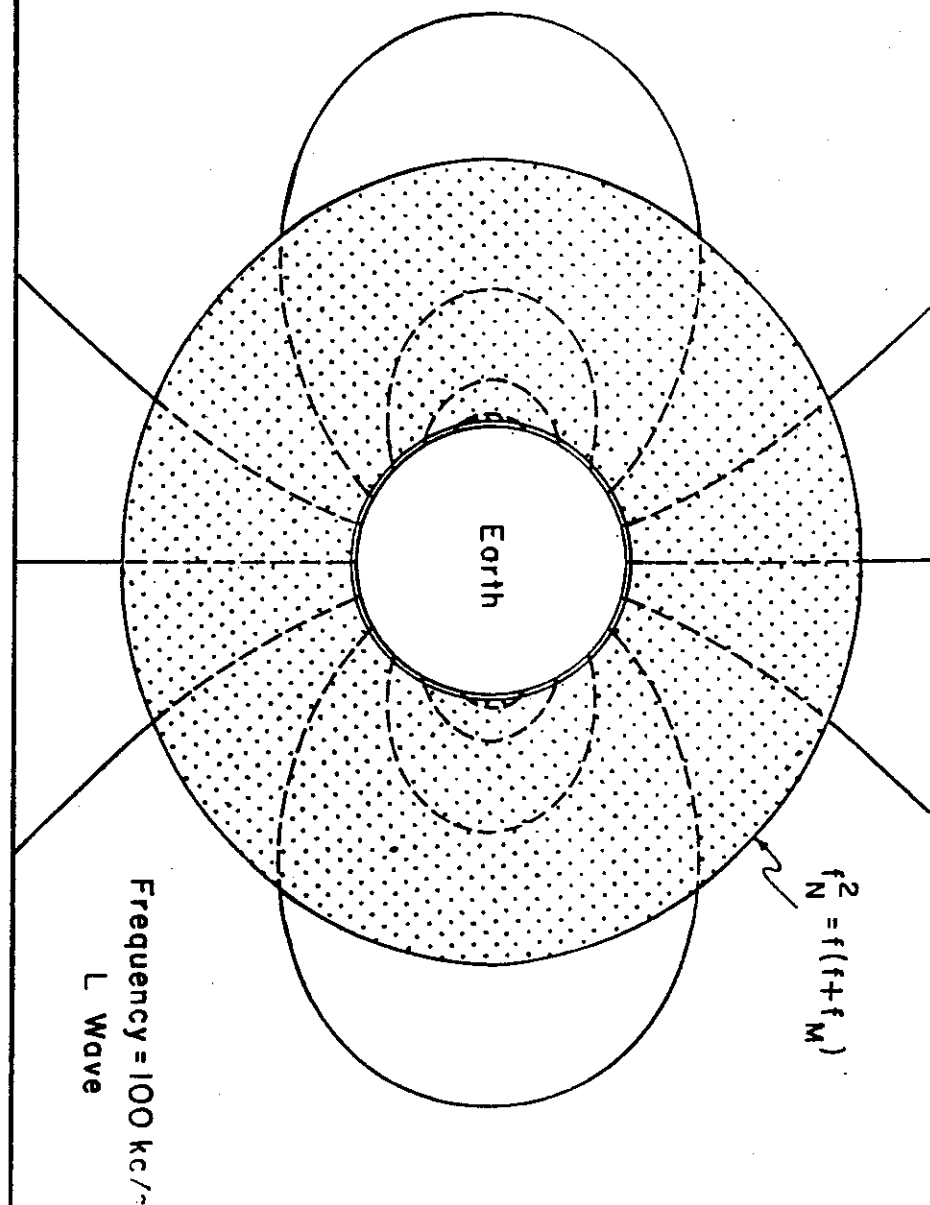


FIG. 10L

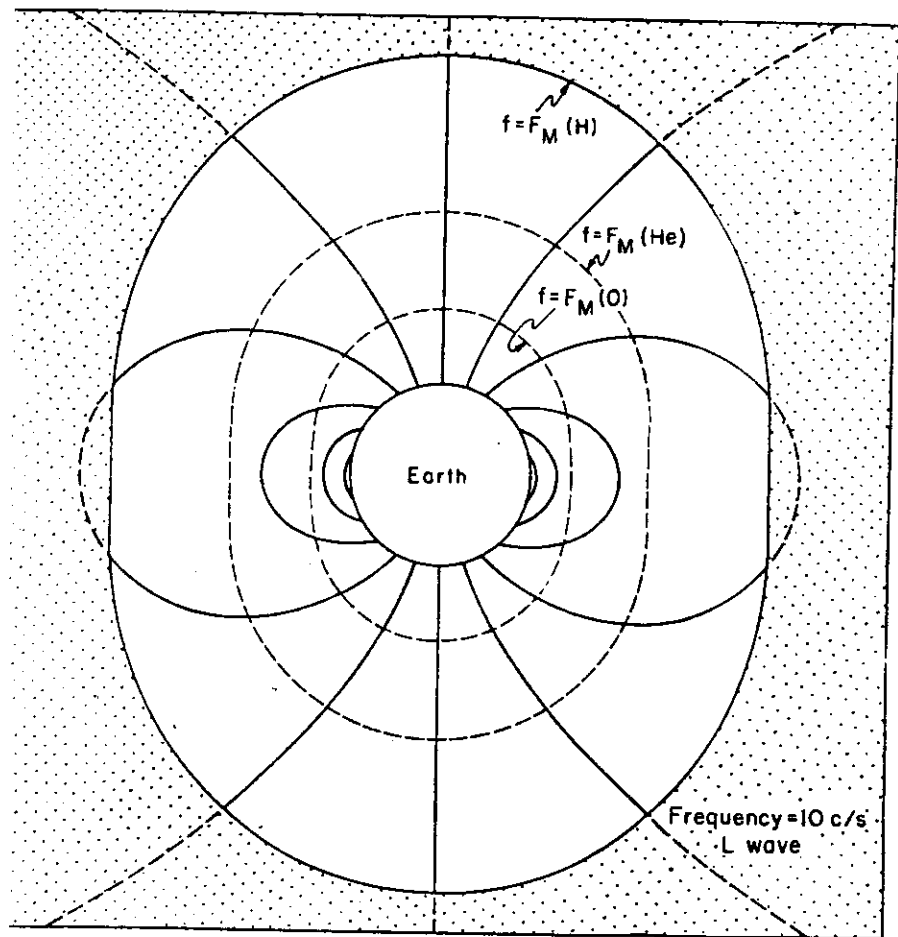


FIG. 40c

FIG. 41

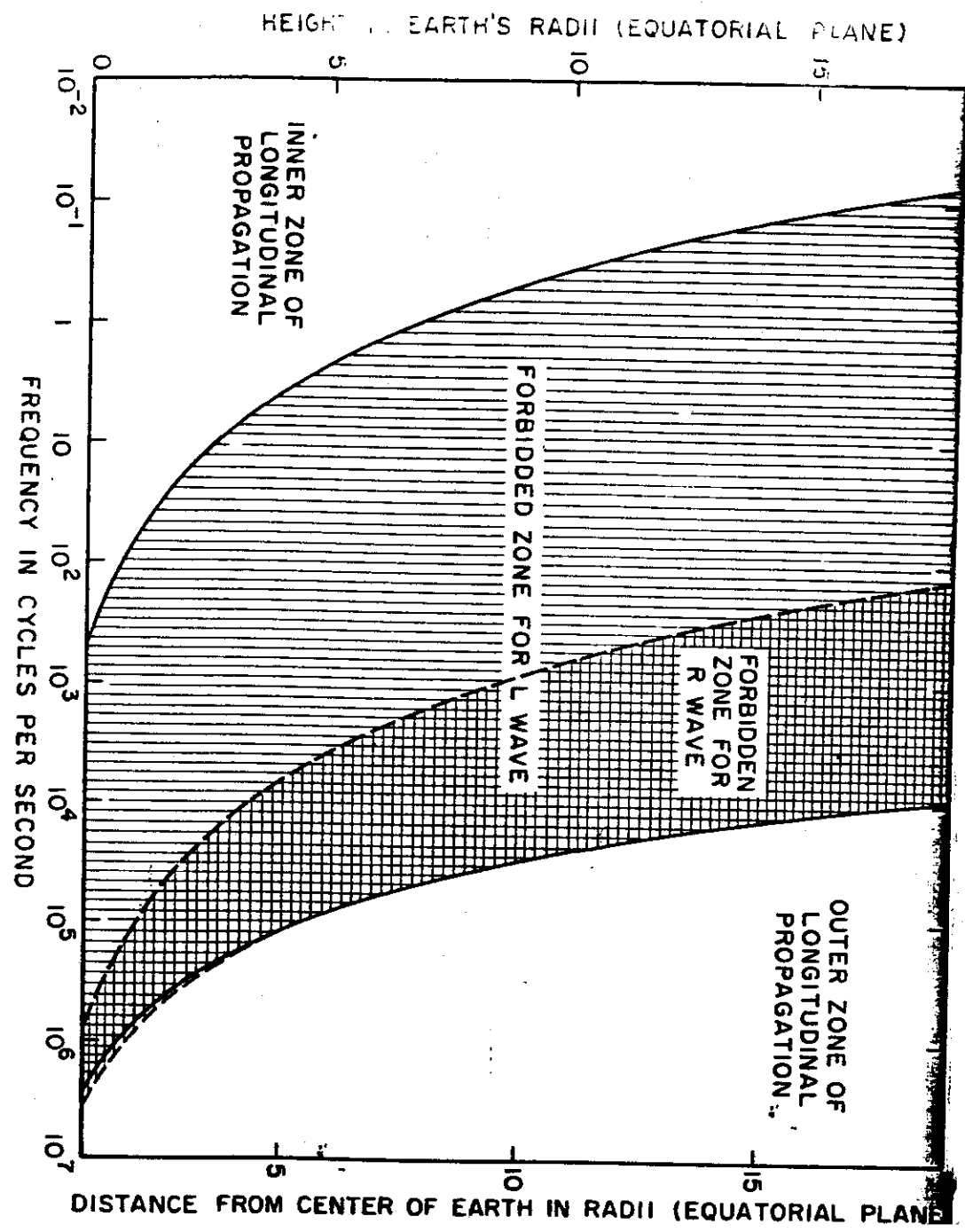


FIG. 42

(29)

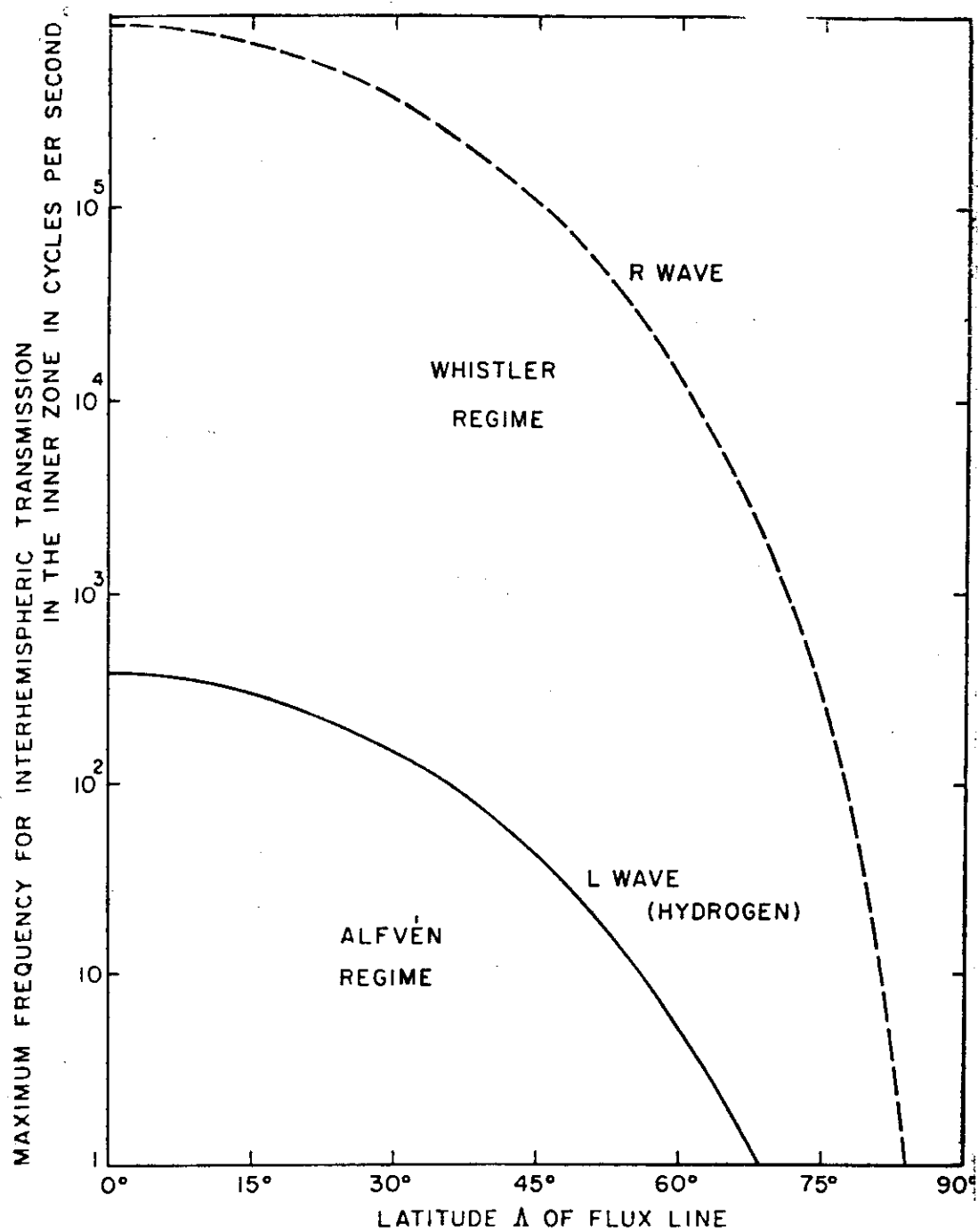


FIG. 43

(30)

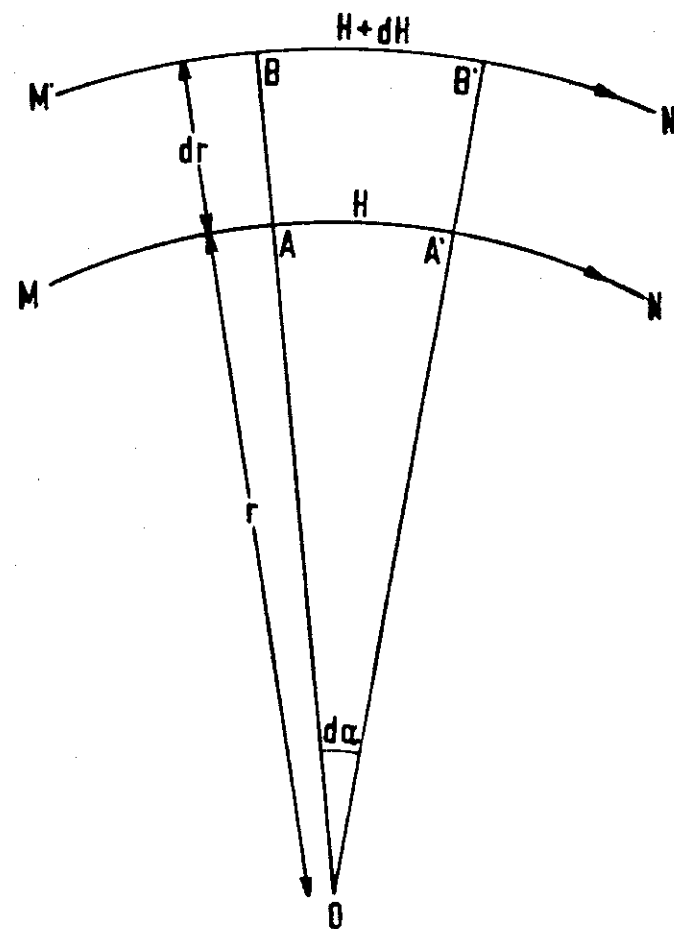
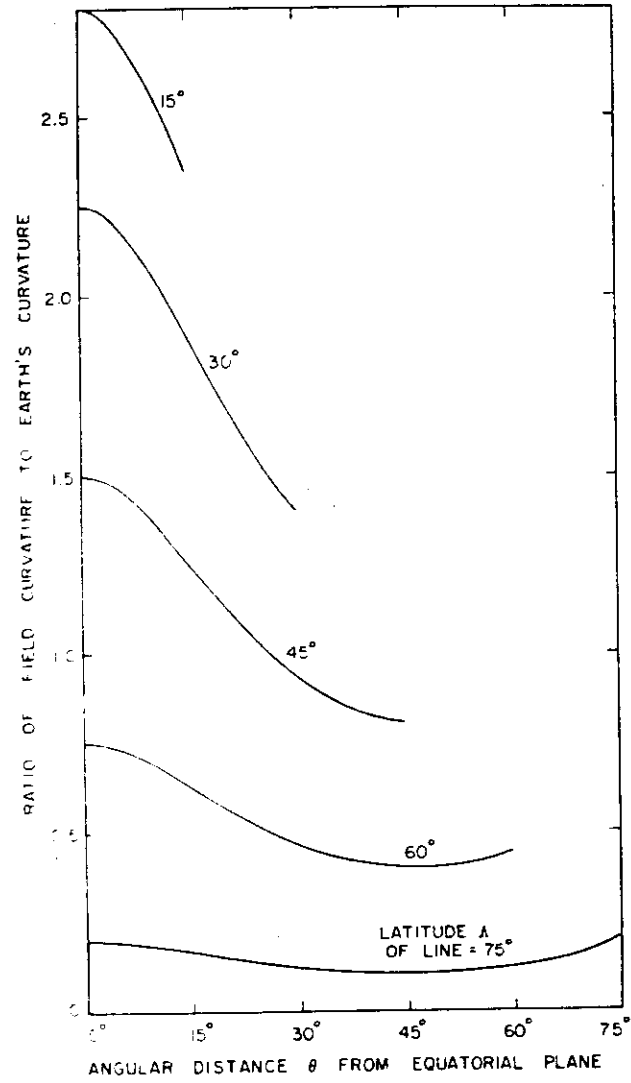


FIG. 44



(31)

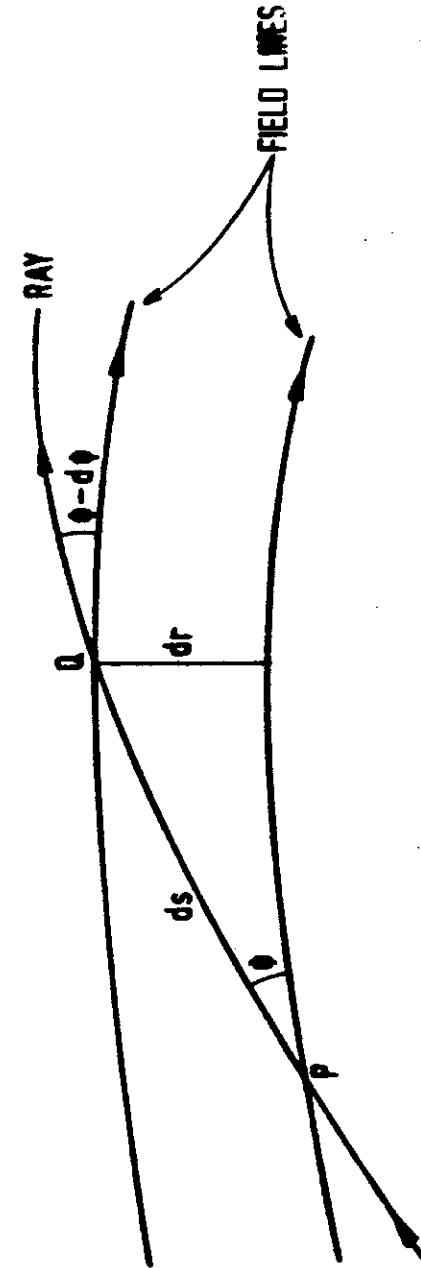
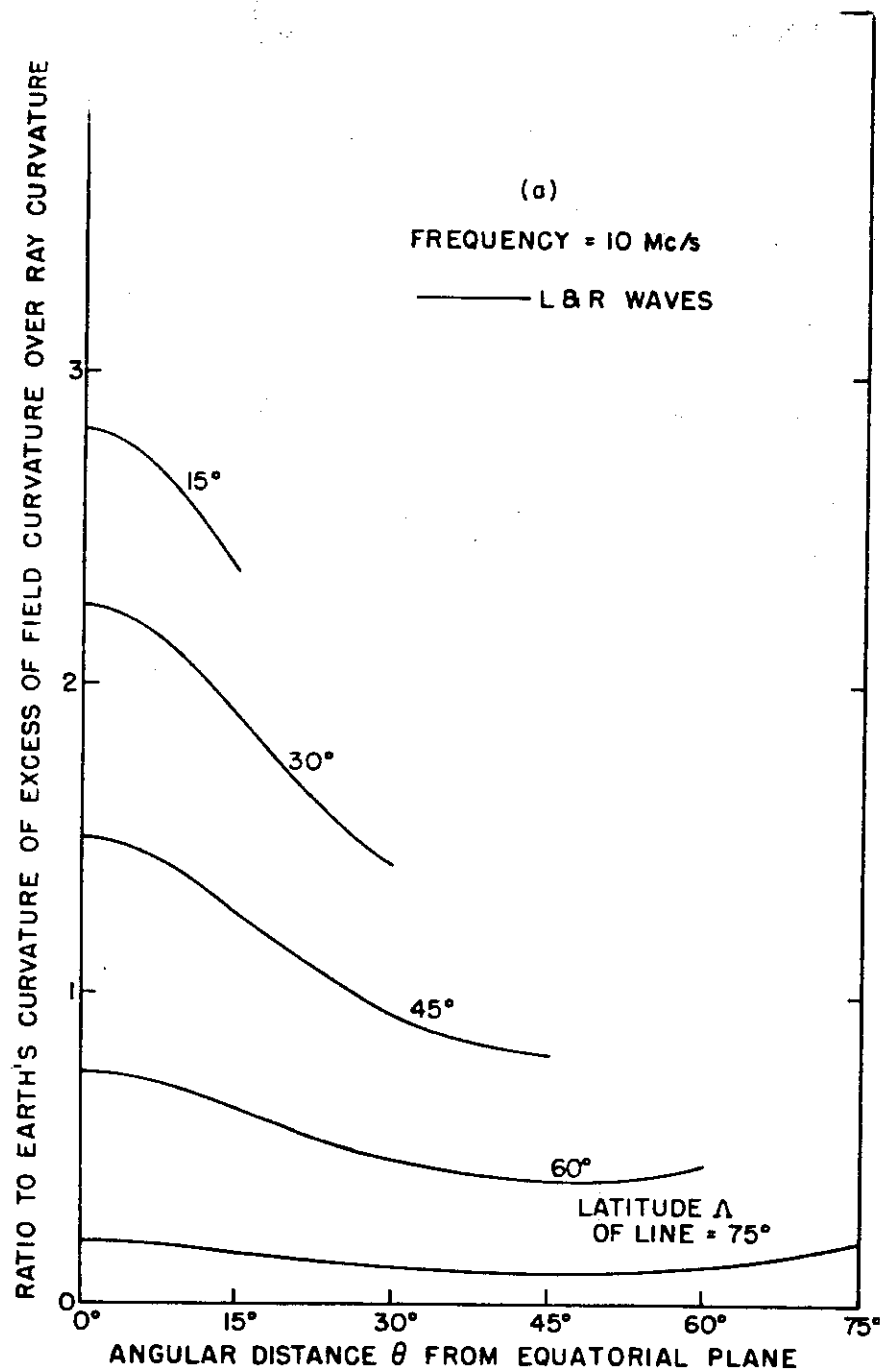


FIG. 45

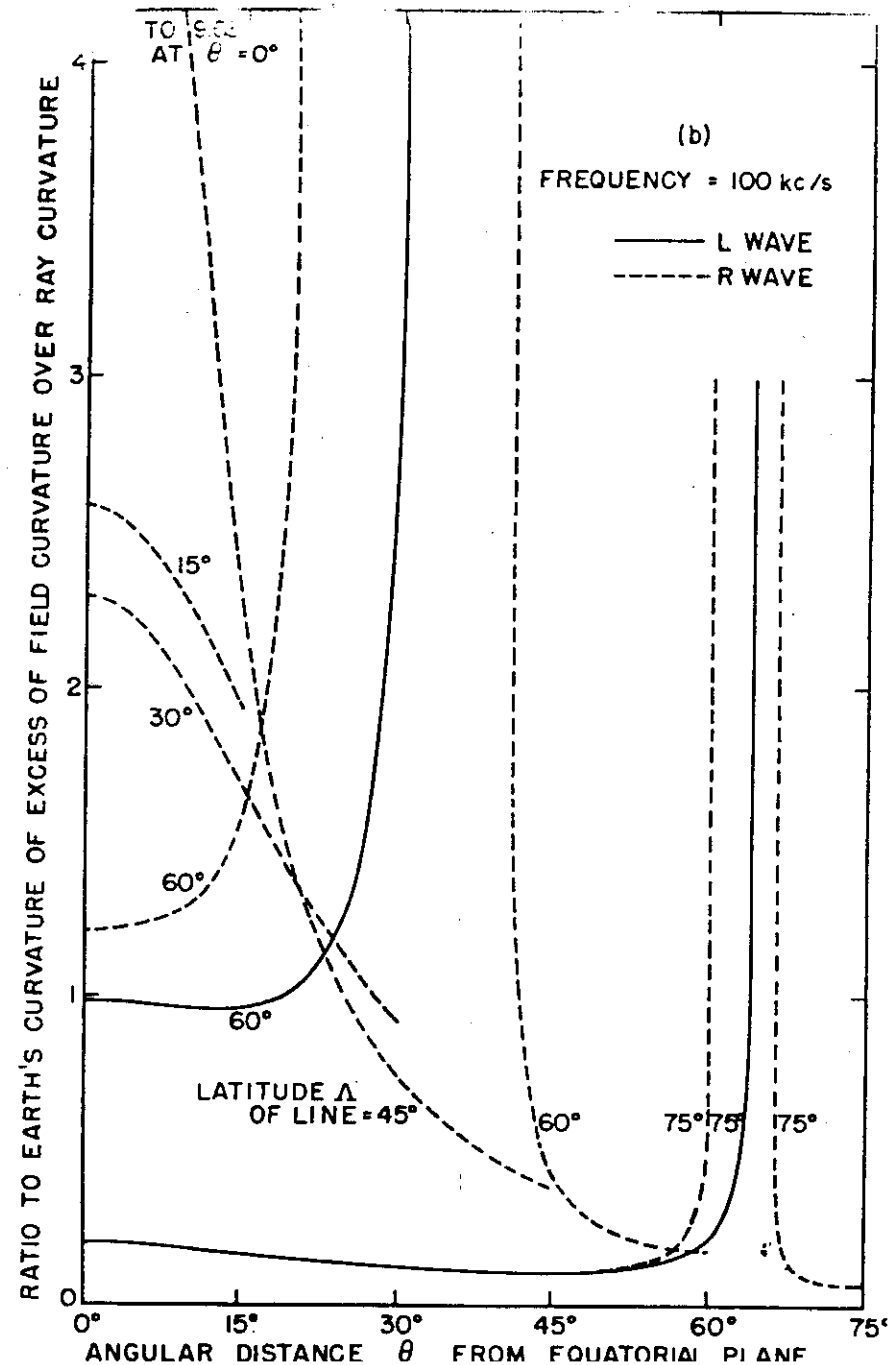
(32)

FIG. 46a



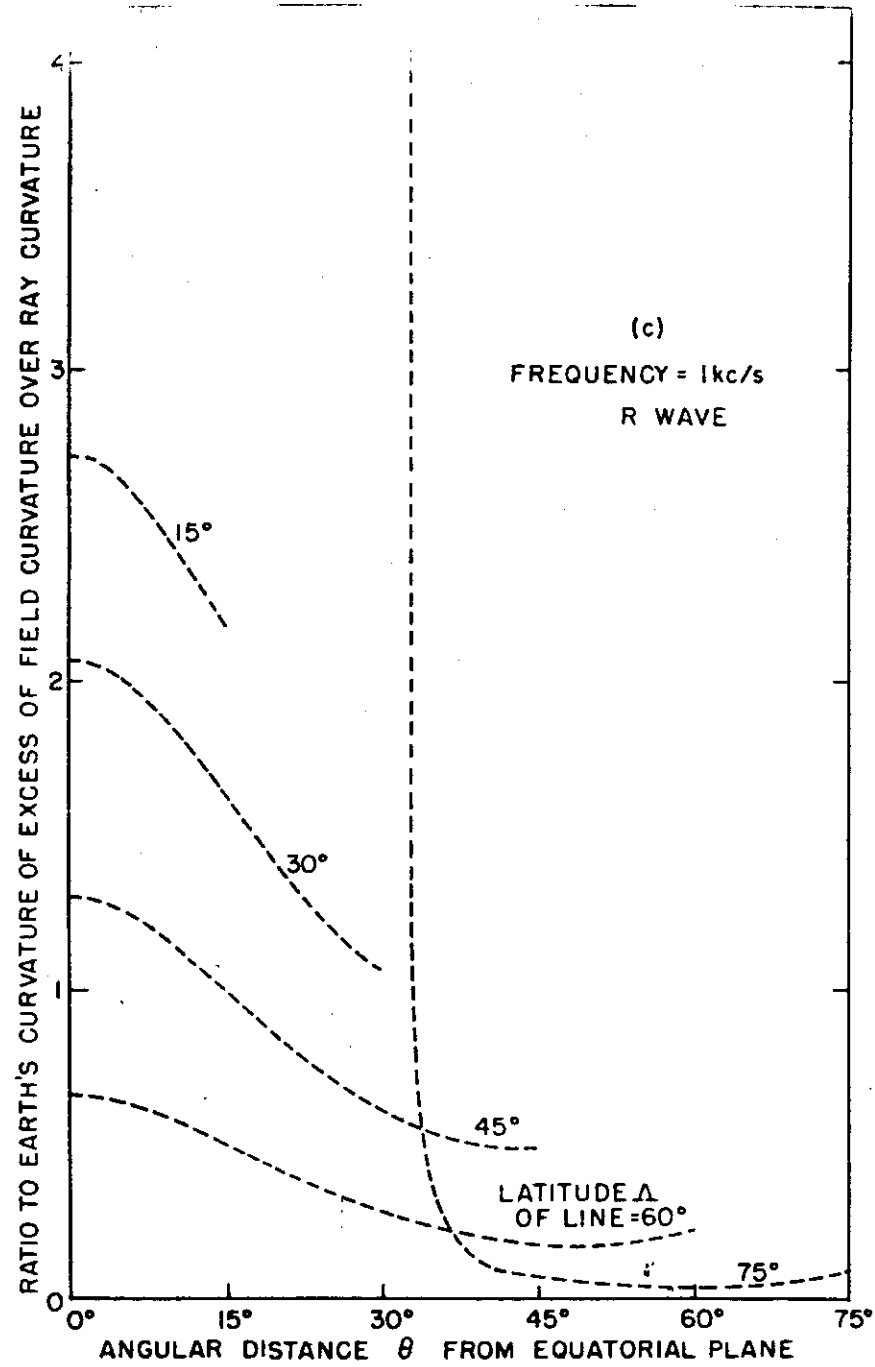
(33)

FIG. 46b



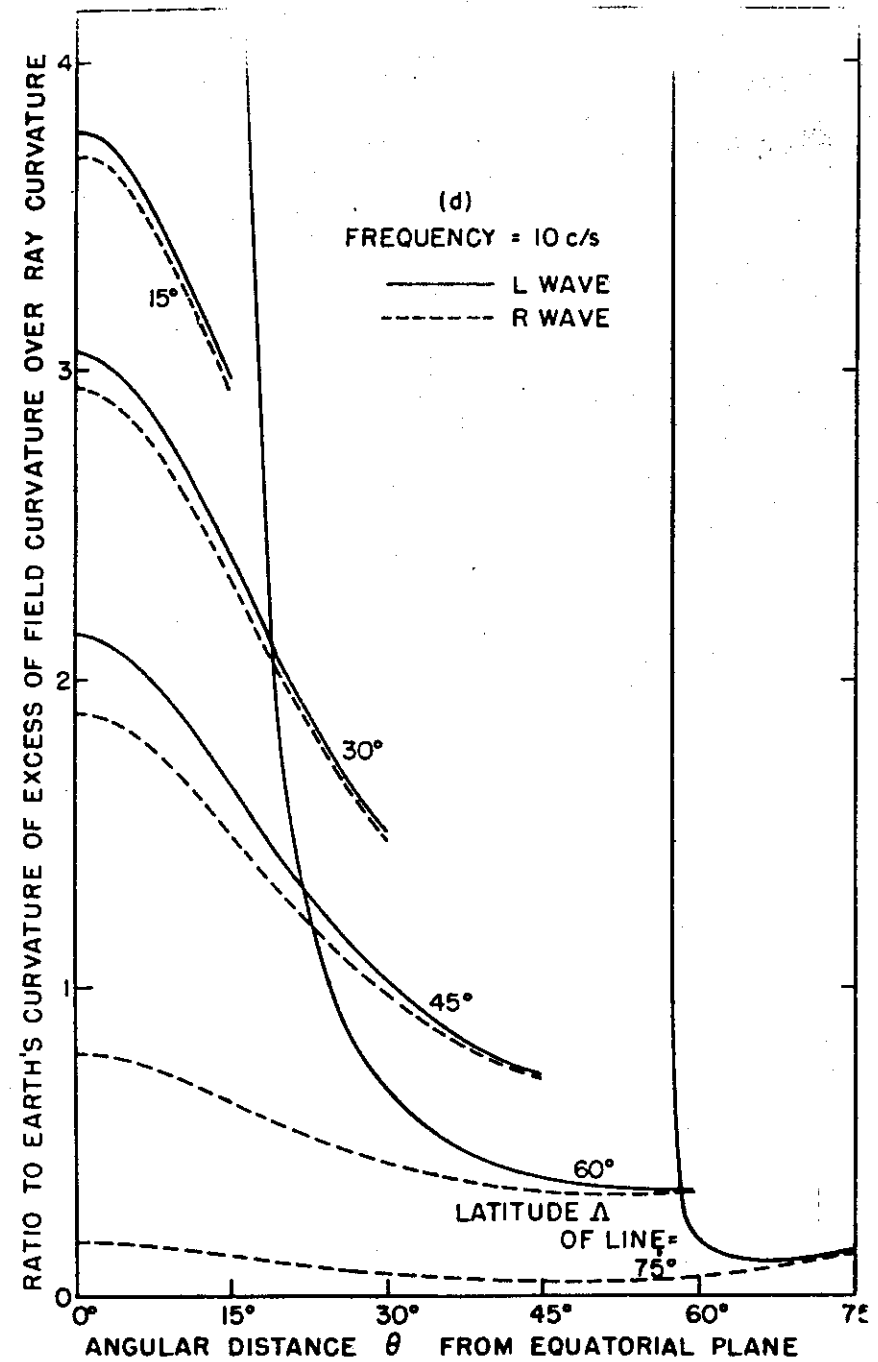
(34)

FIG 46c



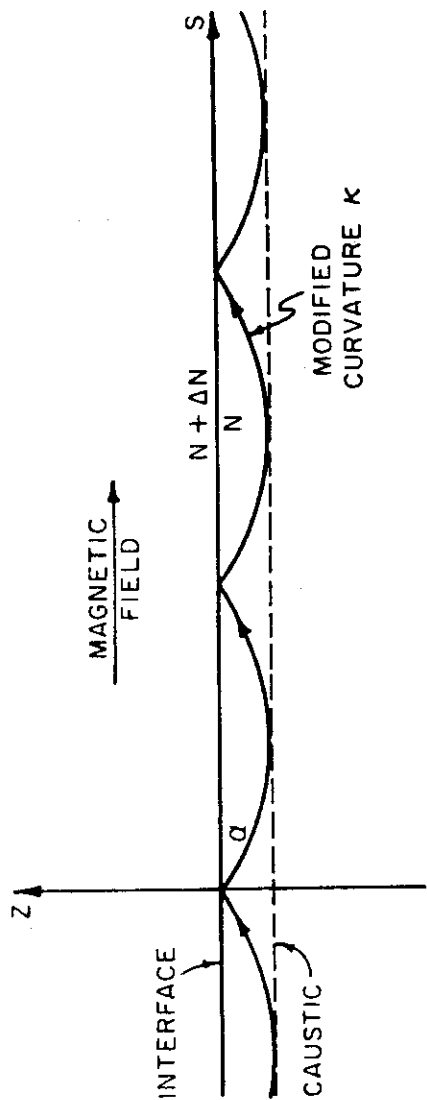
(35)

FIG 46d



(36)

FIG 47



MINIMUM FRACTIONAL INCREASE IN IONIZATION DENSITY $\Delta N/N$ TO GUIDE LOWEST MODE

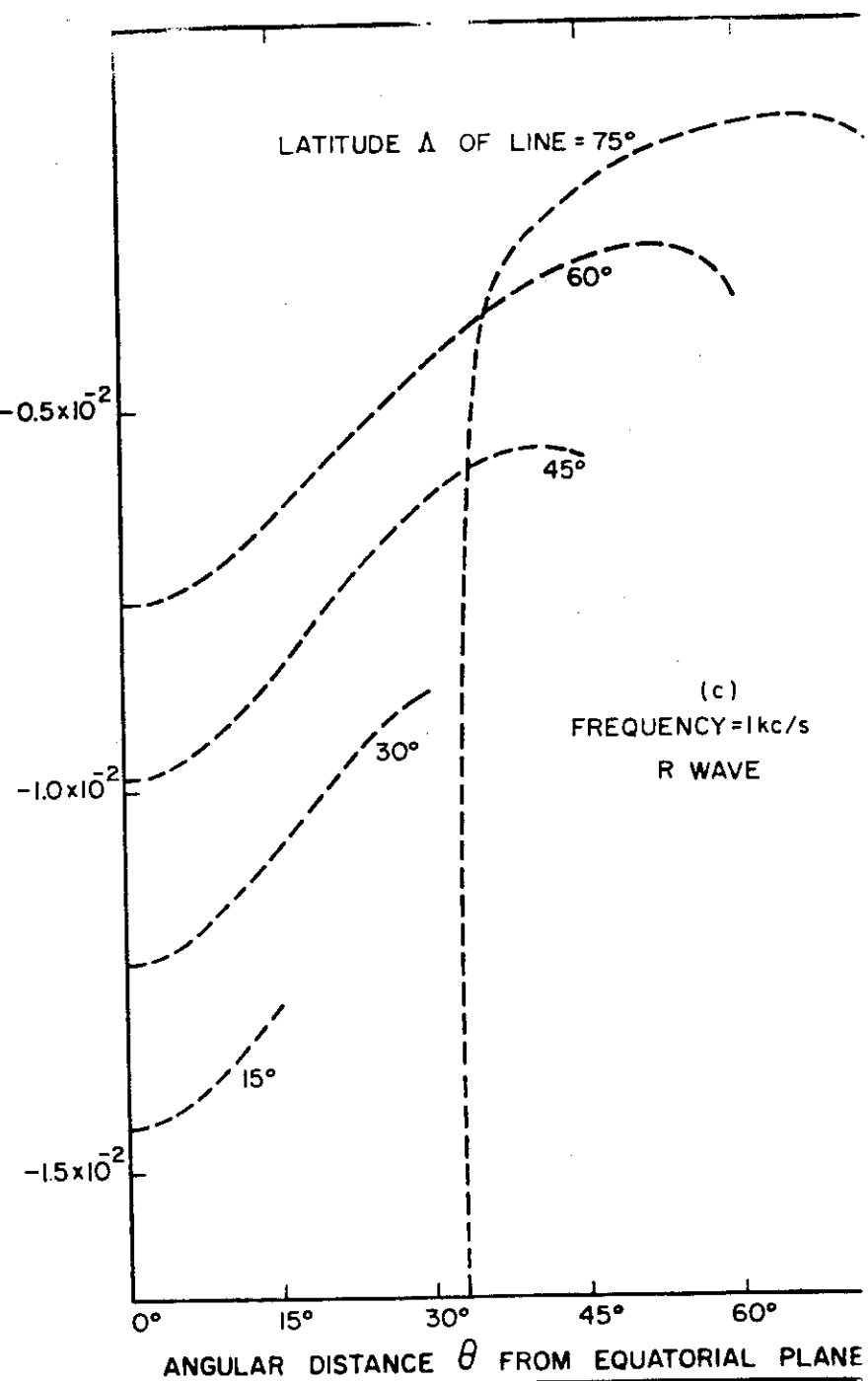


FIG 48a

FIG 48b

(39)

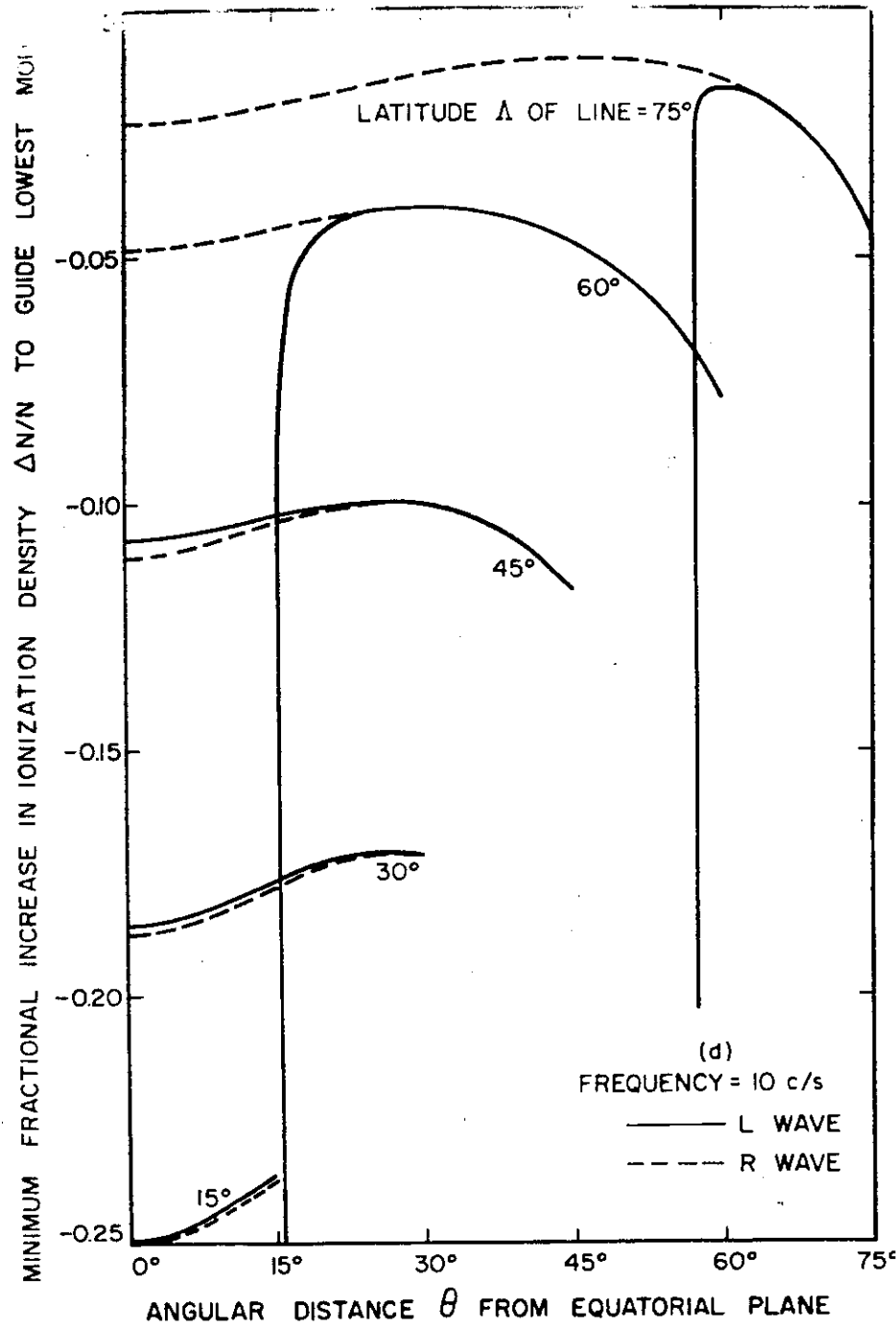


FIG 48c

(40)

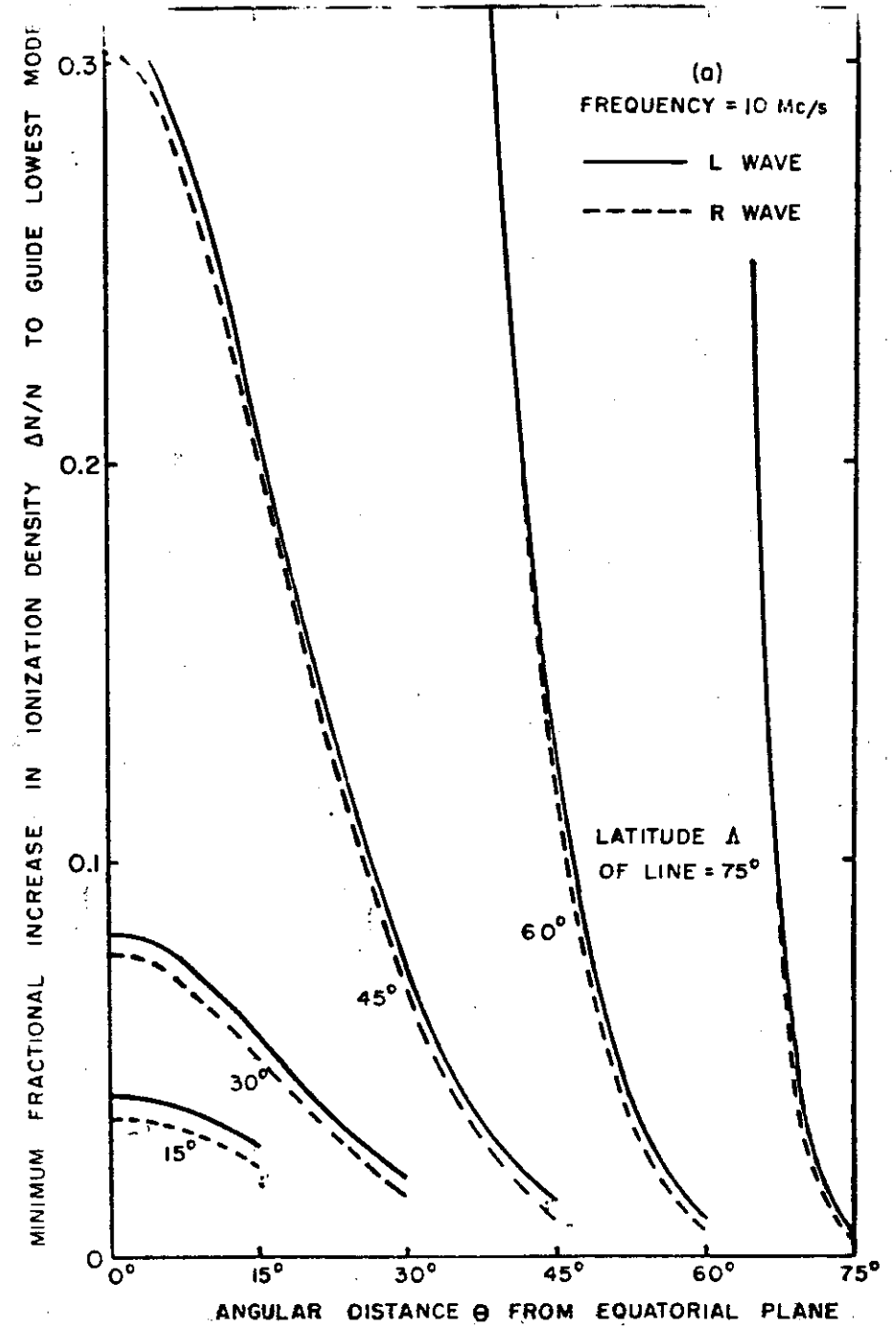


FIG 49a

(41)

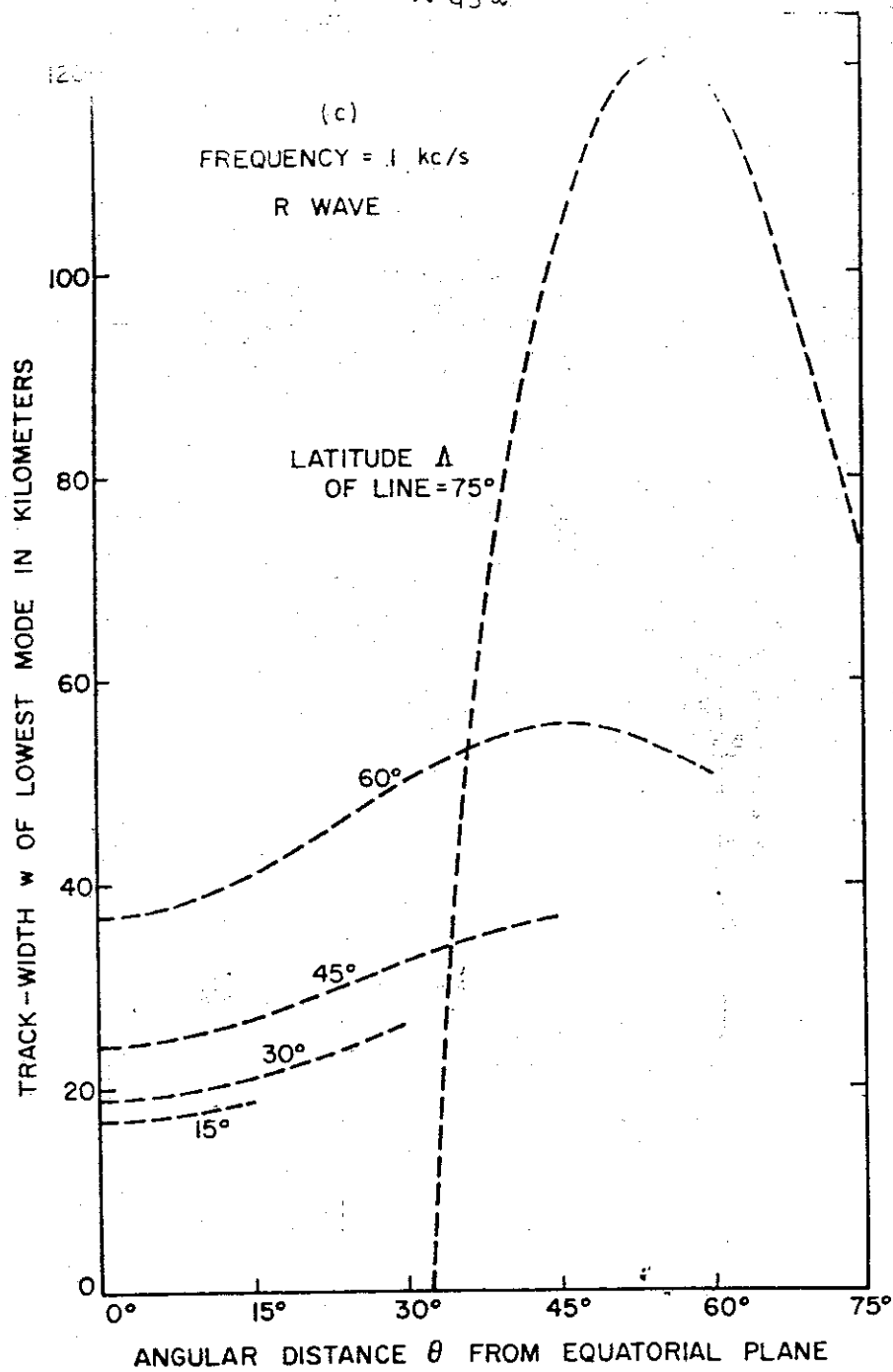


FIG 49b

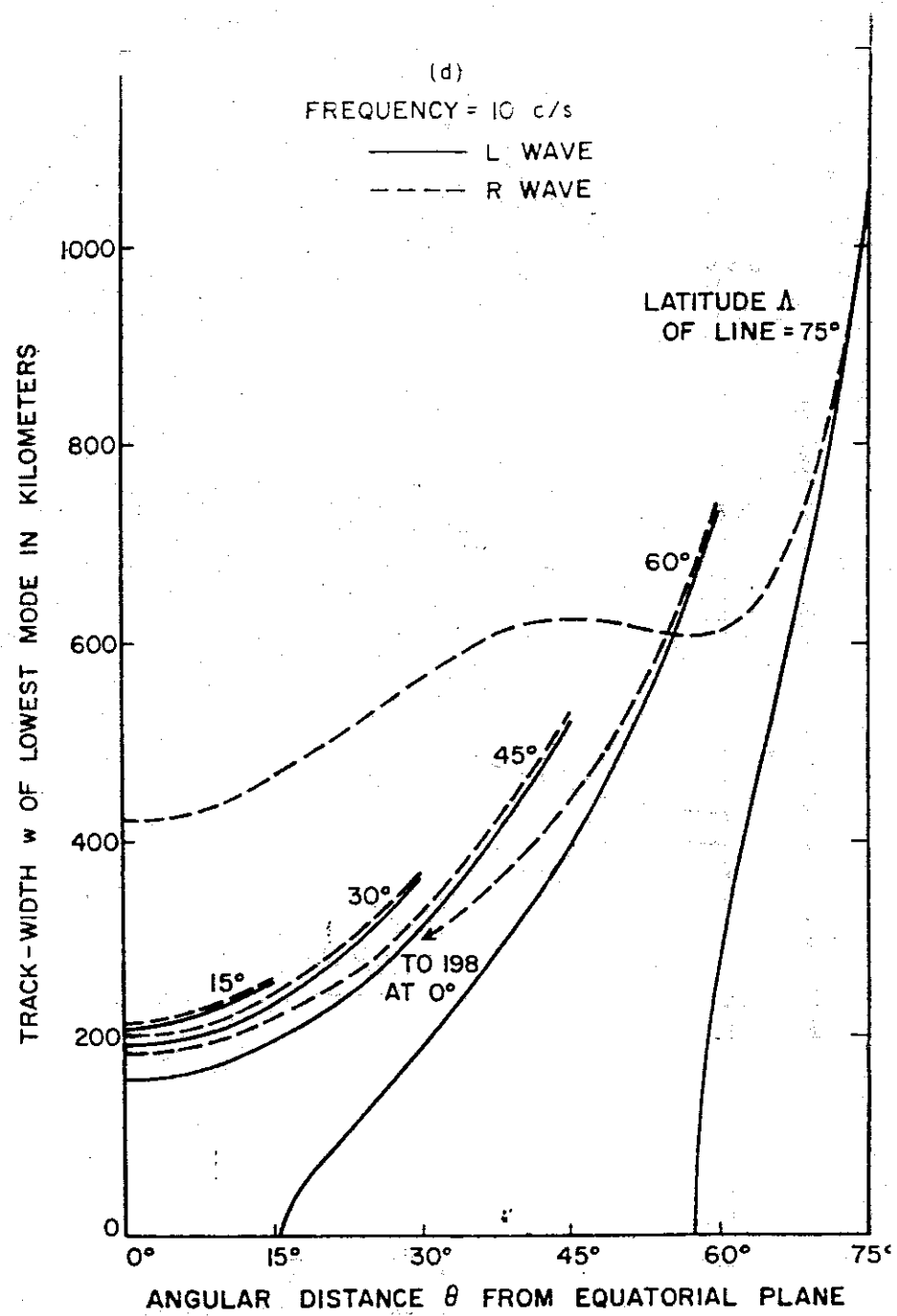


FIG 49c

(43)

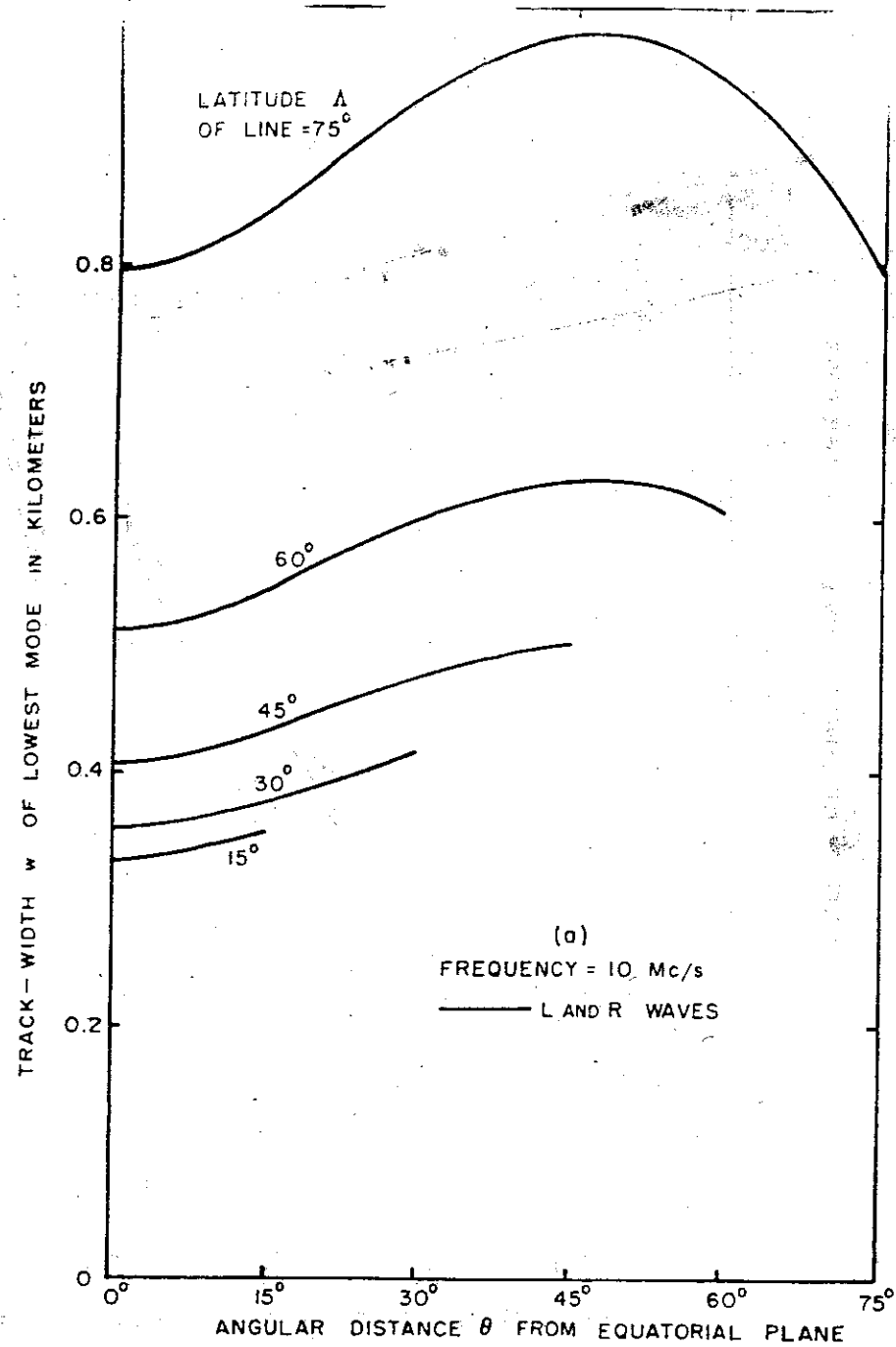


FIG 50a

(44)

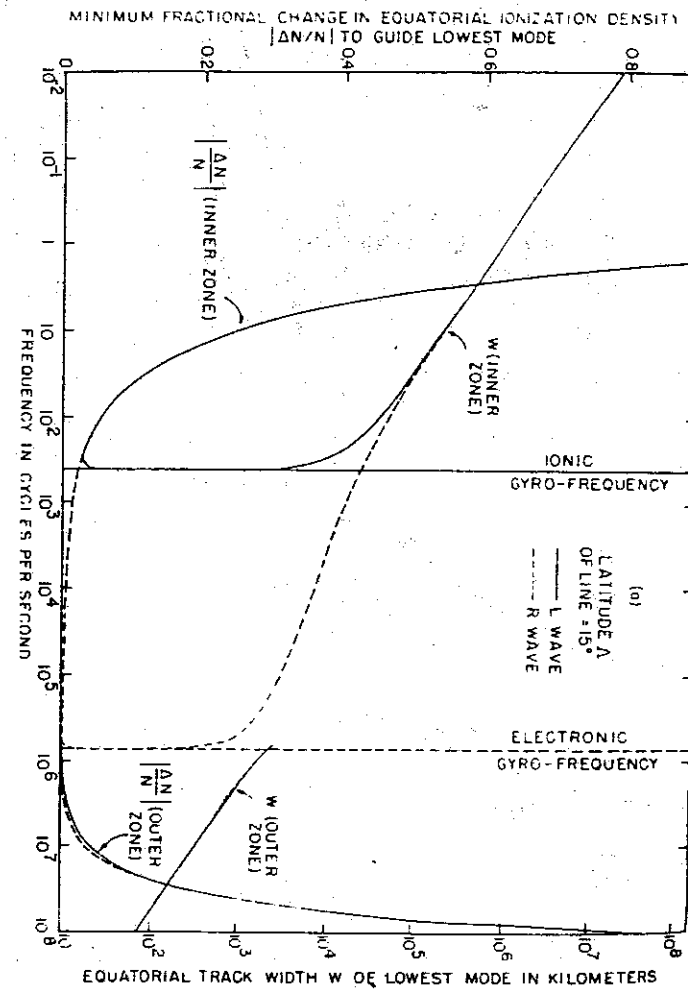


FIG. 50d

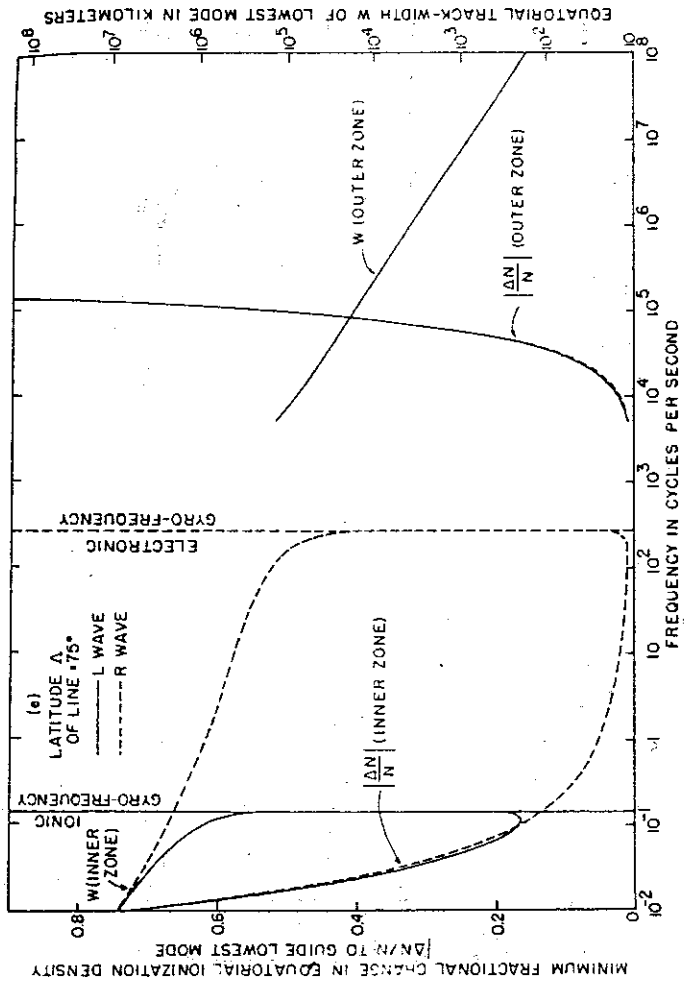


FIG 50b

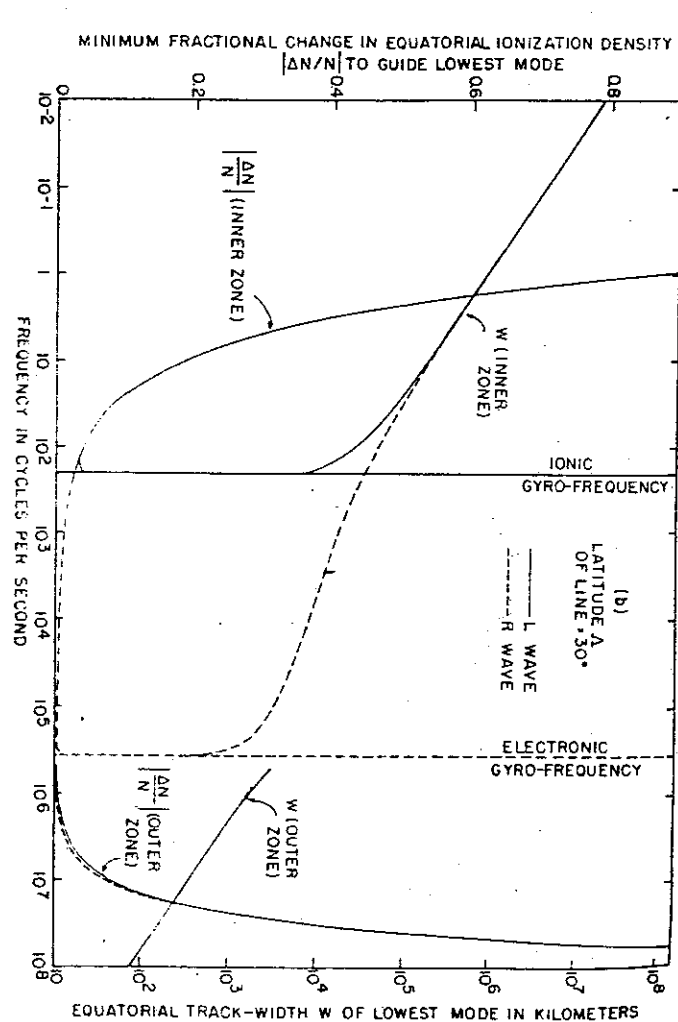


FIG 50c

